Hydrodynamics Forces and Moments on KVLCC2 Hull, with Drift Angle and Rudder Angle Influences

Mohammed Ramzi Chahbi

Master Thesis

presented in partial fulfillment
of the requirements for the double degree:
“Advanced Master in Naval Architecture” conferred by University of Liege
"Master of Sciences in Applied Mechanics, specialization in Hydrodynamics, Energetics and Propulsion” conferred by Ecole Centrale de Nantes

developed at “Dunarea de Jos” University of Galati
in the framework of the

“EMSHIP”
Erasmus Mundus Master Course
in “Integrated Advanced Ship Design”

Ref. 159652-1-2009-1-BE-ERA MUNDUS-EMMC

Supervisor:	Prof. Dan Obreja, “Dunarea de Jos” University of Galati Assist.Prof. Florin Pacuraru, “Dunarea de Jos” University of Galati
Reviewer:	Prof. Lionel Gentaz, Ecole Centrale de Nantes

Galati, February 2014

ABSTRACT

Hydrodynamics Forces and Moments on KVLCC2 Hull, with Drift Angle and Rudder Angle Influences

By **Mohammed Ramzi Chahbi**

The KVLCC2 hull is second variant with more U-shaped stern frame lines of a Very Large Crude Carrier; it was designed at the KRISO (Korea Research Institute for Ships and Ocean Engineering), now MOERI (Maritime and Ocean Engineering Research Institute) around 1997, to be used as a test case for CFD predictions.

The aim of this thesis was to compute the resistance, powering and manoeuvring performances of the KVLCC2 hull using two numerical tools

At the initial design stage, preliminary hydrodynamics performances of KVLCC2 hull were carried out using AVEVA -TRIBON ID code to estimate resistance with empirical formulas (Holtrop and Mennen), the powering and also optimum hydrodynamics performance of the propeller. The manoeuvring performances (turning circle manoeuvre, zig-zag manoeuvre and spiral manoeuvre) were compared with IMO criteria. Preliminary Hydrodynamics Performance (PHP) codes, developed at University of Galati, were used to determine the rudder hydrodynamic and rudder cavitation risk.

SHIPFLOW Code was utilized to apply Computational Fluid Dynamic (CFD) techniques in order to compute the flow around the KVLCC2 bare hull at model scale (1/58) and the still water ship resistance. The numerical computation was carried out with two methods: Potential flow theory combined with Boundary layer theory based on non-linear free surface boundary conditions and Viscous flow theory in order to solve the RANS (Reynolds averaged Navier-Stokes) equations. A grid of 1.9 million of cells was used in the domain of computation. These two numerical results were compared to validate with the experimental results from MOERI, for the range of Froude number from Fn=0.101 to Fn=0.147 (Fn=0.142 represent the design speed).

The second CFD analysis, is the flow around the KVLCC2 bare hull with drift angle β influence (static drift, β = 0°, 2°, 4°, 6°, 8°, 10° and 12°). The calculations were done in deep water, at Froude number Fn=0.142 and Reynolds number $Re=3.7*10^6$, in the same domain of a grid of 1.9 million cells. The numerical results of the non-dimensional hydrodynamics forces X, Y and yaw moment N in horizontal plane are compared to validate with experimental results from towing tank PMM test (INSEAN) at model scale (1/45.714).

The last CFD analysis is the flow around the KVLCC2 hull appended, with drift angle and rudder angle influences (static drift and rudder), with rudder angle δ = -40°,-30°, -20°, -10°, 0°, 10°, 20°, 30°, 40°, the drift angle being the same. The total number of grid is 2 million cells. The non-dimensional hydrodynamics forces X, Y and yaw moment N in horizontal plane are determined.

One may conclude that the CAD-CAE and CFD codes, may be used in naval architecture applications, in order to predict the resistance and propulsion performances and to optimize the shape of the hull. Also, the hydrodynamics forces and moment acting on the ship model in horizontal plane may be evaluated, for different rudder angle and drift angle, with CFD instruments.

Keywords: KVLCC2; CAD-CAE tools; CFD-SHIPFLOW; Resistance; Manoeuvring; Static Drift; Static Rudder and Drift; MOERI; INSEAN

ACKNOWLEDGEMENTS

Enormous gratitude to our coordinator Mr. Philippe RIGO, for always understanding and giving to me the opportunity to participate in this program "EMSHIP" Master in Advanced Ship Design.

I thank especially to my supervisor Mr. Prof. Dan Obreja, who was a great help and a lively input every time. I had questions and for welcoming me in any time and for his comments and observations, where I learnt too much, thanks to him.

I'm also grateful to prof. Florin Pacuraru for his help, advices and comments, it was with pleasure to work with him. Also with Mrs. Oana Marcu for their support in my first steps in Computational Fluid Dynamics with SHIPFLOW .

Many thanks for all teachers of the Université de Liège, Ecole Centrale de Nantes and the University of Galati.

At the end, I dedicated this Master Thesis to my Mom and all my family.

This thesis was developed in the frame of the European Master Course in "Integrated Advanced Ship Design" named "EMSHIP" for "European Education in Advanced Ship Design", Ref.: 159652-1-2009-1-BE-ERA MUNDUS-EMMC.

CONTENTS

Declaration of Authorship

I Mohammed Ramzi Chahbi declare that this thesis and the work presented in it are my own and have been generated by me as the result of my own original research.

"Hydrodynamics Forces and Moments on KVLCC2 hull, with Drift Angle and Rudder Angle Influences"

Where I have consulted the published work of others, this is always clearly attributed.

Where I have quoted from the work of others, the source is always given. With the exception of such quotations, this thesis is entirely my own work.

I have acknowledged all main sources of help.

Where the thesis is based on work done by myself jointly with others, I have made clear exactly what was done by others and what I have contributed myself.

This thesis contains no material that has been submitted previously, in whole or in part, for the award of any other academic degree or diploma.

I cede copyright of the thesis in favour of the "Dunarea de Jos" University of Galati

Date: 26/01/2014 *Signature*

LIST OF FIGURES

LIST OF TABLES

1. INTRODUCTION

For a successful design, the evaluation of the ship hydrodynamics performances is very important, beginning at the initial design stage. However, the main prediction methods are: theoretical mathematical models and empirical formulae used by the CAD-CAE instruments, numerical simulation, also known as Computational Fluid Dynamics (CFD) and experimental fluid dynamics (EFD) on the ship model in the Hydrodynamics Laboratories (towing tank, manoeuvring and seakeeping basin, offshore basin, cavitation tunnel and aerodynamic tunnel).

Nowadays, the scientific researchers are focused on generation and validation of different CAD-CAE or CFD codes, capable to investigate the hydrodynamics performance of the ship (ship resistance and powering, manoeuvrability, seakeeping, etc.).

The CAD-CAE and CFD codes are rapidly improved, in order to be applied not only for straight forward towing conditions (ship resistance and powering problem), but also to solve the behaviour of the ship in oblique towing conditions (manoeuvring problem) or in real sea conditions (seakeeping problem) . The use of CAD-CAE and CFD instruments has become a real procedure, beginning with developing of a new ship design.

In order to validate the CAD-CAE and CFD codes, modern hull forms such as the tanker KVLCC2, the container ship KCS, the surface combatant DTMB 5415, etc., were used as test cases. A large experimental benchmark was summarized by the International Towing Tank Conference (ITTC) and provides a good opportunity to explore the flow phenomena around modern hull forms. Also, the experimental results may be used to validate CAD-CAE and CFD codes results, both for inviscid and viscous flow calculations. The validation is thus expected to reveal the differences between numerical and experimental results. As a consequence, new versions of the computer codes may be develop in order to obtain a satisfactory correlation.

KVLCC2 (KRISO Very Large Crude Carrier) is the most relevant to the current study. The main objective was to investigate the resistance, powering and manoeuvring performances of this ship. Two numerical instruments with specific methods were used in order to determine the hydrodynamics performance of KVLCC2:

- Preliminary theoretical prediction method based on the mathematical models and empirical formulae carried out in AVEVA-Tribon M3 system, which is a specialized software for the initial ship design, comprising the hull surface definition and production level fairing capacities;

- CFD method with SHIPFLOW code used in the initial ship design; the knowledge of the surface ship, of the flow and the pressure field is useful both in the study of the main aspects of the new hull forms and for the performances evaluation.

The structure of the present thesis is described and divided in six chapters, as follows:

Chapter 1, dedicated to introduction;

Chapter 2, for preliminary estimation of the hydrodynamics performance of the KVLCC2 ship, carried out by using the mathematical models of the CAD-CAE tools for initial ship design (AVEVA-Tribon ID code and PHP-Preliminary Hydrodynamics Performance code, developed at University of Galati); the following performances were estimated:

- Ship resistance, optimum hydrodynamics characteristics of the propeller and powering performances, using the regression analysis methods from AVEVA-Tribon ID code;
- Rudder hydrodynamics and rudder cavitation risk on the basis of PHP code, including maximum hydrodynamic torque related to the rudder axis, which is used to select the optimum suitable steering gear;
- Manoeuvring performances using AVEVA-Tribon ID (turning circle, Zig-Zag, and Spiral manoeuvre characteristics), which were compared with IMO criteria.

Chapter 3, for CFD analysis of the flow around KVLCC2 bare hull, in order to perform:

- still water ship resistance;
- the numerical computations was carried out in potential flow theory combined with boundary layer theory, taking non-linear free surface and in viscous flow theory were done with undisturbed water surface, i.e. neglecting the generation of the wave;
- the two computational results were compared to validate with the experimental results obtained from MOERI at model scale (1 :58);

Chapter 4, for CFD computations (on the basis of viscous flow theory) of the hydrodynamic forces and moments of KVLCC2model, in the oblique flow, for static drift angle, in deep water condition; the numerical results were validated with the experimental results from INSEAN at model scale (1:45.714);

Chapter 5, for CFD computation in viscous flow theory of the hydrodynamic forces and moments of KVLCC2model, with deflected rudder and static drift angle; the hydrodynamic forces and moments may be used to determine the numerical hydrodynamics derivatives, from manoeuvring mathematical model;

Chapter 6, dedicated to conclusion and future recommendations.

2. PRELIMINARY HYDRODYNAMICS PERFORMANCES

2.1 AVEVA (Tribon M3) system

The TRIBON M3 is a naval architecture program originally developed by Kockum Computer Systems (KCS) for designing commercial and naval vessels. KCS was spun off from Kockums shipyards as an independent company, later renamed Tribon Systems, which was in turn acquired by AVEVA in 2004.

The TRIBON M3 system is based on the use of a Product Information Model (PIM) database, which has been to handle in an efficient way all design details of the ship (structural and outfit objects, etc.) found in shipbuilding industry. These databases are used to depict a 3D model of ship. The informations in the database contain all the technical data that is needed to define the final product. It addresses all phases in the design and production process. Information from one stage can be used in the next stage. All types of drawing and reports can be derived from the model.

The preliminary hydrodynamics performances (Resistance, Powering, Propeller and Manoeuvring) of the KVLCC2 hull were carried out using the TRIBON M3 initial design. It comprises three basic elements:

- Geometric modeling facility
- Hydrostatics performance calculation routines
- Hydrodynamic analysis programs.

Tribon initial design contains three separate but integrated systems for geometry (hull) modeling:

- **Tribon Form module:** is a modeling program based on the specific parameters, providing the users with the ability to rapidly generate the body line plan.
- **Tribon Lines module:** is used for fairing of a hull form generated with Tribon form; or directly from offset data.
- **Tribon Surface & Compartment module:** is used by the designer to rapidly define the transverse bulkheads, the longitudinal bulkheads and the decks, which are then used to define the ship compartmentation for use in TribonCalc & Hydro module.

Hydrostatics and hydrodynamic performances are done with **TribonCalc & Hydro module**; it comprises separate tools for analyzing:

- **Hydrostatics**

- **Resistance and powering:** module incorporates empirically methods in order to predict the ship resistance, the propeller performance and the powering requirements.
- **Manoeuvring:** module predicts the ship manoeuvring characteristics using semi-empirical formulae, for the following tests: turning circle, zig-zag, spiral and stopping.

Before to predict hydrodynamics performances of KVLCC2, using TribonCalc& Hydro module, KVLCC2 hull has to be design. The process is described as follow.

a. Project creation Module

In this module we create a new Tribon M3 Initial design project (named KVLCC2) using project tool. This module creates and manages projects. A project is established to represent a proposed tender or investigation and so many contain design variants; with input initial values for hull form including length, draught, displacement, block coefficient, beam, etc., (see Figure 1)

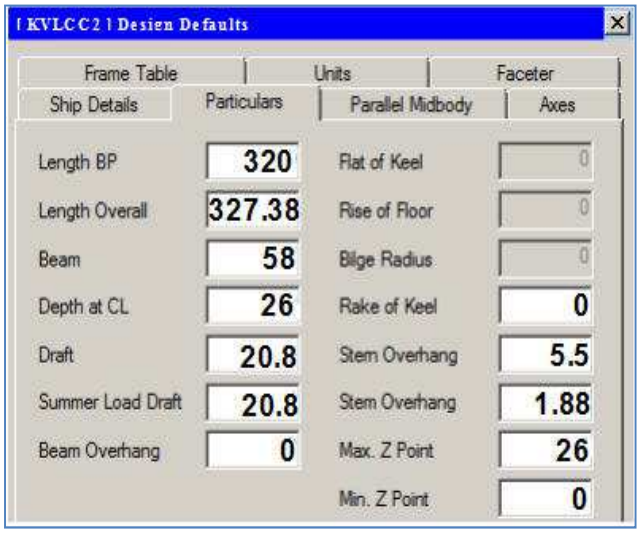

Figure 1. Input Initial Value

b. Tribon Lines Module

The main objective of this module is to create lines of ship shape form and to fair a hull form by means of a series of orthogonal and 3d space curves, generated from offset data. A BRITFAIR FILE (BRI), will be input to the system Lines module.

- BRITFAIR File (BRI) generation:

Taking from hull surface of KVLCC2.iniges file [1], a number of 20 sections are created between aft perpendicular and forward perpendicular, including the section at the transom stern and another section at the end of bulbous bow.

Then points are generated in all sections, to have coordinates (y, z) of these points, which they are input in **Tribon M3 Edit Britfair.**

- Tribon Lines Module:

Here the import of the body lines plan (BRITFAIR file) to the Tribon Lines Module, to make more fairing body lines if it's necessary(see Figure 2).

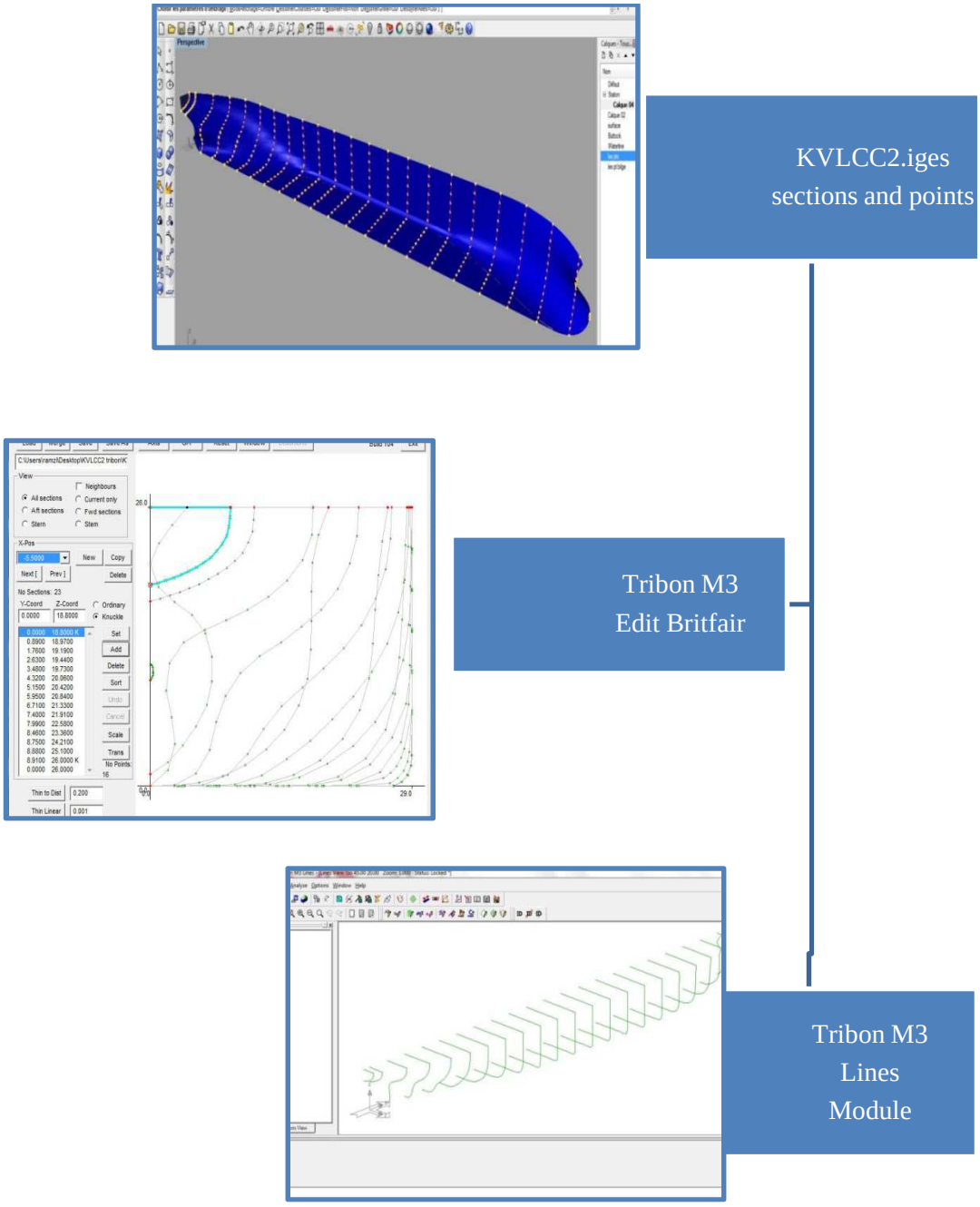

Figure 2. Workflow of Tribon Lines module

c. <u>Tribon Surface & Compartment Module</u>

After opened Tribon Surface & Compartment module (see Figure 3), offset data was used. In order to carry out the detailed analysis in TribonCalc/Hydro, the envelope is set up, it is

therefore useful to obtain the basis information as well as releasing the Calculation Geometry of the profile points and deck edge points are generated.

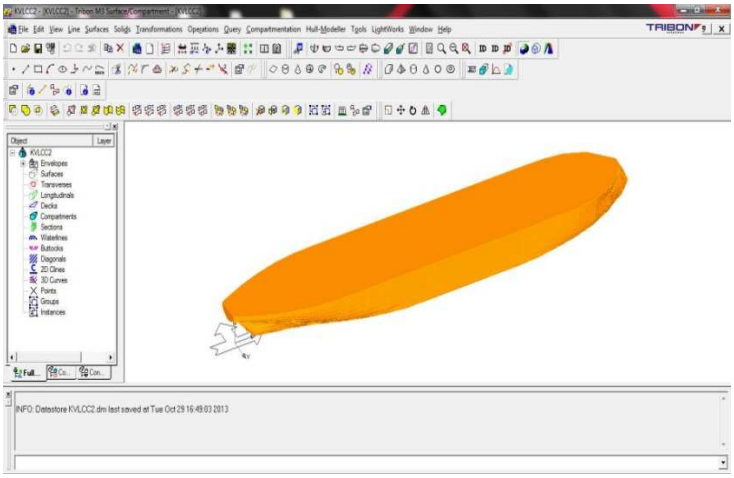

Figure 3.Tribon M3 Surface & Compartment Module

d. Tribon M3 Calc& Hydro Module :

Tribon M3 Calc& Hydro offers the ship designer a comprehensive toolkit of Naval Architectural assessment routines including the calculation of hydrostatics, tank calibration, loading conditions, intact and damage stability, critical KG, longitudinal strength, freeboard, tonnage and launching.

Concerning KVLCC2, we apply only the hydrostatics and sectional area.

- Hydrostatics

Start the module Tribon M3 Calc & Hydro with creating new designs using the output file from the previous module (General Particulars File – GPF and Calculation Geometry from Tribon M3 Surface and Compartment) as input.

In order to produce the hydrostatics calculation of particulars were done in no trim and heel conditions. The results will be presented in graph known as hydrostatic curves (Figure 4) and table (see APPENDIX A1).

The particulars that are calculated are as follows, plotted against different variation of the draft moulded:

- The displacement - Δ
- The longitudinal centre of buoyancy - LCB
- The vertical centre of buoyancy - VCB
- The waterplane area - WPA
- The longitudinal centre of flotation - LCF
- The height of the longitudinal metacentre - KML

- The height of the transverse metacentre - KMT
- The wetted surface area - WSA
- The tonnes per centimetre immersion - TPC
- The moment to change trim one centimetre – MTC

The range of moulded draft is from 0.5 – 21 m with the increment of 0.5 m have been introduced. Additionally, the design draft (20.8 m) has been implemented as additional input draft. The pivot point along the x-axis has been chosen to be at the amidship, at the distance of 160 m from the aft perpendicular.

From the results given in (APPENDEX A1), the coefficients of hull form can be calculated at the design draft (20.8 m):

The block coefficient C_B is determining as follows:

$$C_B = \frac{\Delta}{\rho * L * B * T} \tag{1}$$

$C_B = 0.805$

The waterplane area coefficient is obtained with the following formulae:

$$C_W = \frac{WPA}{L * B} \tag{2}$$

$C_W = 0.897$

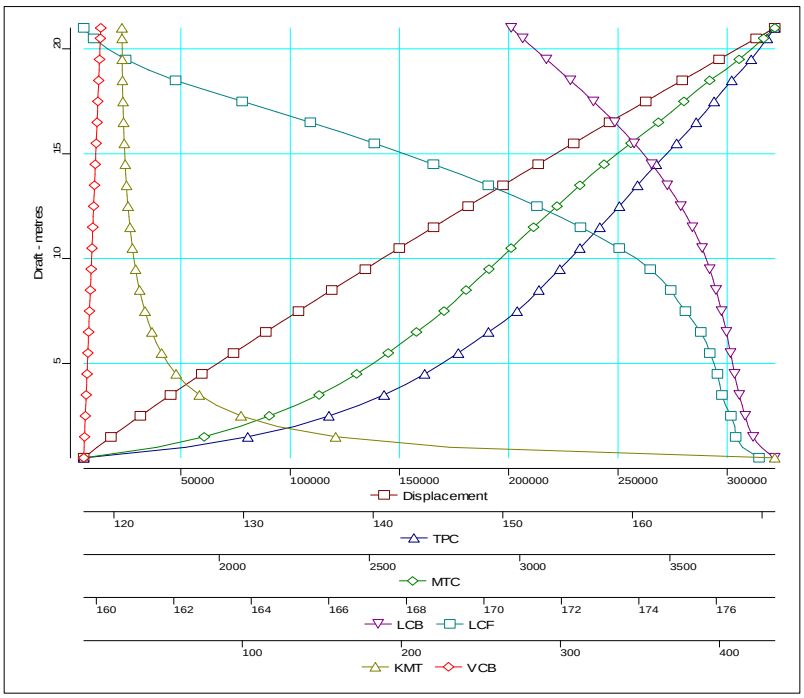

Figure 4. Hydrostatic curves of KVLCC2

The hydrostatic static curves (Figure 4) looks correct, the displacement curve increase proportional with draft.

- Sectional Area Curves

The sectional area is calculated in order to develop Bonjean diagram, where we can obtain the transverse sectional area curves (from section with number -0.125 to 10.25). The aft perpendicular is at section 0 and the forward perpendicular is at section 10, which means the midship section is at section 5.

The sectional area are represented and calculated for different waterline height (draft). The range is from 0 to 21 m, including the design draft 20.8 m.

The results are shown in the following Figure 5

From the table in (APPENDIX A2), the section (area) was extract at a midship at design draft (20.8 m):

$$A_M = 1203.60\ m^2$$

After that the midship section coefficient C_M is described by:

$$C_M = \frac{A_M}{B * T} \tag{3}$$

Finally the prismatic coefficient C_P can be evaluated by the ratio between $C_B$and C_M:

$$C_P = \frac{C_B}{C_M} \tag{4}$$

The results: $C_P = 0.807$, $C_M = 0.997$

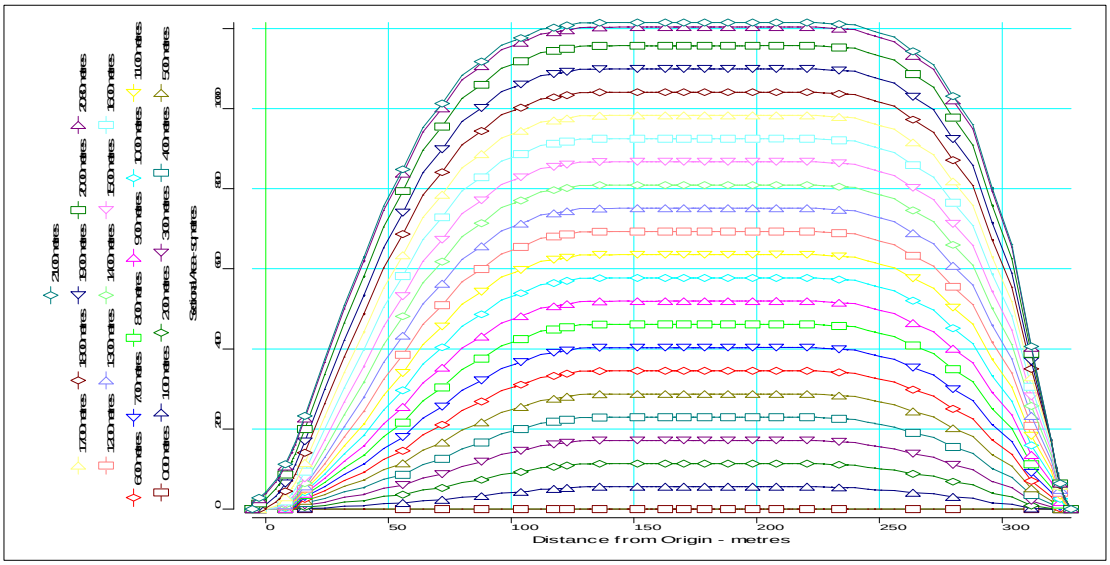

Figure 5. Sectional Area (Bonjean curves) of KVLCC2

2.2 Ship resistance and powering

2.2.1 Ship resistance

The prediction resistance of KVLCC2 is executed in Tribon M3 Calc& Hydro module, providing different empirical methods to estimate the ship resistance.

Holtrop and Mennen method [2] was used to compute the resistance of bare hull KVLCC2. This method is based on statistical regression analysis of experiments for 191 models available at the Netherlands Ship Model Basin (MARIN). Accuracy is claimed to be satisfactory for preliminary design work for 95% of the cases as long as the range of hull parameters is in limitations as shown in the Table 1.

Table 1. KVLCC2 in Limitation of the method

Holtrop and Mennen method	KVLCC2
Fn ≤ 0.24	0.141
Cp ≤ 0.85	0.807
≤ L/B ≤ 7.1	5.517
2.4 ≤ B/T ≤ 3.2	2.788

The KVLCC2 hull parameters are in range of limitations of Holtrop and Mennen method. According this method the bare hull KVLCC2 resistance is calculated using formulae with the total resistance being subdivided as follows:

$$R_{Total} = R_F(1 + k_1) + R_W + R_B + R_{TR} + R_A \quad (5)$$

Where:

R_F : Frictional resistance according to the ITTC 1957 model-ship correlation line.

$(1 + k_1)$: Form factor describing the viscous resistance of the hull form in relation to R_F

R_W : Wave-making and wave breaking resistance

R_B : Additional pressure resistance of the bulbous bow near the water surface

R_{TR} : Additional pressure resistance of immersed transom stern

R_A: Ship-model correlation resistance.

The inputs in **Tribon M3 Calc& Hydro** are: ship form (body shape coefficients), ship speed V=13 – 17 knots with 0.5 knots increment, drafts, bulb information, and form coefficients (see Table 2).

Table 2. The inputs data in Tribon M3, Resistance

Draught aft	20.800	[m]	
Draught fwd	20.800	[m]	
Mean draught	20.800	[m]	
Length aft of AP	5.500	[m]	
Length fwd of FP	0.000	[m]	
Transom area	13.820	[m²]	(1.146 % midship area)
Bulb area	174.030	[m²]	(14.426 % midship area)
Height of Centroid	10.280	[m]	
Displacement	318344	[tonnes]	
Long. centre buoy.	10.823	[m]	(3.382 % LPP fwd midships)
Wetted surface	27699	[m²]	
Half entrance angle	59.950	[deg]	

The form factor K is estimated using the Holtrop and Mennen formula. The form factor correction factor is applied to the value obtained from the formula. The default value for the correction is 1.0 which applies no correction to the Holtrop and Mennen estimate.

$$Form\ factor, k = 0.333$$

Table 3**.** Resistance Coefficients of KVLCC2

Speed kts	**Fn**	**Rn /10^9**	**Cf *10^3**	**Cf x k *10^3**	**Cw *10^3**	**Ca *10^3**	**Ct *10^3**
13.000	0.118	1.832	1.422	0.473	0.272	0.228	2.408
13.500	0.123	1.902	1.415	0.471	0.275	0.228	2.402
14.000	0.127	1.973	1.409	0.469	0.279	0.228	2.398
14.500	0.132	2.043	1.403	0.467	0.286	0.228	2.397
15.000	0.137	2.114	1.398	0.465	0.296	0.228	2.399
15.500	0.141	2.184	1.392	0.464	0.311	0.228	2.406
16.000	0.146	2.255	1.387	0.462	0.332	0.228	2.421
16.500	0.150	2.325	1.382	0.460	0.358	0.228	2.441
17.000	0.155	2.396	1.377	0.459	0.391	0.228	2.467

Thus the resistances are calculated from the resistance coefficients using the following formula:

$$R_F = \frac{1}{2} * \rho * V^2 * WSA * C_F$$

$$R_W = \frac{1}{2} * \rho * V^2 * WSA * C_W \quad (6)$$

$$R_A = \frac{1}{2} * \rho * V^2 * WSA * C_A$$

$$R_T = \frac{1}{2} * \rho * V^2 * WSA * C_T$$

where:

ρ : sea water density [1.025 t/m³]

V: the ship speed

WSA: is the wetted surface area taking from hydrostatic result [27699.27 m²]

C: specific resistance coefficients

Table 4. Resistances of KVLCC2

Speed [kts]	Rf [kN]	kRf [kN]	Rw [kN]	Ra [kN]	Rt [kN]
13	902.71	300.27	172.67	144.74	1528.65
13.5	968.70	322.44	188.26	156.09	1644.39
14	1037.36	345.30	205.41	167.86	1765.51
14.5	1108.05	368.82	225.87	180.07	1893.08
15	1181.55	393.01	250.17	192.70	2027.57
15.5	1256.22	418.74	280.66	205.76	2171.32
16	1333.77	444.27	319.26	219.25	2328.09
16.5	1413.32	470.42	366.11	233.17	2496.32
17	1494.84	498.28	424.46	247.51	2678.13

2.2.2 Hydrodynamics characteristics of the propeller

The propeller of the KVLCC2 ship was designed by MOERI. One fixed pitch propeller, with right hand rotation was used.

In the same module Tribon M3 Calc& Hydro, powering tool, we determine the hydrodynamics performances of the propeller in open water using:

- Propeller series as Wageningen B-series is suitable for normal merchant ships, whereas the Gawn-Burrill series propellers are more appropriate for the higher loading conditions of warships.
- The propulsion factors (wake fraction ω, thrust deduction t and relative rotative efficiency η_R) obtained previously by Holtrop and Mennen empirical.

Reynolds Number correction methods can be used, one of three methods, to correct the propeller design for the actual Reynolds number. ITTC-78 correction was choosing among the others (No correction, correction according to Oostervald and Oossanen).

The input data for propeller design are given in Table 5.

Table 5.Input data of Propeller design

Wageningen B-Series propeller		
Fixed Pitch		
Non-noise Reduced		
Efficiency factor	1.000	-
Shaft height	5.800	[m]
Cavitation SF	1.000	-
Design speed	15.500	[Kn]
Diameter	9.860	[m]
Number of blades	4	-
Min. Effective BAR	0.430	-
Number of screws	1	-
Reynolds number correction using ITTC method		

Three different ways are provided in Tribon M3, to optimize the propeller:

- Given the **ship speed** and **RPM of the propeller** mode, it determines the optimum diameter, pitch and blade area ratio.
- Given the **ship speed** and **the diameter of the propeller** mode, it determines the optimum RPM, pitch and blade area ratio.
- Given the **delivered power** and **RPM** mode, it determines the optimum propeller diameter, pitch and blade area ratio.

According to the input data in propeller design, we choose the ***Given ship speed & diameter*** mode to optimize the propeller of KVLCC2 ship and the results were calculated after we introduced the shaft height (the open water efficiency, the thrust coefficient, torque coefficient, the local cavitation number, etc.). The optimum results are presented in Table 6.

Table 6 The optimum result of the Propeller

Diameter D	9.860	[m]
Pitch ratio	0.801	
Effective BAR	0.516	(0.514 min)
Local Cavitation no	0.680	
Thrust load. coeff.	0.216	(0.217 max)
Kt/J^2	0.993	
Adv. coeff. J	0.443	
Thrust coeff. Kt	0.195	
Torque coeff. Kq	0.0259	
Open water eff.	0.532	

The optimum RPM of the propeller can be calculated using the formulae:

$$J = \frac{V_A}{n * D} \quad \rightarrow \quad n = \frac{V_A}{J * D} \tag{7}$$

where J is the advanced coefficient and D is propeller diameter.

The speed advance V_A is determined from the ship speed V and the wake fraction ω by:

$$V_A = V(1 - \omega) = 15.5 * 0.5144 * (1 - 0.336)$$

$$V_A = 5.294\ m/s$$

So the revolution speed of propeller is:

$$n = \frac{5.294}{0.443 * 9.86}$$

$$\boldsymbol{n = 1.212\ rps = 72.72\ RPM}$$

The open water characteristics (the thrust coefficient Kt, the torque coefficient Kq and propeller efficiency eta0) of the KVLCC2's propeller are given in Table 7 and Figure 7.

Table 7.Propeller characteristics

J	Kt	Kq	eta0
0.236	0.269	0.0330	0.306
0.287	0.252	0.0314	0.367
0.338	0.234	0.0297	0.425
0.390	0.215	0.0279	0.479
0.441	0.196	0.0259	0.530
0.492	0.175	0.0239	0.575
0.544	0.154	0.0217	0.614
0.595	0.132	0.0195	0.644
0.646	0.110	0.0171	0.663
0.698	0.087	0.0146	0.665
0.749	0.064	0.0119	0.638
0.801	0.040	0.0091	0.556

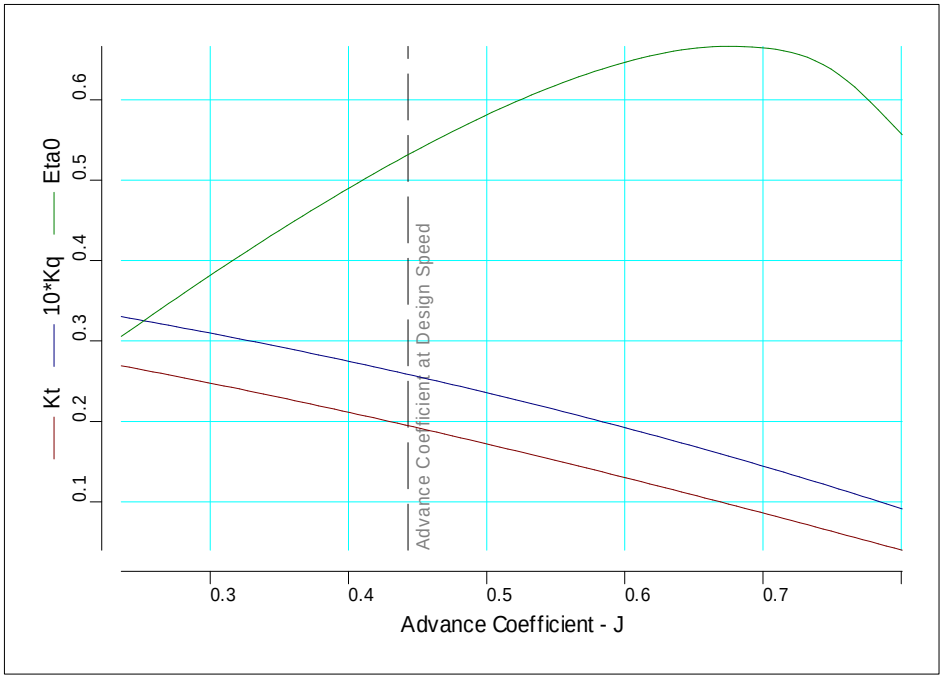

Figure 6. Propeller characteristics

2.2.3 Brake power

After estimate the total resistance of KVLCC2 and the propulsion factors (wake fraction ω, thrust deduction t and relative rotative efficiency η_R) using Holtrop & Mennen method, on the basis of the propeller characteristics (open water efficiency) the powering performance of the ship is calculated.

The main role of the propulsion system is to deliver enough power to overcome the ship resistance and to propel the ship at the required speed (design speed).

The effective power, the delivered power and the brake power must be calculated in order to determine the propulsion power of the engine [3].

- Effective power $\boldsymbol{P_E}$:

The effective power may be calculated using the relation

$$P_E = R_T * V(1 + M_D) \tag{8}$$

where, R_T is the total resistance, V is the ship speed and M_D is the *power design margin* , which is defined as a fraction of the resistance (related to the predicted resistance) or effective power estimate, which is increased to provide the needed margin.

- M_D=0.01 – 0.02 , prediction based on the self-propulsion test with final propeller in the towing tank;
- M_D=0.03 – 0.06, prediction based on the self-propulsion test with stock propeller in the towing tank;
- M_D=0.07 – 0.08, prediction based on the resistance test in the towing tank;
- M_D=0.10, for preliminary theoretical prognosis (Holtrop-Mennen, Guldhammer-Harvald, Taylor, SSPA, etc.).

As the resistance of KVLCC2 was predicted with the empirical formula from Holtrop – Mennen method, so we take $\boldsymbol{M_D}$**=0.10.**

- Delivered Power $\boldsymbol{P_D}$:

The delivered power is calculated with following formula:

$$P_D = \frac{P_E}{\eta_D * np} \tag{9}$$

where: η_D is The Quasi-propulsive efficiency (QPC) and np is Number of propellers.

- Brake power at full rating (100 % MCR):

The brake power at full rating is calculated with relation:

$$P_B = \frac{P_D}{\eta_S * \eta_G * (1 - M_S)} \tag{10}$$

where :

η_S : The line shaft bearing efficiency, is taken equal **0.97**

η_G : The reduction gear efficiency is taken equal 1 because the engine is low speed (rpm < 120).

M_S : The *power service margin:* provide the added power needed in service to overcome the added resistance from hull fouling, waves, wind, shallow water effects, etc. and is defined as fraction of the MCR, usually $M_S = 0.15 - 0.25$, it was choose at the value **0.15.**

- Brake power at service rating P_B^{SR}

The brake power at service rating is calculated with relation:

$$P_B^{SR} = \frac{P_B}{SR} \tag{11}$$

where, *SR* is the service rating of the main engine, P_B is brake power at full rating (100 % MCR). Usually *SR= 0.85 – 0.95 (corresponding to the service rating between 85% MCR – 95% MCR).* In the computation SR was taking equal to **0.9**

Finally the results of powering for KVLCC2 are in function of ship speed (see Table 8).

Table 8. Speed - Powering of KVLCC2

Speed kts	P_E (kW)	THDF t	WFT ω	ETAR η_R	ETA0 η_0	QPC η_D	P_B (kW)	RPM
13	11244.61	0.216	0.335	1	0.532	0.627	24168.16	61.01
13.5	12561.23	0.216	0.336	1	0.532	0.628	26954.99	63.3
14	13985.92	0.216	0.336	1	0.532	0.628	30012.23	65.61
14.5	15532.09	0.216	0.336	1	0.532	0.628	33330.13	67.93
15	17209.24	0.216	0.336	1	0.532	0.628	36929.12	70.29
15.5	19043.57	0.216	0.336	1	0.531	0.628	40865.39	72.7
16	21077.18	0.216	0.336	1	0.531	0.627	45301.42	75.19
16.5	23306.52	0.216	0.337	1	0.529	0.626	50172.98	77.75
17	25761.65	0.216	0.337	1	0.528	0.624	55636.00	80.41

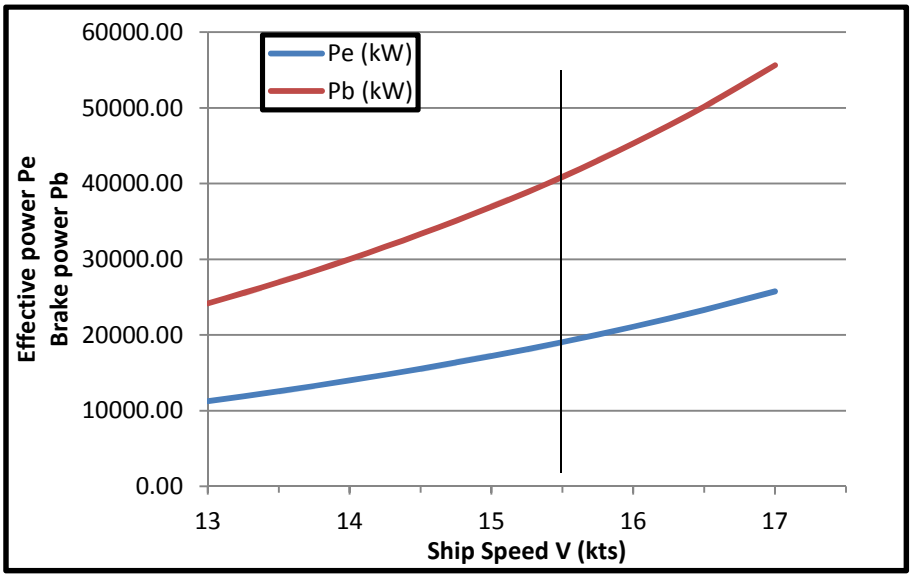

Figure 7. Speed - Powering of KVLCC2

2.3 Manoeuvring performances

The manoeuvring performances of KVLCC2 were executed by Tribon M3 Calc& Hydro module in the early design stage. Using methods of semi-empirical formulae based on mathematical models derived from regression analysis of data sets for the following tests: turning circle manoeuvre, zig-zag manoeuvre and spiral manoeuvre with checking the requirements of IMO criteria.

All the following manoeuvring tests have been performed in a deep water conditions at the design speed (V=15.5 knots)

The KVLCC2 ship was specified as merchant ship type; with the maximum speed for merchant ship is 18 knots and it has to respect and check limitations (see Table 9).

Table 9.KVLCC2 in Merchant ship limitations

Merchant Ship Limits	Min Value	Max Value	KVLCC2
Ship :			
Block coefficient (Cb)	0.48	0.85	0.805
Length/Beam (L/B)	4.0	8.0	5.517
Length/Draft (L/D)	13.66	40.11	15.384
Beam/Draft (B/T)	2.15	6.247	2.788
LCG from midship/Length	-0.05	0.057	0.034
Draft [m]	0.67*Prop Diam	-	20.8
Rudder :			
No. of Rudders	1	4	1
Rudder Area/Length*Draft (A_R/LT)	-	0.075	0.02
Rudder Height [m]	0.75*Prop Diam	Mean draft-Trim	15.79
Aspect ratio	0.75	2.8	1.827
Rudder rate [deg/s]	1.0	7.0	2.34
Propeller :			
Number of propellers	1	4	1
No. of Blades	3	5	4

The input data used in manoeuvring performances of KVLCC2, are:

- General ship information (see Table 10)

Table 10. General ship information

Length	320.000	[m]
Beam	58.000	[m]
Mean Draught	20.8000	[m]
Trim	0.0000	[m]
Block coef.	0.8045	
LCG from Aft Perp.	170.8230	[m]
Bulb present		

- Rudder information (see Table 11)

Table 11. Rudder information

No. of Rudders	1	
Height	15.790	[m]
Area	136.700	[m²]
Aspect ratio	1.827	
Turn rate	2.340	
Type	Conventional	
Distance from midships	160.000	[m]
Distance to load waterline	5.030	[m]

- Propeller information (see Table 12)

Table 12. General information of Propeller

No. of Propellers	1	
No. of blades	4	
Diameter	9.860	[m]
Mean Pitch	7.897	[m]
Blade Area Ratio	0.516	

- Non-Dimensional Hydrodynamic Coefficient, (see Table 13) (calculated and all values multiplied by 10e-5)

Table 13. Non-dimensional hydrodynamic coefficient

Yv	-2282.740	Nv	-855.549		
Yr	531.074	Nr	-374.578		
Yvd	-1566.940	Nvd	N/A		
Yrd	N/A	Nrd	-81.429		
Stabd	-1.88347				
Xrr	N/A	Yr|r|	255.195	Nr|r|	-221.340
Xvv	N/A	Yv|v|	-4423.240	Nrrv	397.216
Xvr	1048.120	Yr|v|	2030.730	Nvvr	-1216.120

2.3.1 Mathematical model

The Abkowitz nonlinear mathematical model of the ship manoeuvring was used [4], which contains the equations of motion for a body moving with six degrees of freedom. We consider the rigid body dynamics, with a right-handed coordinate system Oxyz on body (see Figure 8):

The origin is fixed at the midship section;

The longitudinal x-axis, positive forward is situated in the centreline plane, usually parallel to the keel or the still water plane;

The transverse y-axis, positive to starboard is perpendicular to the plane of symmetry;

The vertical z-axis, positive downward is perpendicular to the still water plane.

δ is rudder angle.

β is drift angle of the ship.

ψ is the heading angle.

u is ship speed component in x-axis, v is ship speed in y-axis, and r is rate angle (angular speed). With corresponding acceleration $\dot{u}, \dot{v}$.

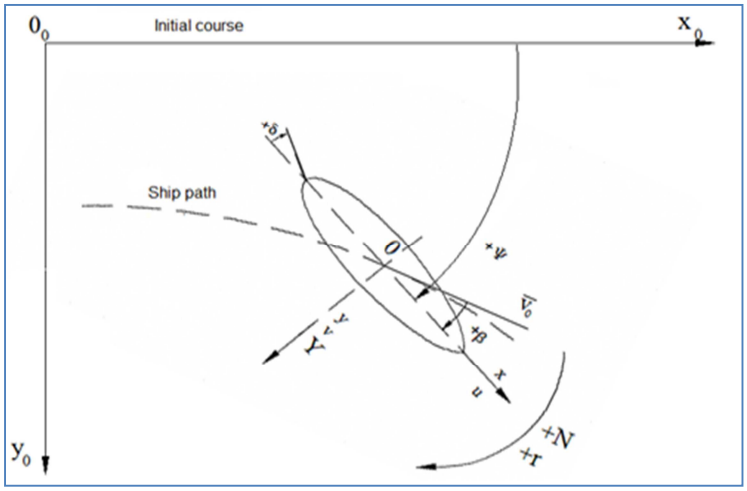

Figure 8. Coordinate system of the ship [4]

To analyse the ship motions with six degrees of freedom the linear momentum theorem and the angular momentum theorem may be used. The linear momentum theorem may be written under this form:

$$\sum_{i=1}^{N} \bar{F}_i = \sum_{i=1}^{N} \frac{d}{dt}(m_i * \bar{v}_i) \tag{12}$$

wherem_i is the mass of the small particle i, F_i is the external force acting on the particle i. and v_i is the speed.

Also, the angular momentum theorem may be written under this form:

$$\sum_{i=1}^{N} (\bar{M}_i + \bar{r}_i * \bar{F}_i) = \sum_{i=1}^{N} \bar{r}_i * \frac{d}{dt}(m_i * \bar{v}_i) \tag{13}$$

wherer_i is the body referenced radius vector and M_i is the external moment acting on the particle i.

If the ship speed in the origin is $\bar{v}_0$ and the angular speed is $\bar{\omega}$, than the total speed has the expression:

$$\bar{v}_i = \bar{v}_0 + \bar{\omega} * \bar{r}_i \tag{14}$$

The equation (14) is replaced in equation (12) to have:

$$\sum_{i=1}^{N} \bar{F}_i = \sum_{i=1}^{N} \frac{d}{dt}\left(m_i * (\bar{v}_0 + \bar{\omega} * \bar{r}_i)\right) = m * \frac{\partial \bar{v}_0}{\partial t} + \frac{d}{dx}\left(\bar{\omega} * \sum_{i=1}^{N} m_i * \bar{r}_i\right) \tag{15}$$

If $m = \sum_{i=1}^{N} m_i$is the total mass of the ship and the centre of gravity vector is noted with $\bar{r}_G$ is possible to note:

$$m * \bar{r}_G = \sum_{i=1}^{N} (m_i * \bar{r}_i) \tag{16}$$

The following conventions will be used:

$$\begin{aligned} \bar{r}_G &= x_G * \bar{\imath} + y_G * \bar{\jmath} + z_G * \bar{k} \\ \bar{v}_0 &= u * \bar{\imath} + v * \bar{\jmath} + w * \bar{k} \\ \bar{\omega} &= p * \bar{\imath} + q * \bar{\jmath} + r * \bar{k} \\ \bar{F} &= X * \bar{\imath} + Y * \bar{\jmath} + N * \bar{k} \end{aligned} \tag{16}$$

The resulting three linear momentum are given for ($\bar{r}_G \neq 0$)

$$\begin{aligned} X &= m\left[\frac{\partial u}{\partial t} + qw - rv + \frac{dq}{dt} z_G - \frac{dr}{dt} y_G + (qy_G + rz_G)p - (q^2 + r^2)x_G\right] \\ Y &= m\left[\frac{\partial v}{\partial t} + ru - pw + \frac{dr}{dt} x_G - \frac{dp}{dt} z_G + (rz_G + px_G)q - (r^2 + p^2)y_G\right] \\ Z &= m\left[\frac{\partial w}{\partial t} + pv - qu + \frac{dp}{dt} y_G - \frac{dq}{dt} x_G + (px_G + qy_G)r - (p^2 + q^2)z_G\right] \end{aligned} \tag{17}$$

The definitions of the moments of inertia are represented on the basis of following relations:

$$I = \begin{vmatrix} I_{xx} & I_{xy} & I_{xz} \\ I_{yx} & I_{yy} & I_{yz} \\ I_{zx} & I_{zy} & I_{zz} \end{vmatrix}$$

$$\begin{aligned} I_{xx} &= \sum_{i=1}^{N} m_i (y_i^2 + z_i^2) \\ I_{yy} &= \sum_{i=1}^{N} m_i (x_i^2 + z_i^2) \\ I_{zz} &= \sum_{i=1}^{N} m_i (x_i^2 + y_i^2) \end{aligned} \tag{18}$$

$$I_{xy} = I_{yx} = -\sum_{i=1}^{N} m_i \, x_i y_i$$

$$I_{xz} = I_{zx} = -\sum_{i=1}^{N} m_i \, x_i z_i$$

$$I_{yz} = I_{zy} = -\sum_{i=1}^{N} m_i \, y_i z_i$$

For the case of the angular momentum theorem, a similar procedure was applied and the following motion equations were obtained:

$$K = \frac{\partial p}{\partial t}I_{xx} + \frac{\partial q}{\partial t}I_{xy} + \frac{\partial r}{\partial t}I_{xz} + rq\left(I_{zz} - I_{yy}\right) + (q^2 - r^2)I_{yz} + pqI_{xz} - prI_{xy} + \\ +m\left[y_G\left(\frac{\partial w}{\partial t} + pv - qu\right) - z_G\left(\frac{\partial v}{\partial t} + ru - pw\right)\right] \quad (19)$$

$$M = \frac{\partial p}{\partial t}I_{yx} + \frac{\partial q}{\partial t}I_{yy} + \frac{\partial r}{\partial t}I_{yz} + pq(I_{xx} - I_{zz}) + (r^2 - p^2)I_{xz} + qrI_{xy} - qpI_{yz} + \\ +m\left[z_G\left(\frac{\partial u}{\partial t} + qw - rv\right) - x_G\left(\frac{\partial w}{\partial t} + pv - qu\right)\right] \quad (20)$$

$$N = \frac{\partial p}{\partial t}I_{zx} + \frac{\partial q}{\partial t}I_{zy} + \frac{\partial r}{\partial t}I_{zz} + pq\left(I_{yy} - I_{xx}\right) + \\ +(p^2 - q^2)I_{xy} + prI_{yz} - qrI_{xz} + \\ +m\left[x_G\left(\frac{\partial v}{\partial t} + ru - pw\right) - y_G\left(\frac{\partial u}{\partial t} + qw - rv\right)\right] \quad (21)$$

If we consider $\bar{r}_G$ = 0, the motion equations become with neglecting the cross-inertia terms in the horizontal plane x – y :

$$X = m\left(\frac{\partial u}{\partial t} + qw - rv\right)$$
$$Y = m\left(\frac{\partial v}{\partial t} + ru - pw\right) \quad (22)$$
$$N = \frac{\partial r}{\partial t}I_{zz} + pq(I_{yy} - I_{xx})$$

If we consider $\bar{r}_G \neq 0$, as the ship is symmetric about the x – z plane, we have $y_G = 0$, w=0, q=0 and for further, neglecting the roll motion influence p=0 and K=0, so the differential equations of the motion in the horizontal plane become:

$$X = m\left(\frac{\partial u}{\partial t} - rv - r^2x_G\right)$$
$$Y = m\left(\frac{\partial v}{\partial t} + ru + \frac{dr}{dt}x_G\right) \quad (23)$$
$$N = \frac{\partial r}{\partial t}I_{zz} + mx_G\left(\frac{\partial v}{\partial t} + ru\right)$$

where, X and Y are the hydrodynamics forces (surge, sway) and N is the vertical hydrodynamic moment (yaw).

2.3.2 Standard manoeuvres and IMO Criteria

The standards for ship manoeuvrability should be used to evaluate the manoeuvring performance of ships.

It should be noted that the standards were developed for ships with traditional propulsion and steering systems (e.g. shaft driven ships with conventional rudders). Therefore, the standards and methods for establishing compliance may be periodically reviewed and updated by the International Maritime Organization, as appropriate, taking into account new technologies, research and development, and the results of experience with the present standards.

The standards are based on the understanding that the manoeuvrability of ships can be evaluated from the characteristics of conventional trial manoeuvres. The following two methods can be used to demonstrate compliance with these Standards [5]:

- Scale model tests and /or computer predictions using mathematical models can be performed to predict compliance at the design stage. In this case full-scale trials should be conducted to validate these results. The ship should then be considered to meet these Standards regardless of full-scale trial results, except where the Administration determines that the prediction efforts were substandard and/or the ship performance is in substantial disagreement with these Standards
- The compliance with the Standards can be demonstrated based on the results of the full-scale trials conducted in accordance with the Standards. If a ship is found in substantial disagreement with the Standards, then the Administration should take remedial action, as appropriate.

➢ <u>Application</u>

The Standards should be applied to ships of all rudder and propulsion types, of 100 m in length and over, and chemical tankers and gas carriers regardless of the length.

The Standards should not be applied to high-speed craft as defined in the relevant Code.

➢ <u>Standards manoeuvres and associated terminology</u>

Standards manoeuvres and associated terminology are as defined below [5]:

1. The test speed (V) used in the Standards is a speed of at least 90% of the ship’s speed corresponding to 85% of the maximum engine output.

2. Turning circle manoeuvre is the manoeuvre to be performed to both starboard and port with 35° rudder angle or the maximum rudder angle permissible at the test speed, following a steady approach with zero yaw rate.
3. Advance is the distance travelled in the direction of the original course by the midship point of a ship from the position at which the rudder order is given to the position at which the heading has changed 90° from the original course.
4. Tactical diameter is the distance travelled by the midship point of a ship from the position at which the rudder order is given to the position at which the heading has changed 180° from the original course. It is measured in a direction perpendicular to the original heading of the ship.
5. Zig-zag test is the manoeuvre where a known amount of helm is applied alternately to either side when a known heading deviation from the original heading is reached.
6. The 10°/10° zig-zag test is performed by turning rudder alternately by 10° to either side following a heading deviation of 10° from the original heading in accordance with the following procedure:
    i. After a steady approach with zero yaw rate, the rudder is put over to 10° to starboard or port (first execute);
    ii. When the heading has changed to 10° off the original heading, the rudder is reversed to 10° port or starboard (second execute); and
    iii. After the rudder has been turned to port/starboard, the ship will continue turning in the original direction with decreasing turning rate. In response to the rudder, the ship should then turn to port/starboard. When the ship has reached a heading of 10° to port/starboard of the original course the rudder is again reversed to 10° to starboard/port (third execute).
7. The first overshoot angle is the additional heading deviation experienced in the zig-zag test following the second execute.
8. The second overshoot angle is the additional heading deviation experienced in the zig-zag test following the third execute.
9. The 20°/20° zig-zag test is performed using the procedure given in 6 above. Using 20° rudder angles and 20° change of heading, instead of 10° rudder angles and 10° change of heading, respectively.
10. Full astern stopping test determines the track reach of a ship from the time an order for full astern is given until the ship stops in the water.

11. Track reach is the distance along the path described by the midship point of a ship measured from the position at which an order for full astern is given to the position at which the ship stops in the water

➢ Conditions at which the standards apply

In order to evaluate the performance of a ship, manoeuvring trials should be conducted to both port and starboard and at conditions specified below:

1. Deep, unrestricted water;
2. Calm environment ;
3. Full load (summer load line draught), even keel condition; and
4. Steady approach at the test speed.

➢ Criteria

The manoeuvrability of the ship is considered satisfactory if the following criteria (see Table 14) are complied with [5]:

1. Turning ability

   The advance should not exceed 4.5 ship lengths (L) and the tactical diameter should not exceed 5 ship lengths in the turning circle manoeuvre.

2. Initial turning ability

   With the application of rudder 10° rudder angle to port/starboard, the ship should not have travelled more than 2.5 ship lengths by the time the heading has changed by 10° from the original heading.

3. Yaw-checking and course-keeping abilities
   a. The value of the first overshoot angle is the 10°/10° zig-zag test should not exceed:
      - 10°, if L/V is less than 10s;
      - 20°, if L/V is 30 s or more; and
      - (5 + 1/2(L/V)) degrees, if L/V is 10s or more, but less than 30 s.

      where L and V are expressed in m and m/s, respectively.
   b. The value of the second overshoot angle is the 10°/10° zig-zag test should not exceed:
      - 25°, if L/V is less than 10 s;
      - 40°, if L/V is 30 s or more; and
      - (17.5 + 0.75(L/V))°, if L/V is 10 s or more, but less than 30 s

c. The value of the first overshoot angle in 20°/20° zig-zag test should not exceed 25°.

4. Stopping ability

The track reach in the full astern stopping test should not exceed 15 ship lengths. However, this value may be modified by the Administration where ships of large displacement make this criterion impracticable, but should in no case exceed 20 ship lengths.

Table 14. IMO Criteria

Ability	Test	Criteria
Turning ability	Turning test with max. rudder angle	Advance < 4.5L Tactical diameter < 5.0L
Initial turning ability	10°/10° Zig-Zag manoeuvring test	Track reach< 2.5 ship length by the time that 10° deviation is reached from the original heading in execution of 10° rudder angle.
Y aw Checking &Course Keeping Ability	10°/10° Zig-Zag manoeuvring test	1) First overshoot angle · 10°, if L/Vis less than 10 sec. · 20°, if L/V is 30 sec. or more. · (5+1/2(L/V)) degrees, if L/V is 10 sec. or more but less than 30 sec. (2) Second overshoot angle · 25°, if L/V is less than 10 sec. · 40°, if L/V is 30 sec. or more · (17.5+0.75(L/V)) degrees, if L/V is 10 sec. or more but less than 30 sec.
	20°/20° Zig-Zag manoeuvring test	First overshoot angle < 25°
Stopping Ability	Stopping Test	Track reach < 15L Stopping distance (track reach) should not exceed 20L

2.3.3 Hydrodynamics of the rudder

a. Rudder Design

Rudder is a hydrofoil pivoting on a vertical, placed at ship's stern behind propeller to produce a transverse force and a steering moment about the ship's centre of gravity.

The type of rudder and its location and placement relative to the propeller and shape of stern hull near is possible, in order to obtain significant influence on rudder effectiveness and good

ship controllability. The Figure 9 below shows the major rudder types available to the designer.

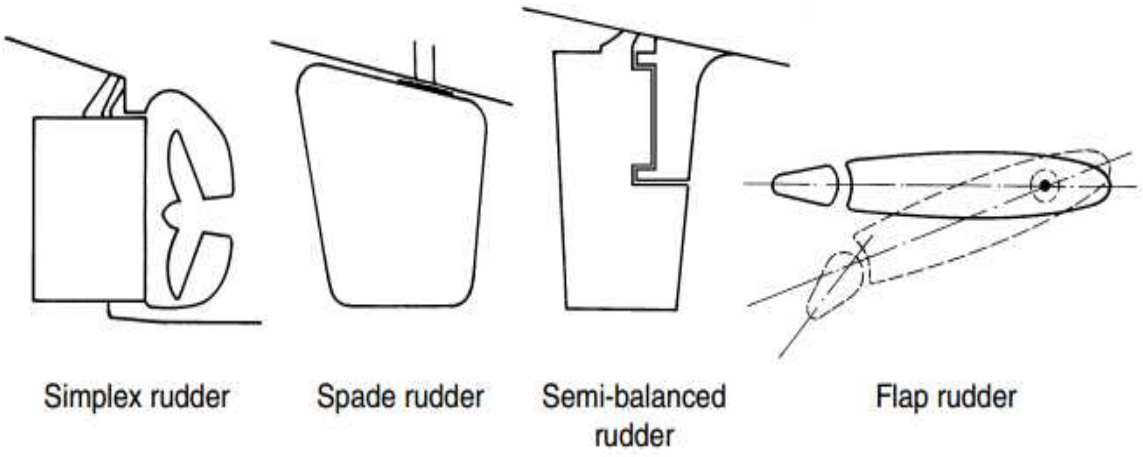

Figure 9.Types of the rudder [6]

The rudder of the KVLCC2 was designed by MOERI at full scale and the geometry was given in (IGES) file format [1]. The description of the rudder is presented in Table 15.

Table 15. Design rudder of KVLCC2

Rudder	**MOERI**
Type	Horn
Surface of rudder (m²)	273.3
Lateral area A_R (m²)	136.7
Turn rate (deg/s)	2.34

The rudder type horn is semi-balanced rudder; a fixed guide-head (horn) extends over the upper part of the rudder, like in Figure 10. This type of rudder has the following properties [6]:

- Decreased rudder bending moment compared to spade rudders
- Reduce rudder effectiveness compared to spade rudders. For steady turning circle, the semi-balanced rudder produces only approximately half the transverse force than a spade rudder of the same area (including the area of the rudder horn). The reasons for the reduced transverse force are:
  - The horizontal gap between horn and rudder opens wide for large rudder angles. Sometimes horizontal plates are attached at the horn along the gap as a remedy for this problem.

- ➢ Unfavourable angle of attack for the rudder horn.
- Drag/Lift ratio of the rudder about twice as high as for spade rudders.

The main geometric elements of the rudder of KVLCC2 ship (see Table16 and Fig. 10)

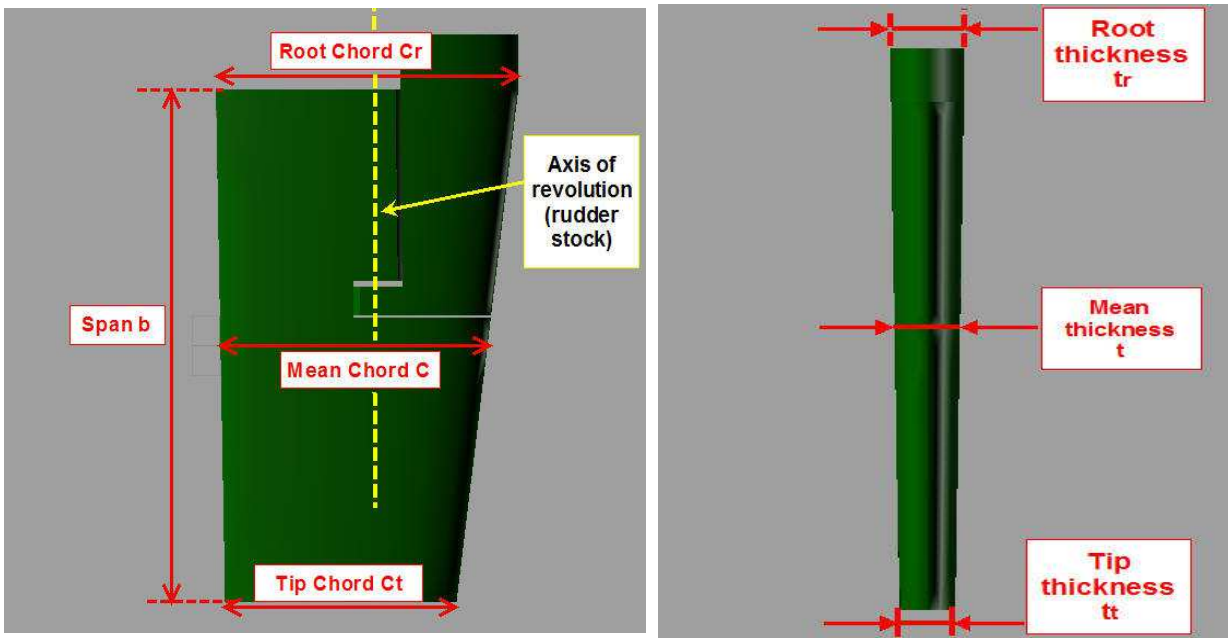

Figure 10. The main geometric elements of the Rudder

Table 16. The main geometric elements of the Rudder

Mean Span, b (m)	**15.79**
Root Chord, Cr (m)	9.79
Tip Chord, Ct (m)	7.49
Mean Chord, C = (Cr + Ct)/2 (m)	8.64
Taper ratio, TR = Ct/Cr	0.765
Root Thickness, tr (m)	1.76
Tip Thickness, tt (m)	1.35
Mean Thickness, t = (tr + tt)/2 (m)	1.555
Aspect ratio, λ = b / C	1.827
Relative Thickness, t / C	0.18

The profile of the rudder is NACA 0018, where last two digits (18) describe the relative thickness, t_{max}/C=0.18 in percent, where t_{max} is the maximum thickness of profile (aerofoil) and C is the mean chord. And (00) indicate the profile is symmetrical (no chamber).

This type of profile (see Figure 11) usually is used to decrease rudder- side cavitation because of the relative thickness.

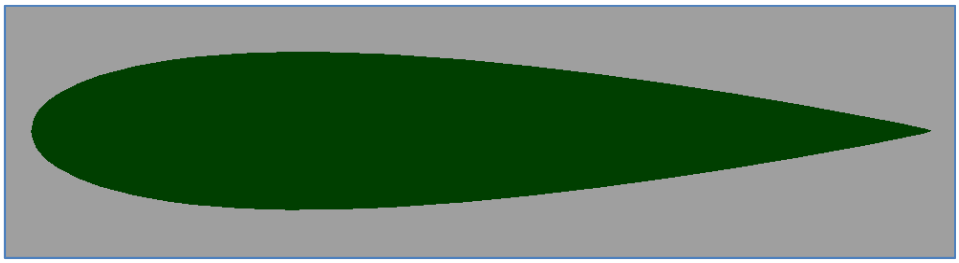

Figure 11.Profile NACA 0018 of the rudder

The rudder cavitation and the hydrodynamics performances was calculated using the Preliminary Hydrodynamics Performance (PHP) program, developed at the Naval Architecture Faculty of the “Dunarea de Jos”, University of Galati (Romania), after designed the rudder of KVLCC2 ship.

b. Rudder cavitation

Using PHP program, the rudder cavitation is investigate, in the design stage of the ship, on the basis of a theoretical method proposed by Brix 1983 [7], which may be applied for immersed point of the rudder situated between 0.7D and D, where D is the propeller diameter and h0 is the immersion of the point on the rudder.

The computation was performed for two inflow angle α, and the results static pressure, dynamic pressure and total pressure are presented in Table 17.

On the basis of the total pressure (static pressure + dynamic pressure) on the suction side, if the resulting minimum pressure is negative or slightly positive, the cavitation occurs only on the side plating of the rudder. For propeller turning clockwise (the cavitation will occur on starboard in the upper part of the rudder and on portside in the lower part of the rudder relative to the propeller axis.

Table 17. Result of rudder pressures

Inflow angle α [deg]	Static pressure [kPa]	Dynamic pressure [kPa]	Total pressure [kPa]
18	219.326	-45.218	174.108
21	219.326	-49.885	169.441

Concerning our results for two inflow angle α, the total pressure is positive that mean no cavitation on sides of the designed rudder.

c. KVLCC2 rudder Hydrodynamics

In order to calculate the hydrodynamic forces and torques acting on the rudder, the method proposed by Y.I. Voitkounski [8] was used in PHP program. In principle, the hydrodynamic torques are calculated against the rudder stock, for ahead and astern ship motion, the maximum value being adopted in order to calculate the diameter and position of the rudder stock and also to choose the steering gear.

- The normal hydrodynamic force P_n in ahead motion.

The normal component of the hydrodynamic force acting on the rudder P_n is calculated using the relation:

$$P_n = 0.5 * C_n^* * \rho * v^2{}_R * A_R \tag{24}$$

where :

v_R : is the flow speed on the rudder

A_R : is the rudder area

ρ : is the water density

C_n^* : is the normal hydrodynamic force coefficient determined by taking account the correction for the corrected attack angle α_{cor}

$$C_n^* = C_y^* * cos\alpha_{cor} + C_x^* * sin\alpha_{cor} \tag{25}$$

The results of hydrodynamic forces P_n on the rudder in ahead ship motion (ship speed V=15.5 kts) with different inflow (attack) angle α [deg,°] from 0° to 40° with 5° increment are presented in Table 18 and Figure12.

Table 18P_n [kN] in ahead ship motion

Alfa α [deg]	$\boldsymbol{P_n}$ [kN]
0	0.000
5	1210.800
10	2446.644
15	3647.082
20	4523.790
25	5159.946
30	5431.297
35	5325.151
40	5225.625

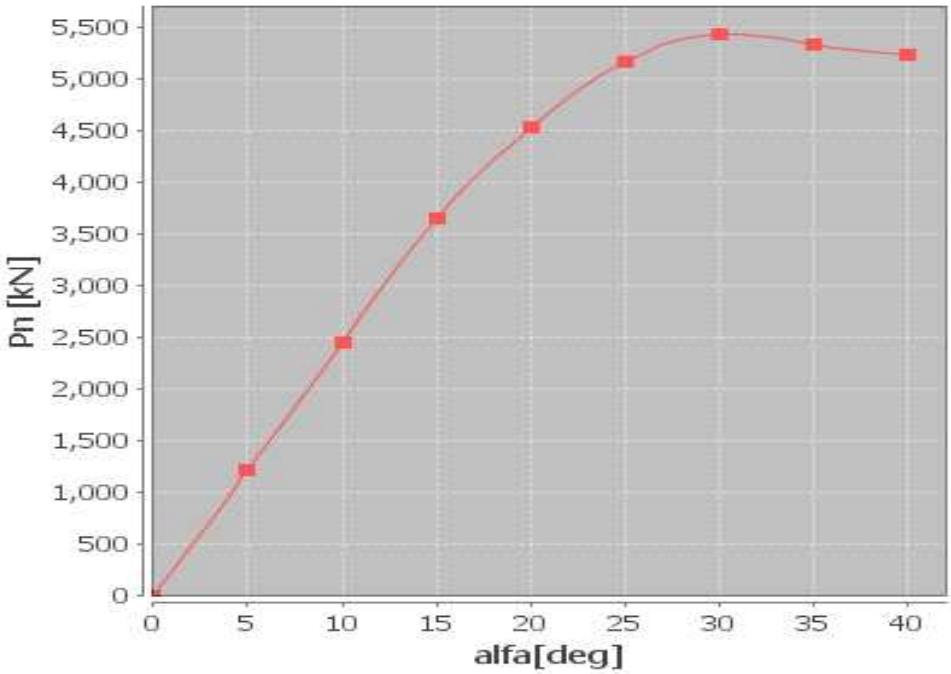

Figure 12.P_n [kN] in ahead ship motion

From the results we can see that the hydrodynamic force P_n start from 0 at inflow angle α=0° and increase proportional with angle α, until it reach maximum P_n =5431.297 kN at α=30°, after that decrease slightly.

- The Hydrodynamic force P_{nb} in astern motion.

The normal component of the hydrodynamic force acting on the rudder P_{nb} is calculated in backwards (astern) ship motion for the attack angle α_{cor} by means of the relations:

$$P_{nb} = 0.5 * C^*_{nb} * \rho * v^2{}_{Rb} * A_R \quad (26)$$

where,v_{Rb} is the speed of the flow on the rudder, and C^*_{nb} is normal force coefficient described as follow:

$$C^*_{nb} = C^*_{yb} * cos\alpha_{cor} + C^*_{xb} * sin\alpha_{cor} \quad (27)$$

The similar results were obtained, in the astern motion case, when the ship speed was considered 60% of speed at ahead motion, so V=9 Kn see (Table 19) and (Fig. 13).

Table 19.P_{nb} [kN] in astern ship motion

Alfa α [deg]	P_{nb} [kN]
0	0.000
5	438.549
10	731.160
15	970.246
20	1212.901
25	1441.227
30	1621.259
35	1609.611
40	1589.198

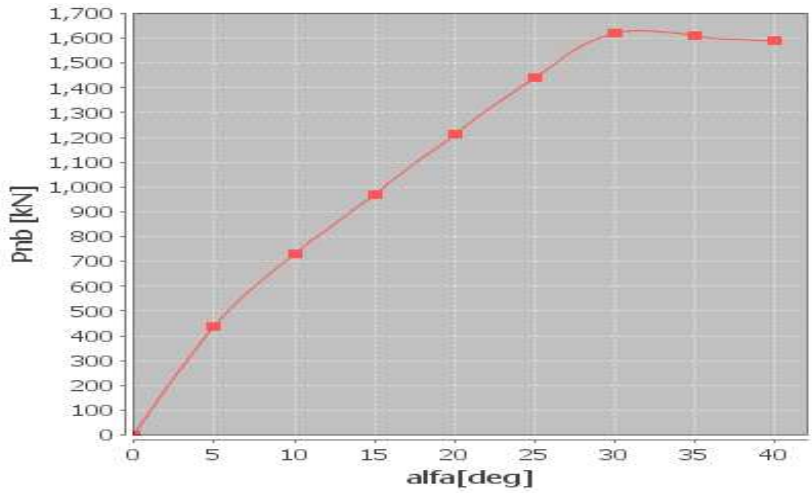

Figure 13.$\boldsymbol{P_{nb}}$ [kN] in astern ship motion

The form of the curve of normal hydrodynamic force P_{nb} on the rudder in astern ship motion is the same as the result in ahead ship motion, but the maximum force at angle α=30° is very small $P_{nb} = 1621.259\ kN$ comparing with one at ahead ship motion.

- <u>The Hydrodynamic torque M in ahead motion</u>

The hydrodynamic torque M towards the leading edge of the rudder iscalculated with relation:

$$M = 0.5 * C_m^* * \rho * {v^2}_R * A_R * \bar{c} \quad (28)$$

where:$C_m^*$is The corrected hydrodynamic torque (moment) coefficient and $\bar{c}$ is The mean chord of the rudder

The results of hydrodynamic torque M, in ahead ship motion, are presented in Table 20 and Figure 14.

Table 20.M [kN.m] in ahead ship motion

Alfa α [deg]	*M* [kN.m]
0	0.000
5	1512.734
10	3500.278
15	6006.727
20	8598.752
25	10668.537
30	12494.372
35	16168.599
40	16623.036

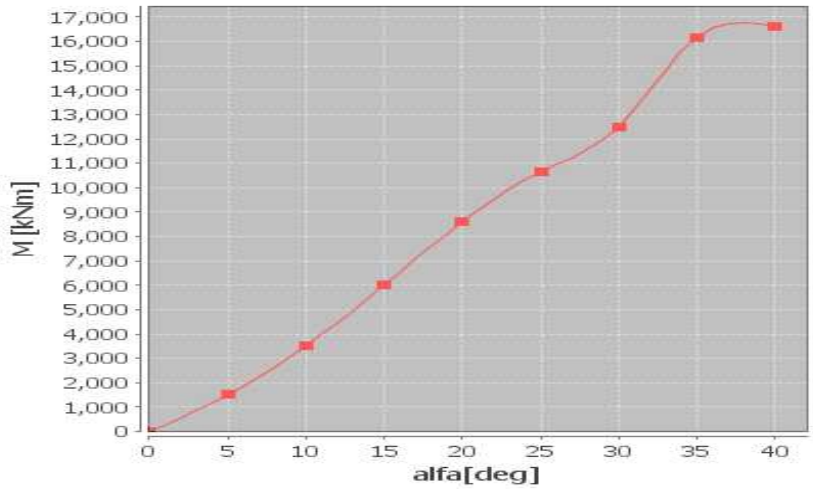

Figure 14.M [kN.m] in ahead ship motion

According to the results in Table 20 and Figure 14, the hydrodynamic torque M in ahead motion increase proportional with the angle α until the maximum $M = 16623.036\, kN.m$ at α=40°.

- The Hydrodynamic torque M_b in astern motion

The hydrodynamic torque M_b to the trailing edge of the rudder, in astern motion is determined using the relation:

$$M_b = 0.5 * C^*_{mb} * \rho * {v^2}_{Rb} * A_R * \bar{c} \tag{29}$$

and the results are presented in Table 21 and Figure 15:

Table 21.M_b [kN.m] in astern ship motion

Alfa α [deg]	M_b [kN.m]
0	0.000
5	-1953.035
10	-2922.304
15	-3818.918
20	-4522.269
25	-5225.506
30	-5879.380
35	-5653.020
40	-6085.071

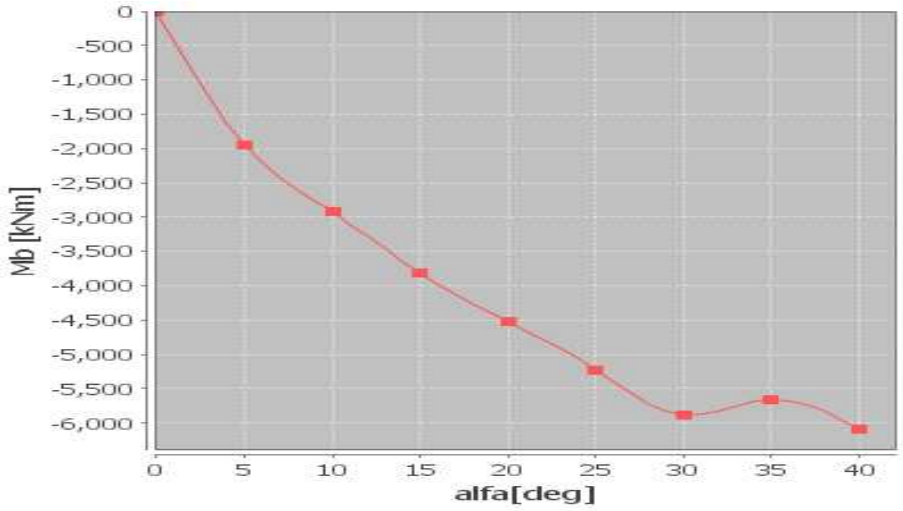

Figure 15.M_b [kN.m] in astern ship motion

The hydrodynamic torque M_b on the rudder in astern motion are decreasing in negative with the angle α, until the maximum $Mb = -6085.071\ kN.m$ at angle α=40°.

- The hydrodynamic torque to the rudder stockM_r in ahead ship motion

The hydrodynamic torque M_r to the rudder stock is compute with the relation:

$$M_r = P_n * (e - d_0) \quad (30)$$

whered_0 is the distance from rudder stock to the leading edge, e is the distance from the pressure centre to the leading edge.

Concerning in astern ship motion, the hydrodynamic torque to the trailing edge of the rudder M_b with the hydrodynamic force P_{nb} give the hydrodynamic torque to the rudder stock M_{rb} in astern motion, using the relation:

$$M_{rb} = \left(M_b - P_{nb} * d_f\right) * k_1 * k_2 \tag{31}$$

withd_f is the distance from the rudder stock to the trailing edge.

In order to determine the optimal distance from the rudder stock to the leading edge, $(d_0)_{optim}$, the calculation are performed for five values of the distance d_0 situated at 15% - 20% - 25% - 30% - 35% of the mean chord of the rudder $\bar{c}$, (d_0 = 1.296, 1.728, 2.160, 2.592, and 3.024 m) . The result of the hydrodynamic torque to the rudder stock is in function of the inflow angle α for these different distances of rudder stock see (Table 22) and (Fig. 16).

Table 22. The hydrodynamics torque $\boldsymbol{M_r}$for different $\boldsymbol{d_0}$

$\boldsymbol{d_0}$ (m)	1.296	1.728	2.160	2.592	3.024
$\boldsymbol{M_r}$[kN.m]	0.000	0.000	0.000	0.000	0.000
	-56.462	-579.528	-1102.593	-1625.659	-2148.724
	329.427	-727.523	-1784.473	-2841.423	-3898.373
	1280.109	-295.431	-1870.970	-3446.510	-5022.049
	2735.921	781.644	-1172.633	-3126.910	-5081.187
	3981.248	1752.151	-476.945	-2706.042	-4935.138
	5455.411	3109.090	762.770	-1583.551	-3929.871
	9267.203	6966.738	4666.272	2365.807	65.342
	9850.625	7593.155	5335.685	3078.215	820.745

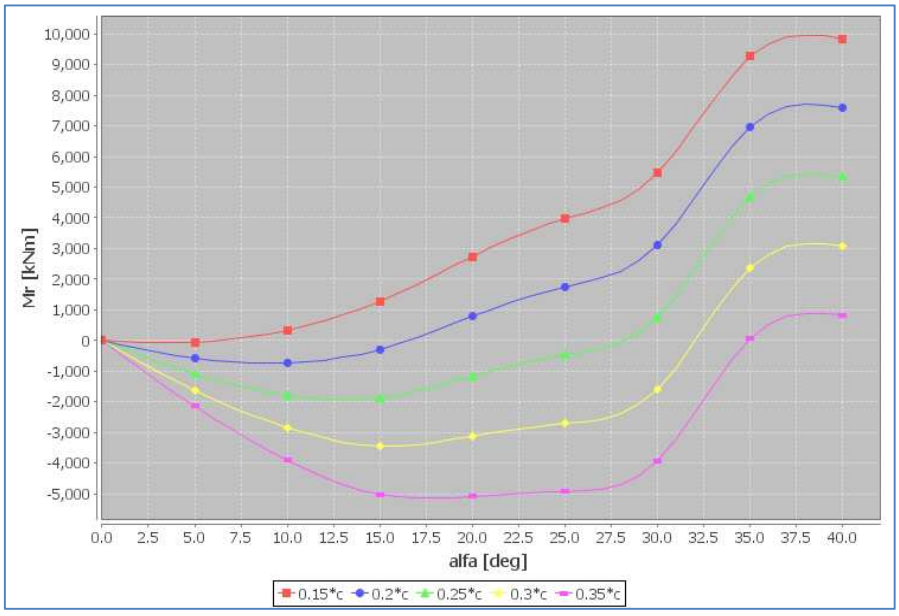

Figure 16. The hydrodynamics torque $\boldsymbol{M_r = f(\alpha)}$ for different $\boldsymbol{d_0}$

From Figure 16 and Table 22, we took the maximum and minimum of the hydrodynamic torque M_r to the rudder stock for each curve of the distance d_0 (1.296, 1.728, 2.160, 2.592, and 3.024 m). The results are presented in Table 23.

Table 23. $\boldsymbol{M_{r_{max}}}$, $\boldsymbol{-M_{r_{min}}}$ for different $\boldsymbol{d_0}$

	The maximum $M_{r_{max}}$ [kN.m]	The minimum $-M_{r_{min}}$ [kN.m]
d_0 = 1.296 m	9850.625	-56.462
d_0 = 1.728 m	7593.155	-727.523
d_0 = 2.160 m	5335.685	-1870.970
d_0 = 2.592 m	3078.215	-3446.510
d_0 = 3.024 m	820.745	-5081.187

In order to determine the optimal position of the rudder stock so that the torque on the stock is minimal, the linear function of the maximum $M_{r_{max}}$ and minimum $-M_{r_{min}}$ of the hydrodynamic torque to the rudder stock are presented in function of the distance of the rudder stock d_0 [m] graphically in Figure 17

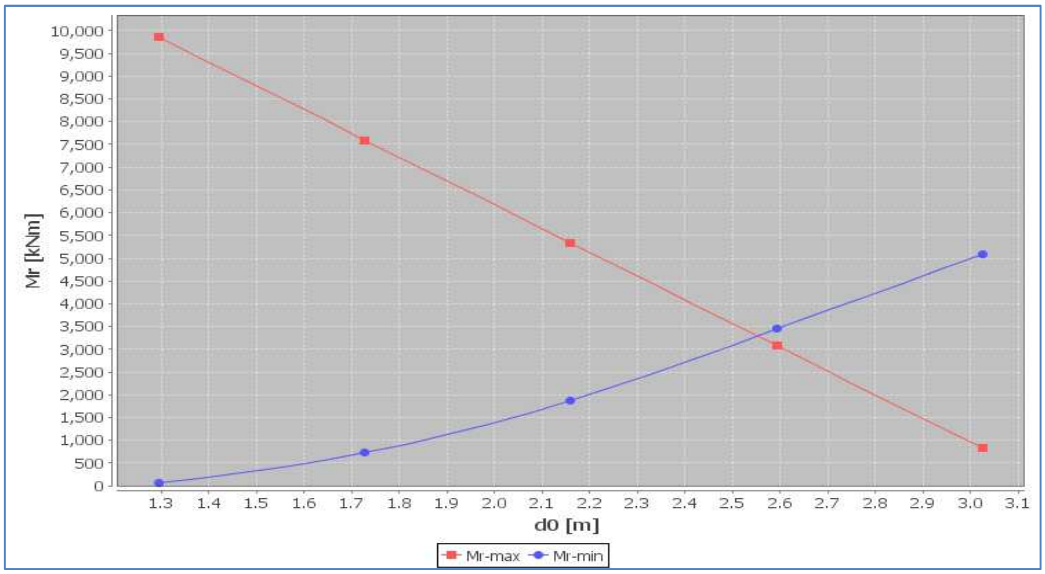

Figure 17. $\boldsymbol{M_{r_{max}}}$, $\boldsymbol{-M_{r_{min}}}$ Curves of in function of $\boldsymbol{d_0}$

According to this Figure 17, the two lines - the maximum $M_{r_{max}}$ and the minimum $-M_{r_{min}}$ they intersect in the optimal point, where the projection gives $\boldsymbol{d_0 = 2.55\ m.}$

Knowing the optimal value of the distance from the rudder stock to the leading edge $(d_0)_{optim}$, the optimum hydrodynamic torque to rudder stock is calculated for ahead ship speed, by means of:

$$(M_r)_{optim} = k_1 * k_2 * P_n * |e - (d_0)_{optim}| \quad (32)$$

wherek_1=1.2 is the safety coefficient for overloads, and k_2 =1.2 is the stock safety coefficient.

The final results of the optimum hydrodynamic torque on the rudder stock and the optimum of the position of rudder stock in ahead ship motion and in astern ship motion are presented in Table 24.

Table 24. Optimum results in ahead and in stern ship motion

Ahead ship motion	
Optimal distance from the rudder stock to the leading edge $(d_0)_{optim}$	2.550 m
Optimal hydrodynamic torque to the rudder stock $(M_r)_{optim}$	4744.979 kN.m
Astern ship motion	
Optimal distance from the rudder stock to the trailing edge $(d_f)_{optim}$	-6.090 m
Optimal hydrodynamic torque to the rudder stock $(M_{rb})_{optim}$	5173.003 kN.m

However the selection of the steering gear depends on the total hydrodynamic torque, which is the sum of the maximum hydrodynamic torque with the supplementary torque due to friction (see Table 25).

The maximum hydrodynamic torque is the comparison of the two optimal hydrodynamic torque to the rudder stock in ahead ship motion and in astern ship motion, where the hydrodynamic torque in astern motion is the maximum.

The torque friction is among the rudder shaft. In an initial approximation, it may be considered that the friction moment may be equal to 20% of the value of the hydrodynamic moment.

Table 25. Hydrodynamic torque of the rudder

Maximum hydrodynamic torque	**5173.003 kN.m**
Supplementary torque due to friction	1034.601 kN.m
Total hydrodynamic torque	6207.603 kN.m

Basing on the total hydrodynamic torque we select in the commercial catalogue from manufacturers of steering gear. The steering gear selected was Kawasaki E Series TYPE FE32 see (Figure. 18) and the particulars of this steering gear are presented in Table 26.

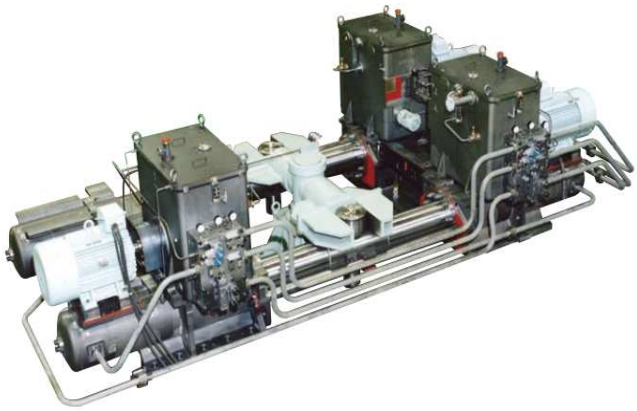

Figure 18. Steering gear Kawasaki E Series TYPE FE32

Table 26. Main Particulars of Kawasaki E Series TYPE FE32

Kawasaki E Series TYPE FE 32	
Torque at max working	6720 kN * m
Rudder turning angle	70°
Rudder turning speed	65/28 °/s
Normal radius of tiller arm	1015 mm
Ram diameter	375 mm

The main dimensions are shown in Table 27 and Figure 19.

Table 27. Dimension of Kawasaki E Series TYPE FE32

A	3920 mm
B	1580 mm
C	375 mm
D	2100 mm
E	2100 mm

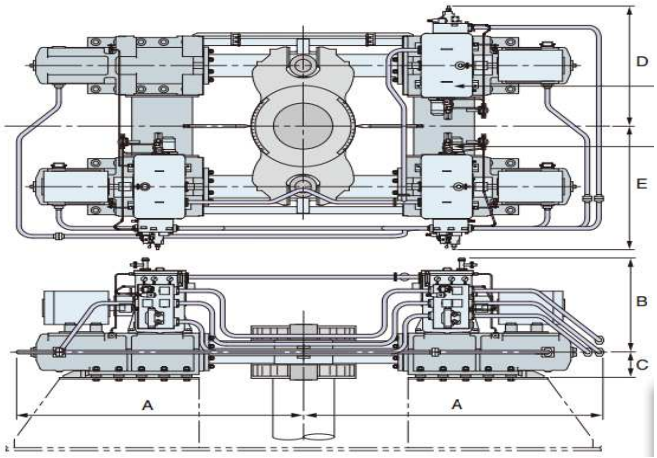

Figure 19. Dimensions of Kawasaki E Series TYPE FE32

2.3.4 Turning circle manoeuvre characteristics

The turning circle manoeuvre of KVLCC2 is performed to starboard with 35° rudder angle as the maximum rudder angle permissible at the design speed (15.5 knots), where the input data are showed in Table 28.

Table 28. Summary of turning circle

Ship name	KVLCC2	
Loading Condition	New	
Approach Speed	15.500	knots
Rudder Command Angle	35.000	deg.
Water depth	Deep	

The rudder angle is executed following a steady approach with zero yaw rate. The essential information obtained from this manoeuvre, tactical diameter, advance, and transfer (Figure20) are given in a non-dimensional form, to compare with IMO criteria (see Table 29). The most important characteristics of the turning circle are presented in Figure 21 and the turning trajectory is depicted in Figure 22.

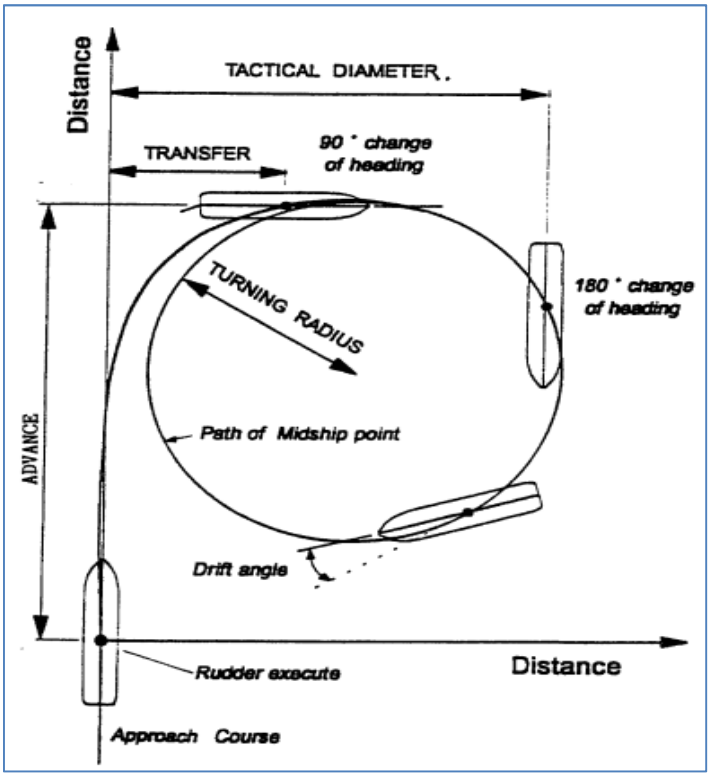

Figure 20.Definition of Turning Circle test [5]

Table 29. The output of turning circle manoeuvre

		TRIBON M3	IMO Criteria
ADVANCE/L	AT 90 DEG	3.32	4.5
TRANSFER/L	AT 90 DEG	1.80	-
MAX TACTICAL DIAM/L		3.88	5
STEADY TURNING DIAM/L		2.25	-
SPEED/APR. SPEED	AT 360 DEGS	0.31	-

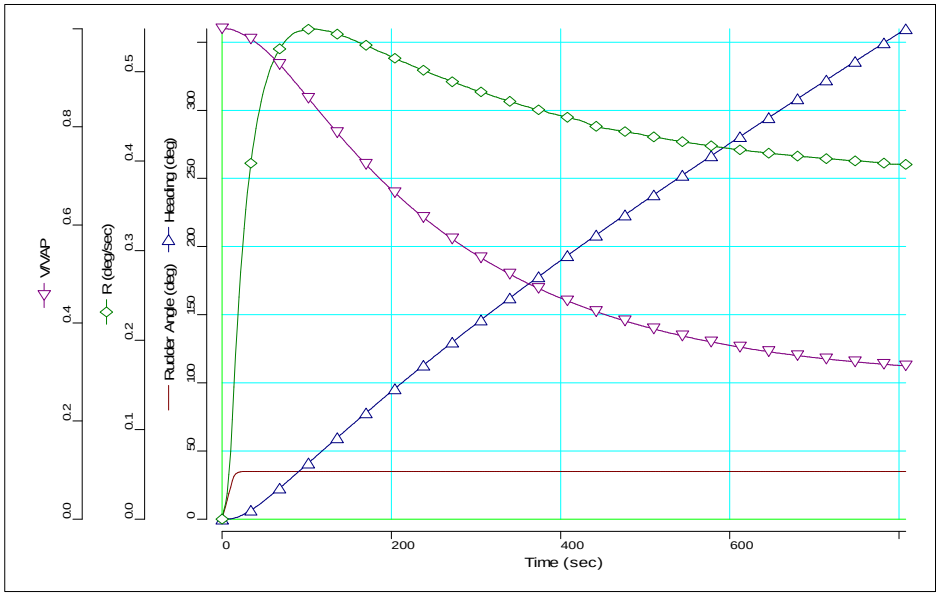

Figure 21.Turning characteristics of the KVLCC2

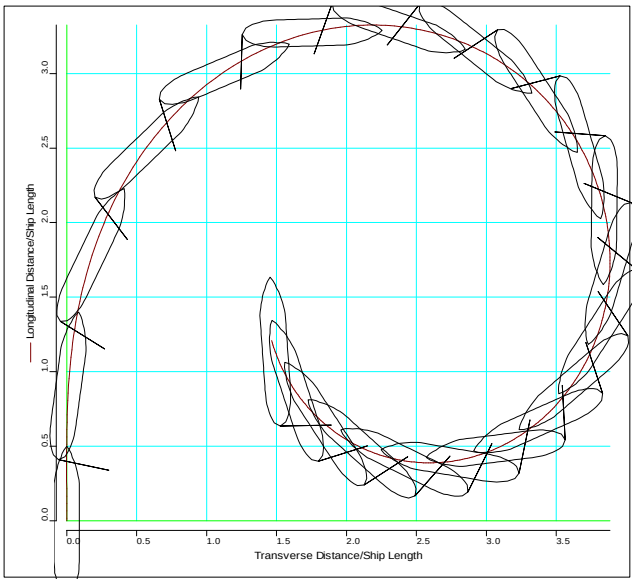

Figure 22.Turning trajectory of the KVLCC2

It can be observed from Table 28 and the Figure 20 that the results obtained are lower than the maximum values from IMO criteria requirement. So the KVLCC2 ship has good course keeping ability.

2.3.5 Zig-Zag manoeuvre characteristics

A zig-zag test should be initiated to starboard and begins by applying a 10° rudder angle to an initially straight approach ("first execute"). The rudder angle is then alternately shifted to either side (port) after a specified deviation from the ship's original heading is reached 10° ("second execute" and following) (see Figure 23).

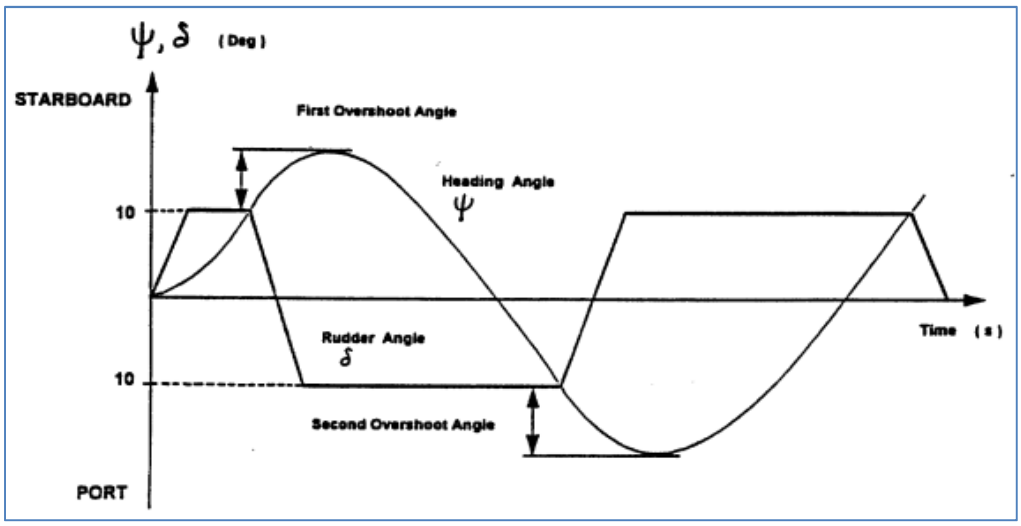

Figure 23. Definition of Zig-Zag test [5]

The essential information to be obtained from these tests is the overshoot angles, initial turning time to second execute and the time to check yaw. The input data are showed in Table 30.

Table 30. Input data of Zig-Zag (10°/10°) of KVLCC2

Ship name	KVLCC2	
Loading Condition	New	
Approach Speed	15.500	knots
Rudder Command Angle	10.000	deg.
Heading Check Angle	10.000	deg.
Water depth	Deep	

The result of the zig-zag (10°/10°) test is showed in Table 31 and is compared with the IMO criteria requirement.

The IMO criteria are specified for Zig-Zag (10°/10°) at first overshoot angle and second overshoot angle, depending on the value of L/V, where L [m] is the length between perpendicular and V [m/s] is the design ship speed. The value is as follow:

$$\frac{L}{V} = \frac{320}{15.5 * 0.5144} = 40.13\ sec$$

Table 31. The output results of Zig-Zag manoeuvre

	TRIBON M3	IMO Criteria	
1ST OVERSHOOT ANGLE	5.43	< 20	DEG
2ND OVERSHOOT ANGLE	7.23	< 40	DEG
PERIOD	388.00	-	SEC
INITIAL TURNING TIME	70.00	-	SEC

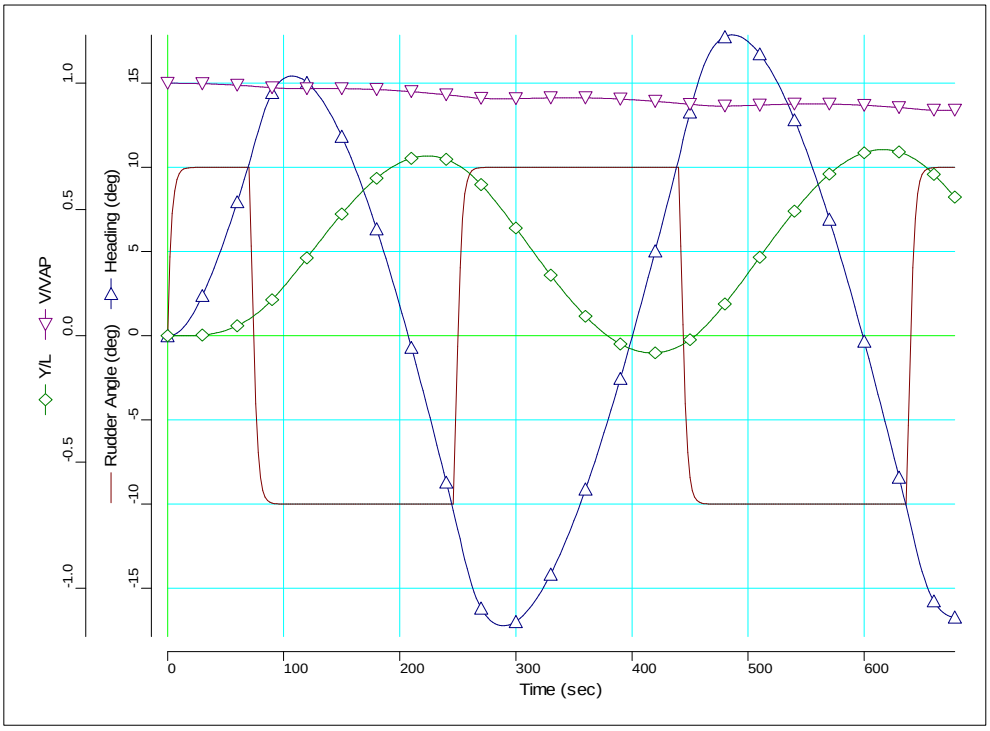

Figure 24. Zig-Zag (10°/10°) characteristics of the KVLCC2

2.3.6 Spiral manoeuvre characteristics

The spiral manoeuvre is performed to provide and to check the directional stability of the KVLCC2 ship. Where the yaw rate is versus rudder angle relationship, it has been carried out for starboard and port sides in function of rudder angles from Figure 25.

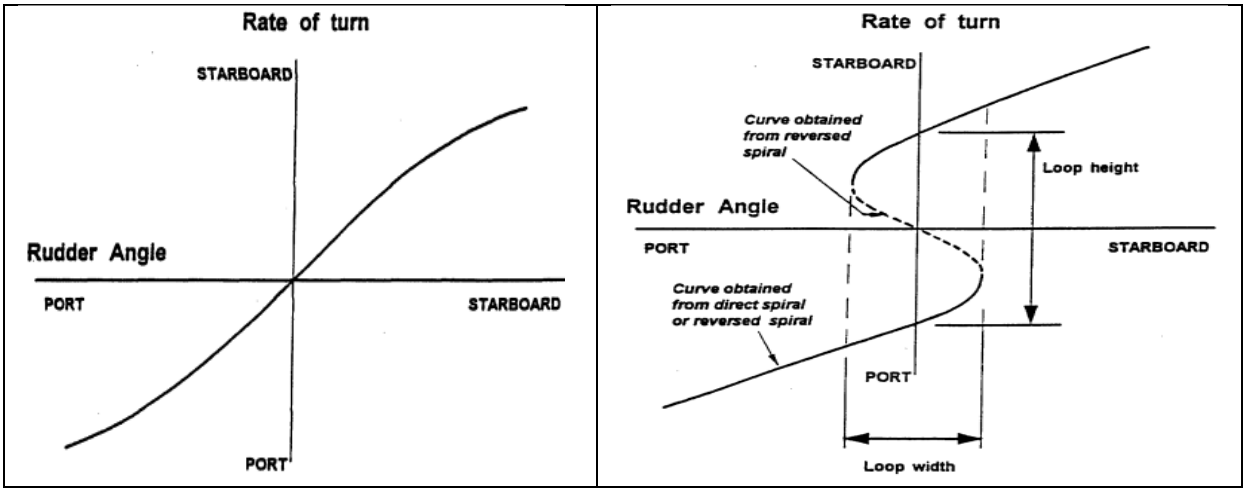

Figure 25. Definition of spiral test [5]

In spiral test, the ship is steered to obtain a constant yaw rate and the mean rudder angle required to produce this yaw rate is measured. The rudder is deflected to about 35° starboard and held until the rate of change of heading is constant. The rudder angle is then decreased by 5° and again held until steady conditions of turning have been obtained, until 10° of rudder angle. After 10° the rudder angle is decreasing with small angles until 0°, to start doing the same to the port by increasing the rudder angle. The input data of the spiral test are presented in Table 32.

Table 32. Summary the Reverse spiral of KVLCC2

Ship name	KVLCC2	
Loading Condition	New	
Approach Speed	15.500	[knots]
Water depth	Deep	

The evolution of the yaw rate in function of the rudder angle, in dimensional form, was obtained and presented in Table 33 and Figure26 the red curve.

Table 33. Output result (dimensional) of Spiral manoeuvre

STARBORD		**PORT**	
Rudder Angle [deg]	Yaw Rate [deg/sec]	Rudder Angle [deg]	Yaw Rate [deg/sec]
0.00	0.00	0.00	0.00
1.16	0.06	-1.18	-0.06
2.69	0.12	-2.80	-0.13
4.66	0.18	-4.82	-0.19
7.14	0.24	-7.29	-0.25
10.20	0.29	-10.35	-0.30
15.00	0.34	-15.00	-0.35
20.00	0.37	-20.00	-0.38
25.00	0.39	-25.00	-0.40
30.00	0.39	-30.00	-0.40
35.00	0.40	-35.00	-0.40

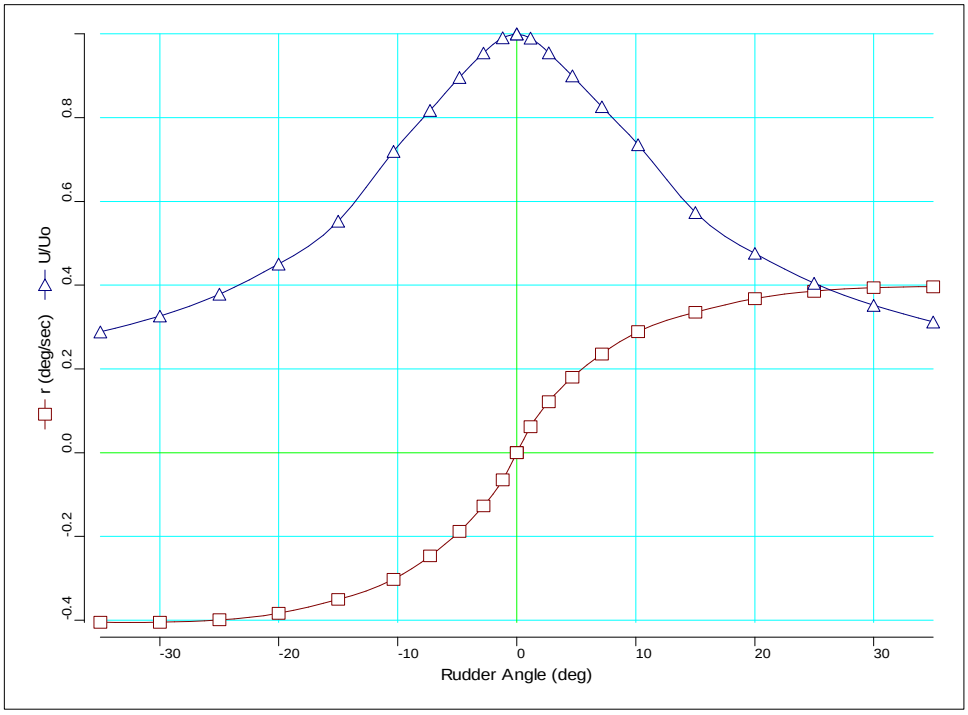

Figure 26 (Dimensional) Spiral manoeuvre of KVLCC2

According to the Figure 26, because of the red curve is without hysteresis domain, the KVLCC2 ship will be stable on route.

3. CFD ANALYSIS OF THE FLOW AROUND THE KVLCC2 HULL

3.1 CFD – SHIPFLOW

The CFD analysis of the flow around the KVLCC2 hull has been employed todetermine the ship hydrodynamic performances. The simulations have been performed using the software FLOWTHECH SHIPFLOW v5.0. This software is specialized for naval applications. In order to analyze the flow around the hull, two approaches have been designed in this software. These approaches are Global approach and Zonal approach. The simulation in this work was based on a Global approach. In order to run SHIPFLOW code needs two files, offset and command (see Figure 27).

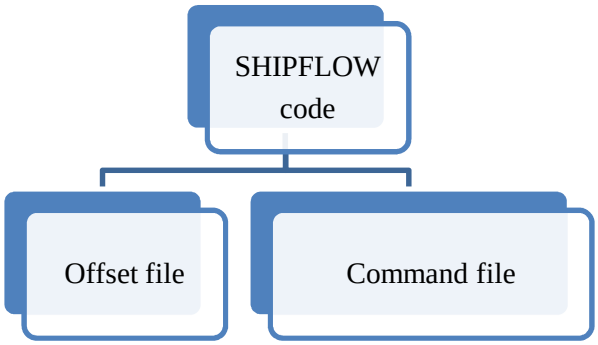

Figure 27. Workflow of SHIPFLOW

a. <u>The offset file</u>

The purpose of the offset file is to describe the geometry of the hull. This is done by a list of coordinate values of points lying on the hull surface. A point is defined by its x, y and z coordinates. A station is a set of points that describe the intersection between the hull and a constant x plane. A group describes the shape of a part of the hull. Typically one group is used to describe the main part of the hull, the bulb, the keel or the bossing. One or more groups can be used to describe the main part of the hull. Label name of an offset group used to identify the group. In the same manner, every point has a status flag that tells the program how to treat the point (firs point of station, point that belongs to the station or end point of the group).

The stations have been generated by sectioning the hull surface with x constant planes. Sections on the hull surface from bow to stern have been created. Each section has been discretized by 70 points ordered from keel to deck. A hull can be divided into several groups. A hull can be divided into several groups. For KVLCC2 hull four groups has been created as follows (see Figure 28):

- Hull is H1GR group
- Bulb is FBGR group
- Overhang is OGRP group
- Bulbstern is ABGR group

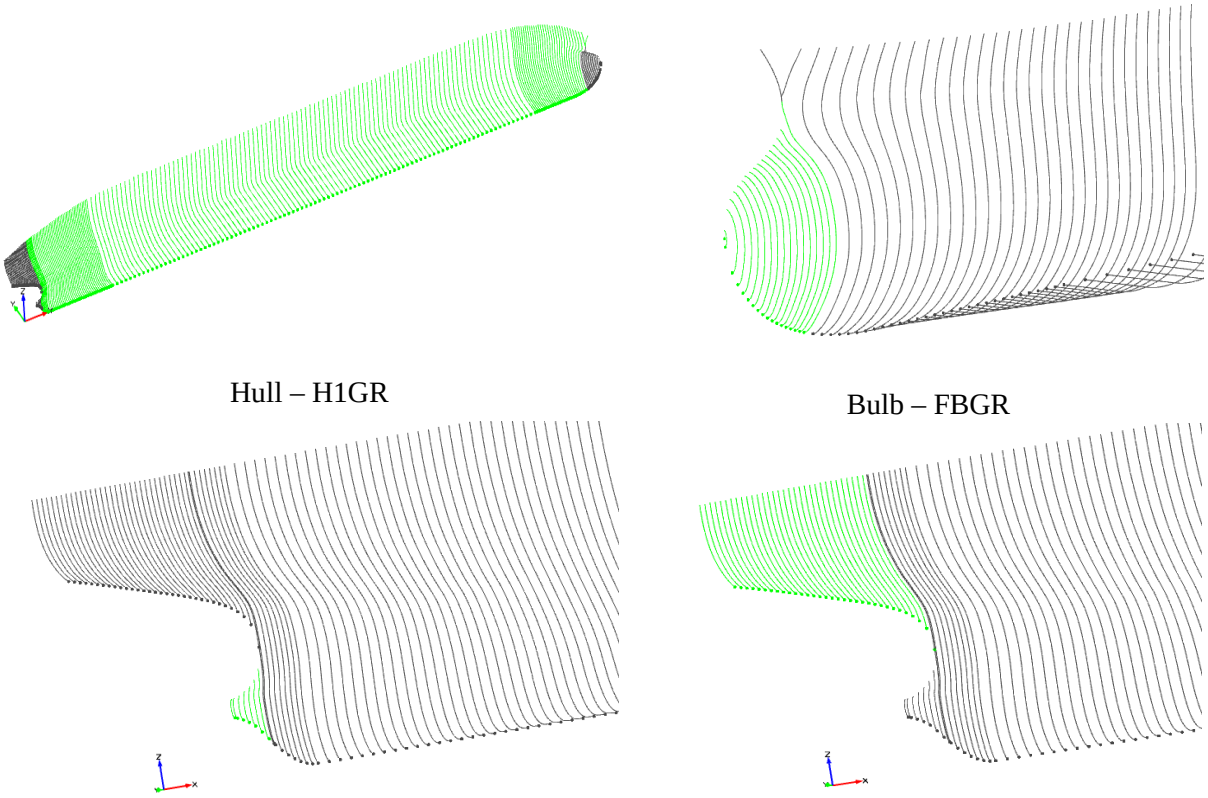

Hull – H1GR

Bulb – FBGR

Bulbstern – ABGR

Overhang – OGRP

Figure 28. The groups in the Offset file

b. <u>The command file</u>

The command file is used to instruct the code how to run different modules and, on the other hand, to define the general physical properties of the problem: initial ship position and speed, onset flow, hull type, propeller geometry, fluid characteristics and symmetry. It contains:

- The title
- Information of what modules (programs) should be execute
- Name of the offset file and the definition of the coordinate system used in the offset file
- Definition of the groups in the offset file
- Ship speed, length scale and type of hull

The command file is used to run SHIPFLOW by means of Notepad++.

The CFD process is divided in three steps (see Table 34): pre-processing, processing and post-processing. For the pre-processing XMESH and XGRID modules have been used. XPAN, XBOUND and XCHAP modules have been employed for the processing and Tecplot to visualize the output files.

Table 34. The SHIPFLOW process

PRE-PROCESSING	PROCESSING			POST-PROCESSING
	Potential Flow	Boundary Layer Theory	Navier-Stokes	
XMESH XGRID	XPAN	XBOUND	XCHAP	Tecplot Spost

The methods and modules used to compute the Resistance and Manoeuvring performances are presented in Figure 29. First, a combination of the potential flow based on Rankine source method and boundary layer method for viscous effects is used for a set of preliminary computations in order to investigate the flow around bare hull. In order to perform preliminary ship resistance computations three modules have been used:

- XMESH is the panel generator for the potential flow module XPAN
- XPAN is the potential flow solver. It solves the flow around three dimensional bodies using surface singularity panel method and using the mesh generated by XMESH with free surface flows using non-linear free surface boundary condition.
- XBOUND is flow solver (processing), a program for thin turbulent boundary layer computations and it also capable to compute the laminar and transition boundary layer.

In the present work, the viscous flow methods have been used in order to determine the hydrodynamic forces on hull and on rudder for different cases of drift and rudder angle. Therefore, an understanding of the flow around the stern part of ship is of great practical interest. Viscous flow theory used in the thesis computes the solution using Reynolds Averaged Navier Stokes equations solver (RANS hereafter). The solver computes the incompressible RANS equations on structured overlapping grids using finite volume method formulation, involving EASM turbulence model. The RANS computation does not include the propeller effect. RANS method has been used to compute the forces acting on ship hull and rudder by simulating the oblique flow with static drift and rudder- static drift. The computations have been performed by means of two models:

- XGRID is pre-processing module who generates the grid used for the viscous computations in XCHAP
- XCHAP is the viscous flow method. It was executed to solve the Reynolds Averaged Navier-Stokes (RANS) equations based on finite volume code. Uses different

turbulence models (EASM, k-ω BSL, k-ω SST). This solver was used in a global approach

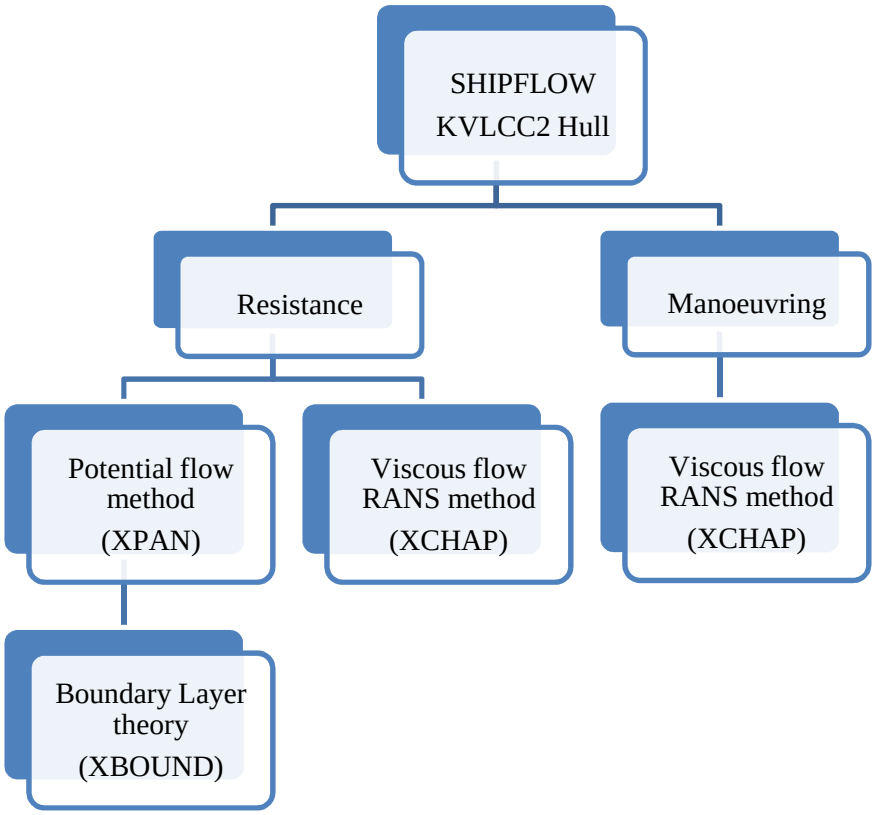

Figure 29. Workflow of resistance and manoeuvring of KVLCC2 in SHIPFLOW

3.2 Potential Flow

3.2.1 Mathematical model

Assumption is made that the ship hull advances in the undisturbed water with a constant velocity U_∞. The potential flow assumption of inviscid and irrotational flow is made for the steady flow around the hull. Equation field and boundary conditions are expressed in terms of velocity potential. The problem is numerically solved making use of distribution of Rankine sources on the boundary surface. Potential flow theory determines wave resistance component of the total resistance and it is based on integration of the pressure acting on the ship hull when it is moving through the water. The ship is specified in a coordinate system having its x-axis parallel to the longitudinal direction, the y-axis to the direction of starboard and the z-axis pointing upwards. Considering that the flow is inviscid, which means that the fluid is frictionless and it is irrotational, the governing equation of the flow is continuity equation. The incompressibility of the fluid is generally assumed in all physical modelling of

phenomena in which fluid is water. Moreover, when the flow is steady the pressure does not depend on time and it is constant so its derivative with respect to time is removed. The continuity equation becomes:

$$\frac{\partial u}{\partial x}+\frac{\partial v}{\partial y}+\frac{\partial w}{\partial z}=0 \tag{33}$$

From mathematical point of view, if the flow is inviscid, irrotational, and incompressible, a scalar function named the velocity potential ϕ can be defined. Thus, velocity vector can be expressed as a gradient of velocity potential:

$$u=\frac{\partial \phi}{\partial x} v=\frac{\partial \phi}{\partial y} w=\frac{\partial \phi}{\partial z} \text{ or } \mathbf{V}=\nabla \phi \tag{34}$$

In the end, by introducing the velocity (34) into the continuity equation (33) the Laplace equation is obtained:

$$\frac{\partial^2 \phi}{\partial \mathrm{x}^2}+\frac{\partial^2 \phi}{\partial \mathrm{y}^2}+\frac{\partial^2 \phi}{\partial \mathrm{z}^2}=0 \text{ or } \nabla^2 \phi=0 \tag{35}$$

Laplace equation is linear and solutions can be superimposed. The Panel Method described in [8]is used for finding solutions to the Laplace equation.

Bernoulli equation shows that pressure, kinetic energy and, potential energy must be constant along streamline.

$$\rho+\frac{\rho u^2}{2}+\rho g h=C \tag{36}$$

One can consider the total velocity potential as a sum of double model velocity potential and the perturbation velocity potential due to presence of free surface:

$$\phi=\phi_0+\phi_w \tag{37}$$

Boundary Conditions for Potential Flow Method

Boundary conditions on the hull

The velocity potential is subject to the several conditions on the hull and free-surface boundaries. First boundary condition imposed on the hull surface requires that no fluid particle penetrate the hull surface:

$$\frac{\partial \phi}{\partial n}=0 \tag{38}$$

Upstream disturbance by a moving ship vanishes at infinity:

$$\lim_{r \to \infty} \nabla \phi=U \tag{39}$$

Boundary conditions on the free surface

Kinematic boundary condition is the mathematical formulation of the physical condition that a particle at the surface should remain at the surface all the time and it can be expressed as:

$$\frac{\partial \phi}{\partial x}\frac{\partial h}{\partial x}+\frac{\partial \phi}{\partial y}\frac{\partial h}{\partial y}-\frac{\partial \phi}{\partial z}=0 \tag{40}$$

The other condition to be satisfied on the free surface comes from the fact that the pressure on the free surface must be equal to the atmospheric pressure, which we assume that is constant. This condition is derived from Bernoulli equation

$$h+0.5(\left(\frac{\partial \phi}{\partial x}\right)^2+\left(\frac{\partial \phi}{\partial y}\right)^2+\left(\frac{\partial \phi}{\partial z}\right)^2-U_\infty{}^2=0 \tag{41}$$

Upstream disturbance by a moving ship vanishes at infinity:

$$\lim_{r\to\infty}|\nabla\phi|=0 \tag{42}$$

Finally, the radiation condition must be imposed (enforced) to avoid upstream waves. The radiation condition cannot be described by an exact mathematical expression, which means that it has to be enforced by numerical schemes.

In the end, forces an moments, including wave resistance are computed by integrating pressure over the ship hull as follow:

$$Rw=-\iint_S \rho n_x dS \qquad T=\iint_S \rho n_z dS \qquad MT=\iint_S \rho n_z (x-x_0)dS \tag{43}$$

Limitations are in wave breaking, forming sprays as well as viscous interaction on wave making. All theoretical mathematic derivations have been referenced from [8], [9]. Boundary layer theory is used to assist potential flow with computing friction coefficient to compute the total resistance. It has capabilities of simulating streamlines as well as limiting streamlines (show the flow direction at the hull surface) and calculation with free surface. Method is accurate over main part of the hull and captures transition from laminar to turbulent flow. The theory usually fails to compute complicated flows such as regions around stern of the ship. In the aft part, usually there are developed turbulent phenomena, which cannot be captured by this methodology. More theoretical methodology about boundary layer theory can be found[10].

3.2.2 Panelization

The panelization has been done by XMESH module for ship hull and free surface. The calculation are done for surface domain of 0.75 ship length upstream, 2.5 ship length downstream, the width of the free surface is 0.7 ship length (see Figure 30).

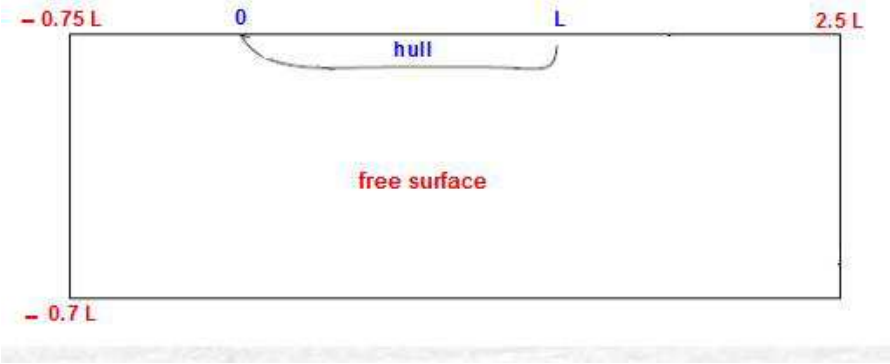

Figure 30. Domain of computation in Potential flow

The panelization of the hull surface was done with BODY command. This is used to specify the panels. The number of panels depends on the curvature of hull surface and to use stretching function towards regions of the high curvature at the bow and the stern of hull. Stretch function number 5 it was applied for stations in Hull group (see Figure 31). The stretching function options are: 0 – uniform distribution; 1 – hyberbolic tangent stretching, one end specified; 2 – exponential stretching, one end specified; 3 – hyberbolic sine stretching, one end specified; 4 – geometric stretching, one end specified; 5 – hyperbolic tangent stretching with spacing specified at two ends.

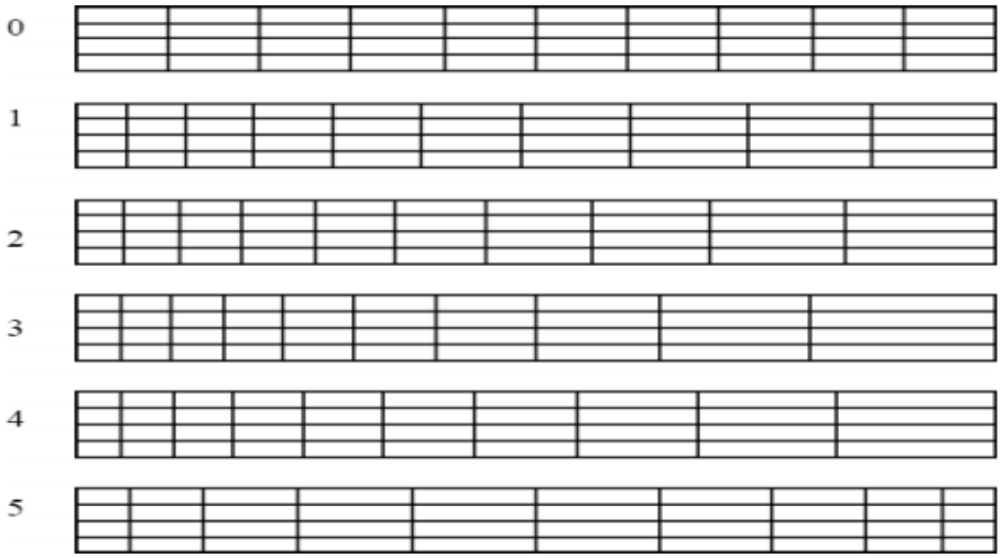

Figure 31. Different stretch function for stations or points

The panels on the hull surface were created by stations and points for each offset group (Hull, Bulb, Bulb stern and Overhang) as shown in the Table 35. The hull is discretized using 2858 panels. The hull panelization has been shown in Figure 32.

Table 35.Panelization of body

	Stations	Points
Hull	100	25
Bulb	8	22
Bulbstern	5	8
Overhang	10	14

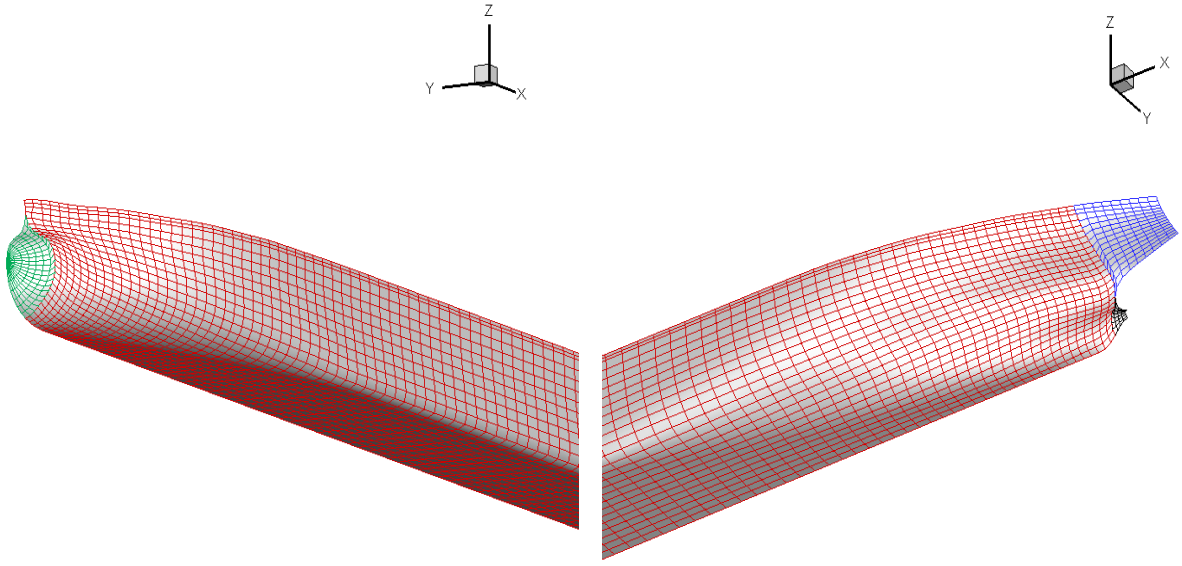

Figure 32.Panelization of Body

The panelization of free surface it was executed by FREE command to specify panels on the free surface. Experience with the method shown that a minimum of 25-30 panels per unit length are necessary to obtain a solution which gives a good representation of wave pattern. Moreover, stretching functions must be also used for cluster the panels towards the regions where it is expected to develop wave crests. The numbers of panels on the free surface are determined by the Froude number and domain dimensions. Considering the computational time and the accuracy of the solution, 25 panels has been chosen for transversal directions. The total number of panels in free surface and body (hull) is equal to 15314. The free surface panelization is presented in Figure 33.

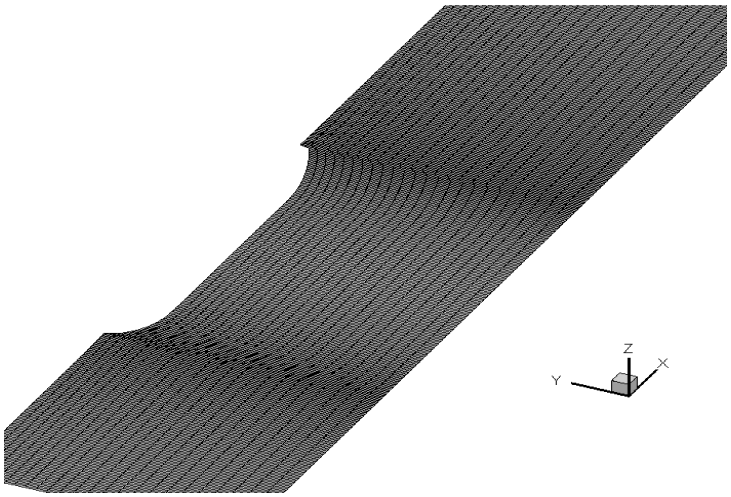

Figure 33.Free Surface panelization

3.2.3 Potential Flow Computation

Potential flow method (XPAN) and Boundary layer theory (XBOUND) has been employed to simulate free-surface flow around the KVLCC2 bare hull model. The scale of the model has been chosen 1:58 for validation purposes. In this case the following dimensions were used:$L_{pp} = 5.5172\ m$and$T = 0.3586\ m$where, L_{pp} is the length between perpendicular and T is the model draft. Numerical results obtained have been compared with experimental data by MOERI [1] for a range of speed from 0.743 to 1.0807 m/s, which corresponds to Fn between 0.101 and 0.147. The model speed of 1.047 m/s corresponds to the full scale ship speed of 15.5 Kn. A set of 8 non-linear free-surface computation has been carry out in order to investigate the flow around KVLCC model and also to determine the ship resistance coefficients as skin friction coefficient, C_F and wave cut resistance coefficient, C_{WTCW}. was computed by mean of boundary layer momentum integral method along streamlines of the hull traced from a potential flow computation. C_{WTWC} was computed from transverse wave cuts by analyzing the wave patterns. The wave cut method approximates the wave elevation in each wave cut by the sum of a series of elemental waves. With the first requirement is to respect the location of the wave cuts in region where the wave pattern is relatively smooth (first wave cut not to be too close to the stern) and second requirement is that wave cuts cover at least one in wavelength[11]. The computed results are presented in Table 36.

Table 36. Resistance coefficients in Potential flow

V (m/s)	Fn	C_F	C_{WTWC}
0.743	0.101	3.57E-03	4.01E-06
0.8105	0.110	3.52E-03	9.17E-06
0.8781	0.119	3.47E-03	1.50E-05
0.9456	0.129	3.42E-03	2.60E-05
0.9794	0.133	3.40E-03	2.99E-05
1.0132	0.138	3.38E-03	3.85E-05
1.0469	0.142	3.36E-03	4.42E-05
1.0807	0.147	3.34E-03	5.55E-05

The resistance coefficients obtained by computing the flow around KVLCC hull are compared with the experimental results obtained from MOERI. The comparison is done for wave resistance coefficient, friction resistance coefficient and the total resistance coefficient.

a. ***Wave resistance coefficient***

The numerical transverse wave cut resistance coefficient C_{WTWC} is compared with the experimental wave resistance coefficient (see Figure 34 and Table 37). Significant differences may be observed.

Table 37. Comparison the wave cutC_{WTWC} with the experimentC_W

Fn	Cwwavecut (Potential)	CwExp	Error(%)
0.101	4.01E-06	1.59E-05	-74.80%
0.110	9.17E-06	3.63E-05	-74.72%
0.119	1.50E-05	5.73E-05	-73.84%
0.129	2.60E-05	7.18E-05	-63.80%
0.133	2.99E-05	8.15E-05	-63.29%
0.138	3.85E-05	9.02E-05	-57.37%
0.142	4.42E-05	9.88E-05	-55.23%
0.147	5.55E-05	1.10E-04	-49.63%

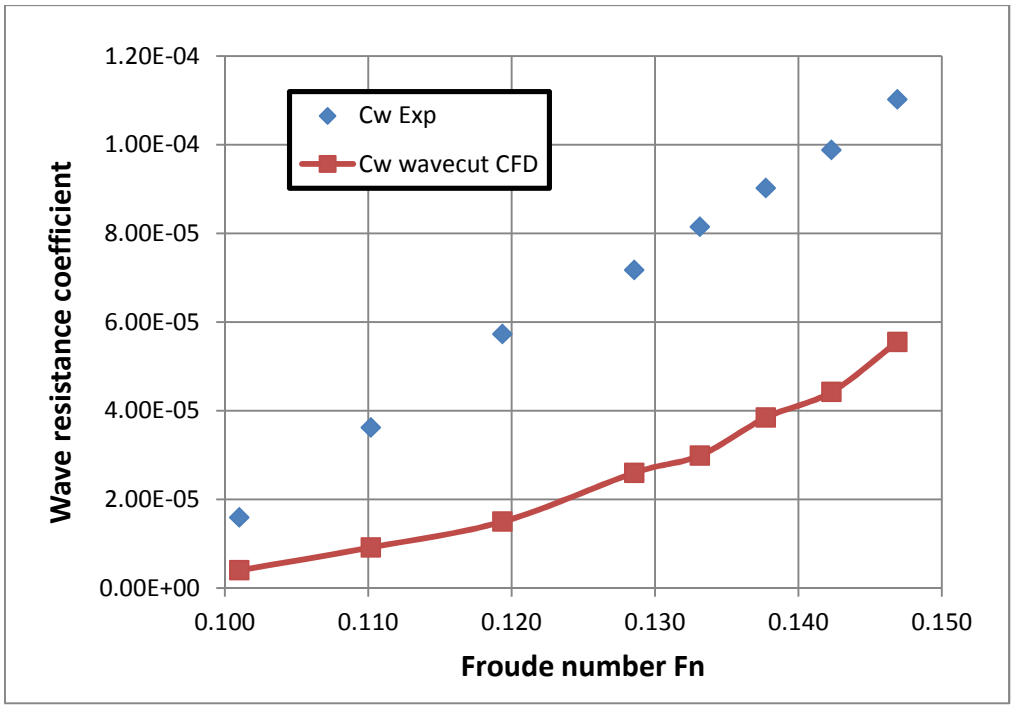

Figure 34. Comparison the wave cut C_{WTWC} with the experiment C_W

b. Frictional resistance coefficient

The skin friction resistance coefficient computed with boundary layer theory is compared with the friction resistance coefficient determined by ITTC 1957. The results presented in Table 38 and Figure 35 shown a good agreement between skin friction resistance coefficient computed be boundary layer theory and one computed by ITTC 1957 formula.

Table 38. Comparison of C_F (ITTC1957) and C_F (Boundary layer)

Fn	C_F Boundary layer	C_F (ITTC 1957)	Error (%)
0.101	3.57E-03	3.52E-03	1.28%
0.110	3.52E-03	3.47E-03	1.44%
0.119	3.47E-03	3.42E-03	1.59%
0.129	3.42E-03	3.37E-03	1.57%
0.133	3.40E-03	3.35E-03	1.57%
0.138	3.38E-03	3.33E-03	1.66%
0.142	3.36E-03	3.31E-03	1.64%
0.147	3.34E-03	3.29E-03	1.59%

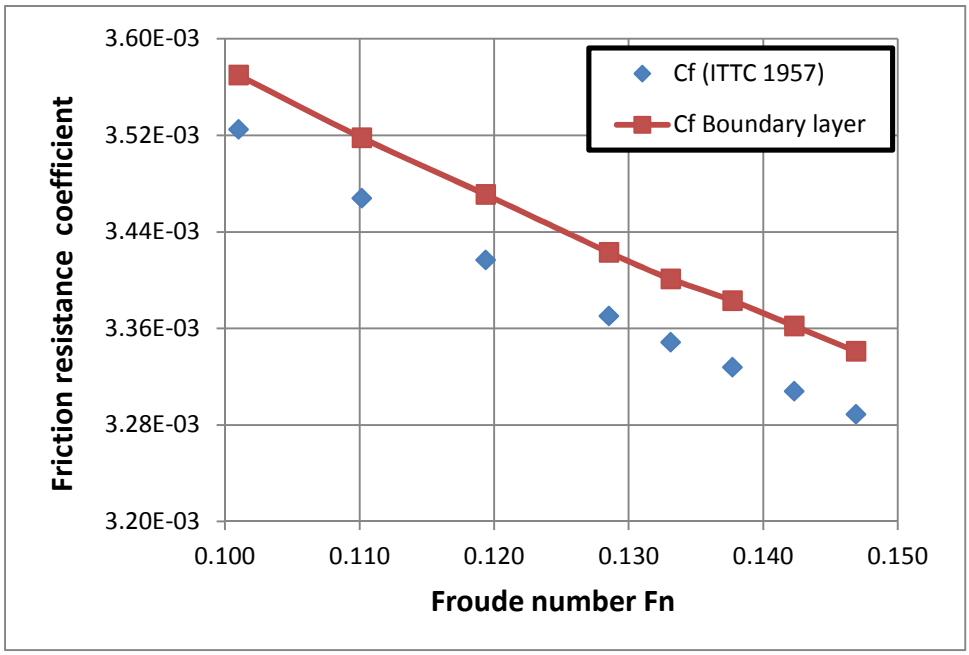

Figure 35. Comparison of C_F (ITTC1957) and C_F (Boundary layer)

c. *Total resistance coefficient*

The total resistance coefficient from MOERI experiment is compared with the total resistance coefficient of the potential flow, which was calculated by the following relation:

$$C_T = (1+k)_{Hughes-Prohaska} * C_F + C_{WTWC} \quad (44)$$

where (1+k) is 1.2135 and C_F is computed by boundary layer theory.

The results of comparison are presented in Table 39 and plotted in Figure 36, function of Froude number. The experimental and potential (SHIPFLOW) values of the total resistance coefficient decrease proportional with the increasing of Froude number. A satisfactory correlation between numerical and experimental results may be observe.

Table 39. Comparison of C_T Potential and C_T Exp

Fn	C_T Potential	C_T Exp	Error (%)
0.101	4.34E-03	4.29E-03	1.00%
0.110	4.28E-03	4.24E-03	0.79%
0.119	4.23E-03	4.20E-03	0.56%
0.129	4.18E-03	4.16E-03	0.44%
0.133	4.16E-03	4.14E-03	0.29%
0.138	4.14E-03	4.13E-03	0.37%
0.142	4.12E-03	4.11E-03	0.27%
0.147	4.11E-03	4.10E-03	0.21%

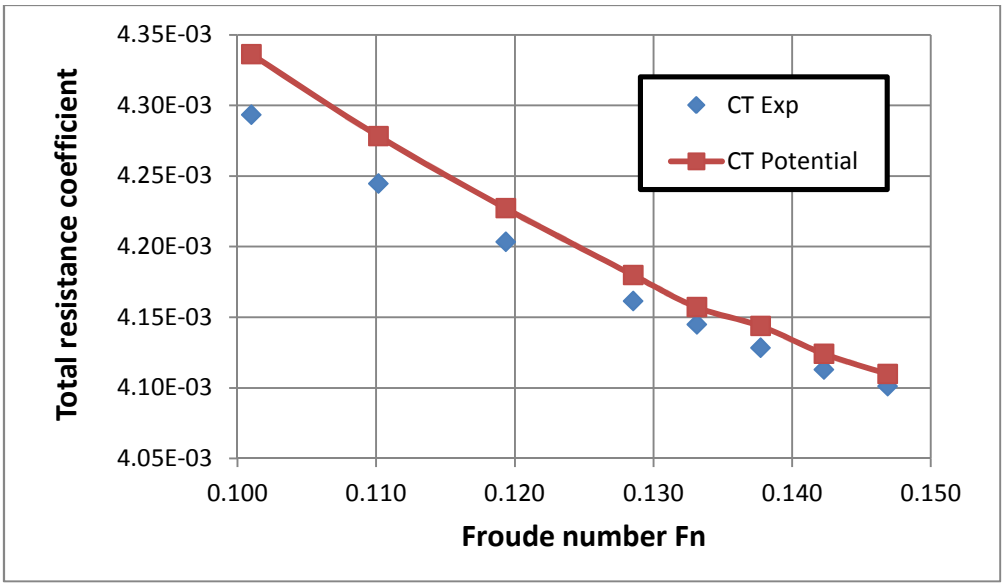

Figure 36. Comparison of C_T Potential and C_T Exp

3.2.4 Numerical study of the free surface potential flow

The potential flow computation around KVLCC2 hull has been performed not only to determine the ship resistance, but also to investigate the hydrodynamic parameters of the flow. In order to investigate the features of the flow around the KVLCC2 hull, the pressure contours on the hull, wave pattern and wave profile along the waterline has been plotted.

a. <u>Pressure distribution on hull</u>

The pressure contours on the hull are presented in Figures 37 and 38.

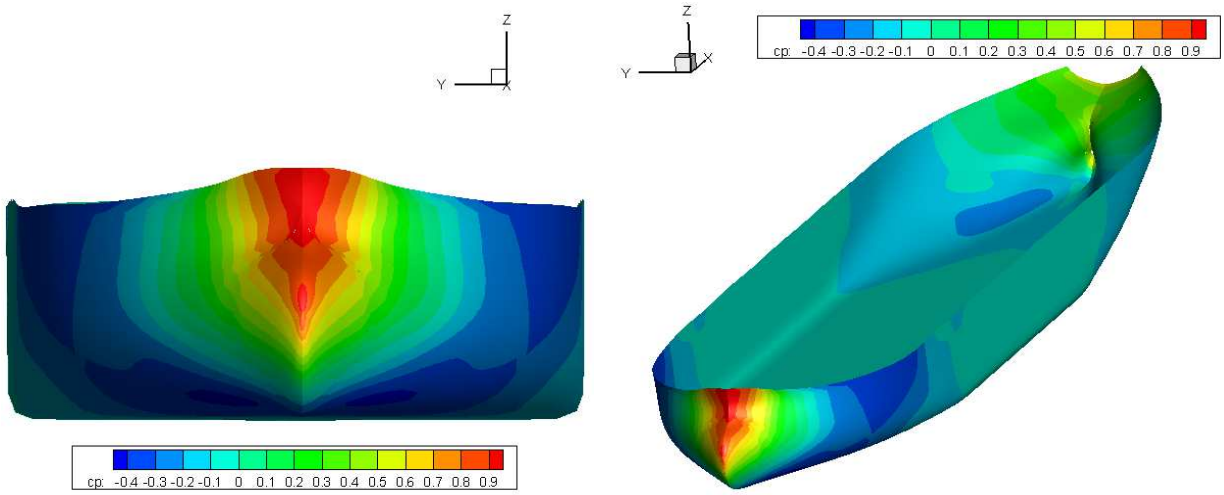

Figure 37. Pressure contour for design speed V=1.047 m/s.

The pressure distribution on the hull for model speed V = 1.047 m/s, corresponding to design speed at full scale (V=15.5 Kn), has been plotted in Figure 37. The pressure is increased on the bow part at the waterline, because of the high entrance angle (60°). A medium pressure distribution may be observed at the aft part of the ship. The Figure 38 present the comparison of pressure contour at design model speed V = 1.047 m/s with other speeds (V = 0.743m/s, 0.8781m/s and 0.9794 m/s).

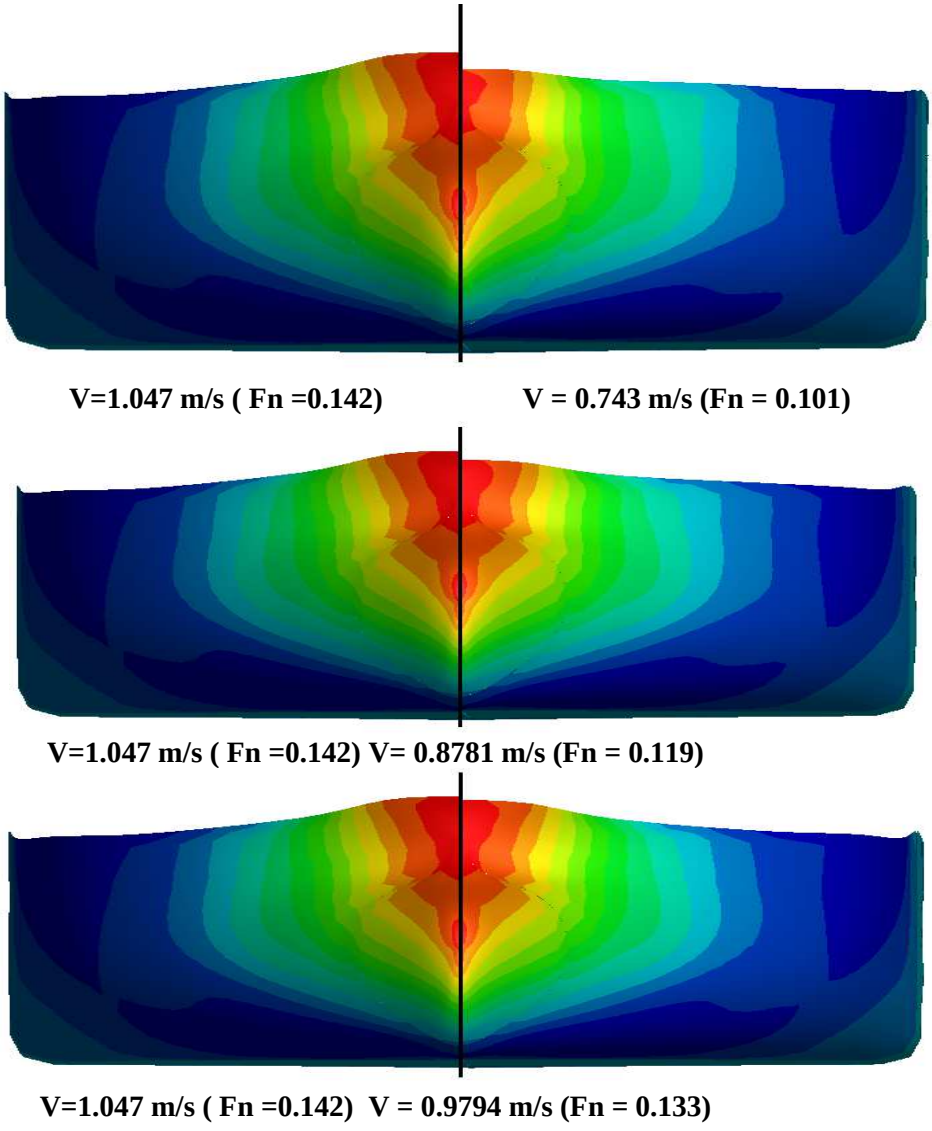

Figure 38. Comparison between design speed and three other speed of model

According to the Figure 38, the pressure at bow increase proportionally with increasing the model speed.

b. Wave pattern

When a ship advances in calm water, it generates waves on the disturbed air – water interface (free surface). The ship has to supply energy continuously to the generated wave system following the ship. The generated waves can be divided into transverse and divergent wave components depending on the wave-propagating direction. [12]. The transverse wave components have the crest line normal to the X-direction with the phase velocity similar to the ship speed, while the divergent wave components are located at the edge of the so-called Kelvin triangle with the shorter wavelength and slower phase velocity (SNAME 1967). The Figure 39 shows the wave pattern at design speed of model $V = 1.047$ m/s corresponding to a Froude number of 0.142.

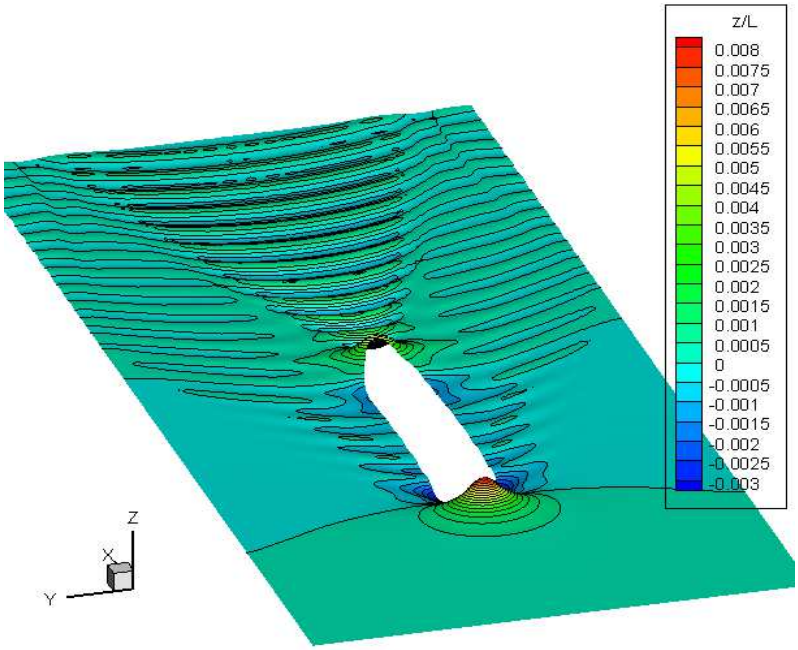

Figure 39. Wave pattern at Design model speed V=1.047m/s

From Figure 39 one can see that the free surface elevation is high, both at the bow and aft part of the model, because of the high pressure. The wave pattern (free surface elevation represented on starboard) at $V = 1.047$ m/s has been compared with wave pattern at smallest speed of model $V = 0.743$ m/s, plotted in portside (see Figure 40). The wave patterns generated at the design model $V = 1.047$ m/s are double than the case at the model speed $V = 0.743$ m/s .

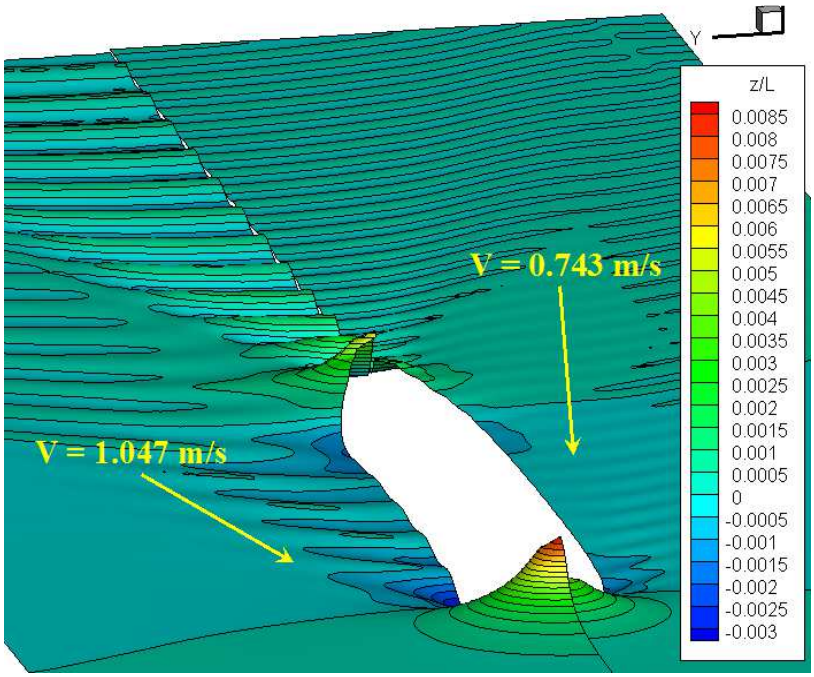

Figure 40. Wave pattern for V=1.047 m/s and V=0.743 m/s.

- **Comparison with the Experimental**

Wave pattern around KVLCC2 obtained in SHIPFLOW with potential flow solver (see Figure 41) is compared with the wave pattern measured in the experimental (see Figure 42) [12]. One can see that the non-dimensional wave height is almost the same, in the both cases.

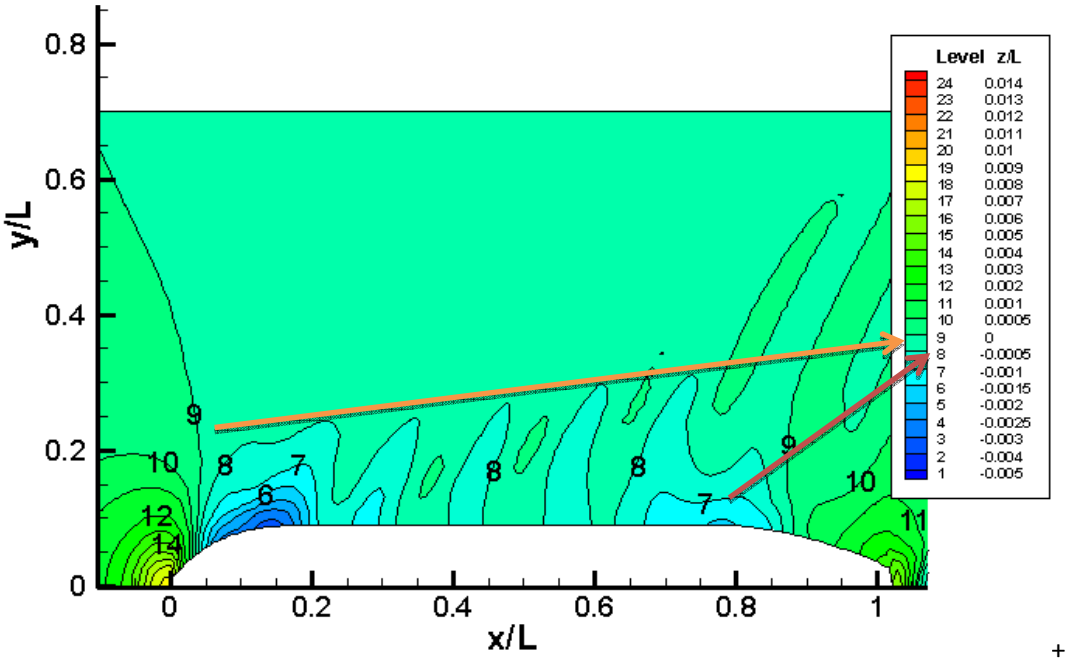

Figure 41. Wave pattern around KVLCC2 in SHIPFLOW

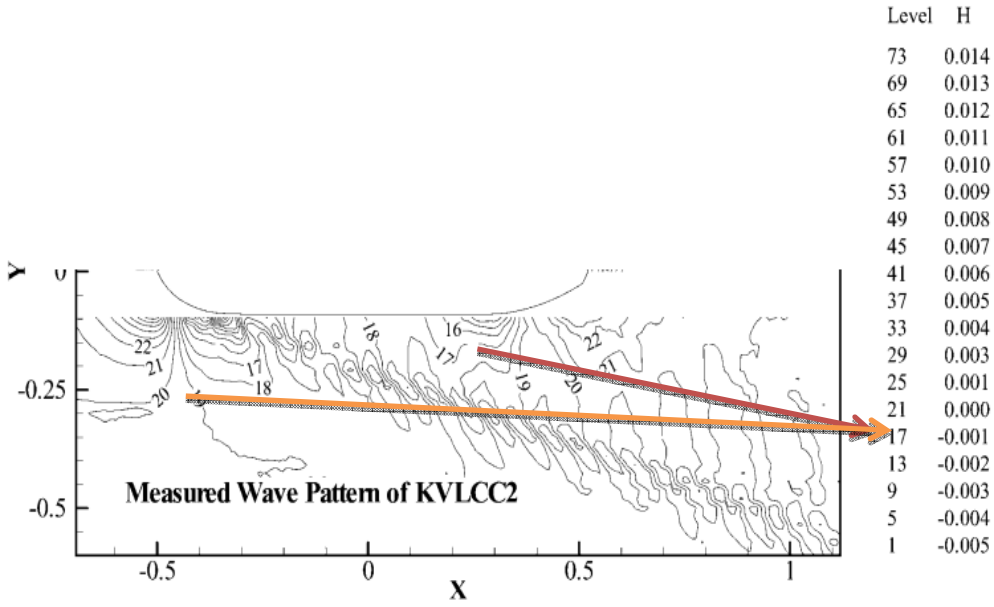

Figure 42. Measured wave pattern around KVLCC2 Experimental [12]

c. Wave profile along the waterline

The wave profile for the model speed V = 1.047 m/s is depicted in Figure 43.

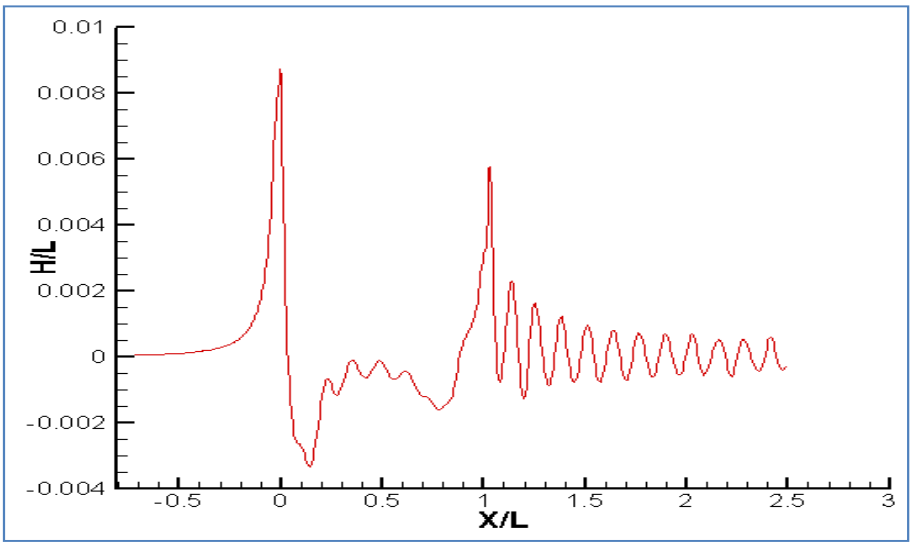

Figure 43. Wave profile along the waterline at V=1.047 m/s

Figure 43 reveals two peaks of high elevation of free surface, as follows:

- **At the bow :** H/L = 0.00866 so the height of wave elevation **H = 0.0477 m**
- **At the transom :** H/L =0.00552 so the height of wave elevation **H = 0.0304 m.**

We can see the influence of the bulbous bow. The wave elevation is decreased along the ship, after the bulbous bow. Modern commercial ships have a bulbous bow to reduce wave generation around the bow region. The waves generated by the bulbous bow under the free surface interact with the waves generated near the design waterline. It is believed that wave resistance can be reduced if the bow bulb is properly located. [12]

The effect of model speeds on wave elevation is shows in details in Figure 44 and Table 7. The wave profile comparison between design speed and speeds of 0.743 m/s, 0.8781 m/s and 0.9794 m/s is presented in Figure 44.

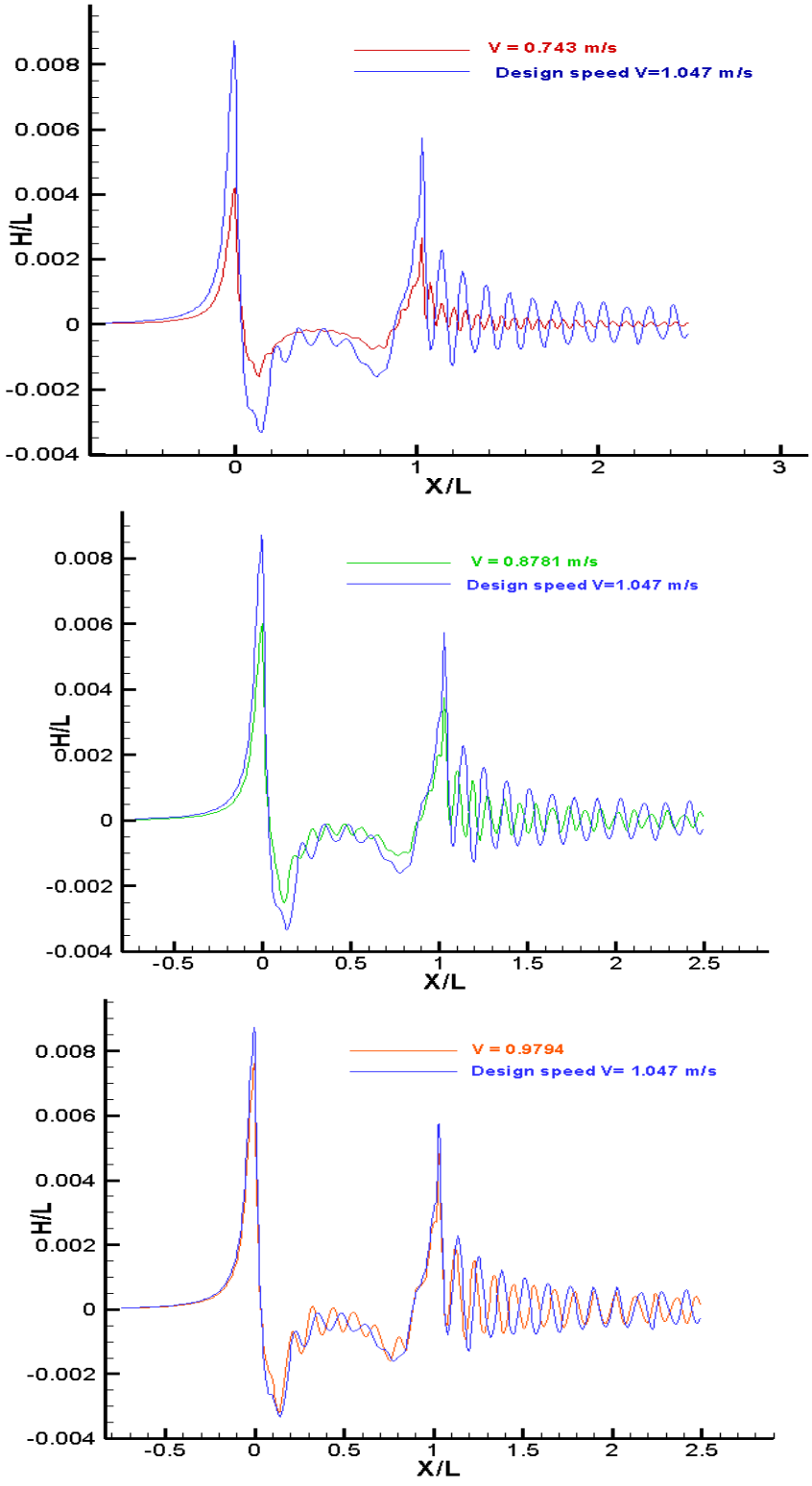

Figure 44. Comparison of wave profile at design speed other three speeds

Also, the wave profile comparison between bulbous bow and transom stern is shown in Table 40. According to the (Figure 44 and Table 40) we observe that the wave profile (elevation) increase with the model speed, both for the bulbous bow and transom.

Table 40. Wave profile (elevation) at bulbous and transom for different model speeds

	Bulbous		Transom	
	H/L	H (m)	H/L	H (m)
V = 0.743 m/s	0.00419	0.023	0.00263	0.014
V = 0.8781 m/s	0.006	0.033	0.00376	0.02
V = 0.9794 m/s	0.0076	0.042	0.00483	0.026
V = 1.047 m/s	0.00866	0.047	0.00552	0.03

- **Comparison with the experimental test**

The result of wave profile along the hull surface obtained from potential flow computations (see Figure 46) is compared with the wave profile measured from the experimental (Figure 45) towing tank tests performed by Korea Research Institute of Ships and Ocean Engineering (KRISO) [12] at the same scale ratio 1/58 of the model and at the same model speed V = 1.047 m/s.

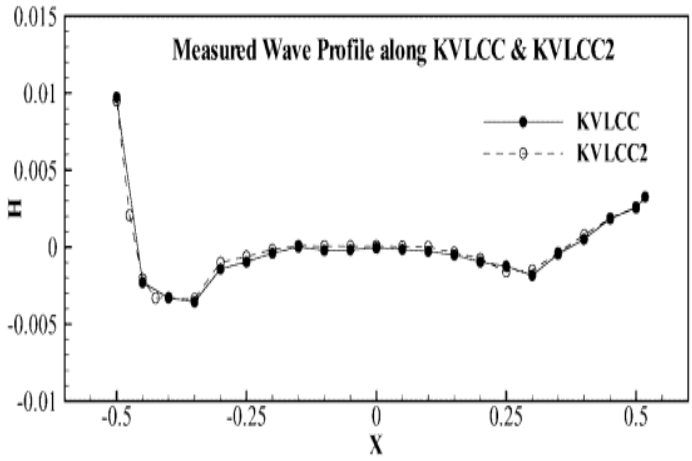

Figure 45. Wave profile of KVLCC2 from Experimental [12]

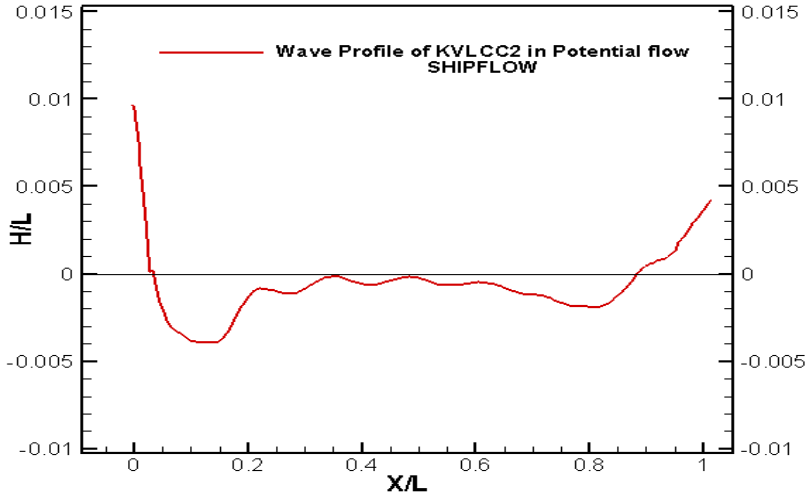

Figure 46. Wave Profile from Potential flow - SHIPFLOW

In the Figure 45 the value X= -0.5 represent forward perpendicular and X= 0.5 represent aft perpendicular. In the Figure 46, the forward perpendicular is at X/L=0 and the aft at X/L=1. The comparison shows that the two results curves are the same. That means the result of wave profile along hull surface from potential flow is validated by the experimental result.

3.3 Viscous Flow

3.3.1 Mathematical model

Viscous flow theory is second alternative of investigation ship resistance in the software SHIPFLOW. Using RANS (Reynolds-Averaged Navier-Stokes) equations larger boundary layers can be handled and turbulent flows in the wake region around stern part of the hull can be captured.

3.3.2 Governing Equations

The Navier-Stokes equations can be solved numerically by resolving all scales for turbulent flows, which requires extremely dense grids to resolve the smallest turbulent length scales. In the present model, the continuity equation states that mass is conserved:

$$\frac{1}{\rho}\frac{\partial \rho}{\partial t}+\frac{\partial U_i}{\partial x_i}=0 \tag{45}$$

Only incompressible flow is considered in the present study. That means that the changes in density are negligible. Then the continuity equation can be written:

$$\frac{\partial U_i}{\partial x_i}=0 \tag{46}$$

The Navier-Stokes equations of motion can be written in the following form:

$$\rho\frac{\partial U_i}{\partial t}+\rho\frac{\partial (U_j U_i)}{\partial x_j}=\rho R_i+\frac{\partial \sigma_{ij}}{\partial x_j} \tag{47}$$

where σ_{ij} is the total stress and for a Newtonian fluid can be written as:

$$\sigma_{ij}=-P\delta_{ij}+2\mu\left(S_{ij}-\frac{1}{3}S_{kk}\delta_{ij}\right) \tag{48}$$

where S_{ij} is the strain-rate defined as following:

$$S_{ij}=\frac{1}{2}\left(\frac{\partial U_i}{\partial x_j}+\frac{\partial U_j}{\partial x_i}\right) \tag{49}$$

S_{kk} in (16) is zero for incompressible flow

$$S_{kk} = \frac{1}{2}\left(\frac{\partial U_k}{\partial x_k} + \frac{\partial U_k}{\partial x_k}\right) = \frac{\partial U_k}{\partial x_k} = 0 \tag{50}$$

The RANS equations can be derived from (47) by splitting the instant velocity components U_i and the instant pressure, *P*, in time mean velocity u_i, and pressure, *p*, and time fluctuating velocity $u_i^{"}$, $U_i = \overline{U_i} + u_i^{"} \equiv u_i + u_i^{"}$ and fluctuating pressure, $p^{"}$, $P = \overline{P} + p^{"} \equiv p + p^{"}$. Following some simple mathematic manipulations, the time averaged continuity equation and N-S equation for incompressible flow can be written as follows:

$$\begin{gathered}\frac{\partial u_i}{\partial x_i} = 0 \\ \frac{\partial u_i}{\partial t} + \frac{\partial (u_j u_i + \overline{u_j^{"} u_i^{"}})}{\partial x_j} = \overline{R_i} - \frac{1}{\rho}\frac{\partial p}{\partial x_i} + \frac{\partial}{\partial x_j}\left(\upsilon\left(\frac{\partial u_i}{\partial x_j} + \frac{\partial u_j}{\partial x_i}\right)\right)\end{gathered} \tag{51}$$

3.3.3 Turbulence Modeling

In an EASM model, the Reynolds stress components are explicitly determined from the tensor functions of the velocity gradients, turbulent kinetic energy, and turbulent length scale. These models have the advantage explicit solution of the Reynolds stresses, at each iteration. The model is relatively complex and assumes that convective effects are negligible. In this approach, the EASM model approximates the predictions of a full Reynolds stress closure model, which is an approximation in itself. The Boussinesq assumption

$$\rho\overline{u_i^{"} u_j^{"}} = \mu_T\left(\frac{\partial u_i}{\partial x_j} + \frac{\partial u_j}{\partial x_i}\right) + \frac{2}{3}\rho k\delta_{ij} \tag{52}$$

is a linear eddy viscosity model. Since it is a linear model it sometimes fails to give satisfactory results and to improve this, nonlinear terms can be added. The Explicit Algebraic Stress Model (EASM) is such a model that includes nonlinear terms. The Reynolds stress tensor is then given by

$$\rho\overline{u_i^{"} u_j^{"}} = \frac{2}{3}\rho k\delta_{ij} - \mu_T\left(S_{ij} + a_2 a_4\left(S_{ik}W_{kj} - W_{ik}S_{kj}\right)\right) - a_3 a_4\left(S_{ik}S_{kj} - \frac{1}{3}S_{mn}S_{mn}\delta_{ij}\right) \tag{53}$$

whereas the turbulent viscosity by $\nu_T = \max\left(-k\alpha_1, \frac{0.0005k}{\beta^* \omega}\right)$. Here $\alpha_1, \beta^*, a_2, a_3, a_4$ are numerical coefficients of the model, while W_{ij} is the rotation-rate.

3.3.4 Boundary conditions

A **boundary fitted coordinate system** is employed to allow a more accurate formulation of the boundary conditions, which requires the **no-slip condition** for the velocity the hull surface, a **Neumann-type condition** for the pressure, while for k and ω, **Dirichlet conditions** are used. The **zero-gradient Neumann** conditions are imposed for all the variables in the symmetry plane. At the upstream, the oncoming flow velocity is supposed constant, as k and ω are, whereas the pressure is extrapolated with zero-gradient. At the downstream, the velocity, k and ω are extrapolated with zero-gradient, while the dynamic pressure has the zero value. Boundary conditions used to describe the problem are given in Table 41 and Figure 47.

Table 41. Boundary conditions for the domain

	No slip	Slip	Inflow	Outflow
u	$u_i = 0$	$u_i n_i = 0, \frac{\partial u_i}{\partial \xi_B} = 0$	$u = \text{Constant}$	$\frac{\partial u_i}{\partial \xi_B} = 0$
p	$\frac{\partial p}{\partial \xi_B} = 0$	$\frac{\partial p}{\partial \xi_B} = 0$	$\frac{\partial p}{\partial \xi_B} = 0$	$p = 0$
k	$k = 0$	$\frac{\partial k}{\partial \xi_B} = 0$	$k = \text{Constant}$	$\frac{\partial k}{\partial \xi_B} = 0$
ω	$\omega = f(u_T, ...)$	$\frac{\partial \omega}{\partial \xi_B} = 0$	$\omega = \text{Constant}$	$\frac{\partial \omega}{\partial \xi_B} = 0$

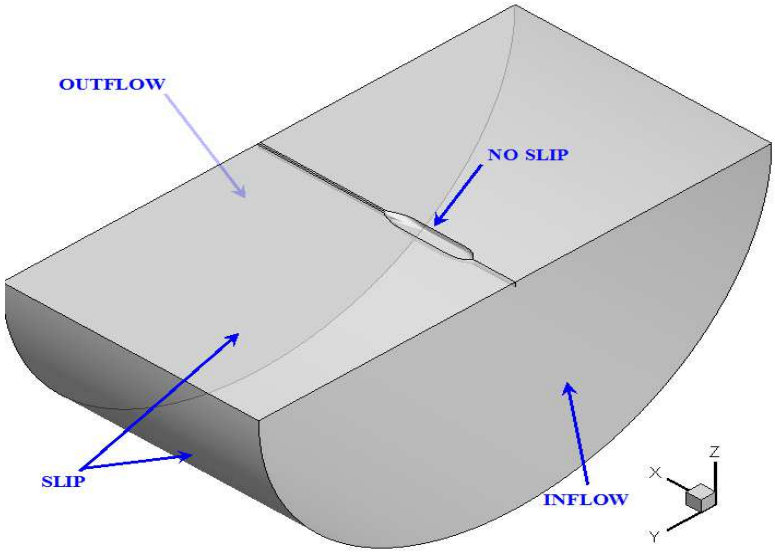

Figure 47.Boundary condition of the domain

3.3.5 Domain of Computation and Grid

For complex geometries such as a ship hull, the grid generation is a very complicated and time consuming task to accomplish. In the present particular case of the tanker hull, both port and starboard sides are included in the solution domain to simulate the asymmetric flows. In Figure 48, XSTART, XFPU, XFPD, XAPU, XAPD and XEND represent x – coordinates non-dimensionalized by Lpp. This parameters define the dimensions of the domain and the areas where the grid lines are clustered on x direction, as fallow: XSTART is x – coordinate of the inflow of the computation; XFPU is the x – coordinate of the change in stretching of the bow region upstream of the FP (forward perpendicular); XFPD is the x – coordinate of the change in stretching of the bow region downstream of the FP; XAPU is the x – coordinate of the change in stretching of the stern region upstream of the AP (aft perpendicular); XAPD is the x – coordinate of the change in stretching of the stern region downstream of the AP; END is x – coordinate of the end of the grid and domain. The parameters that have been utilized in the viscous flow computations around KVLCC are presented in Table 42.

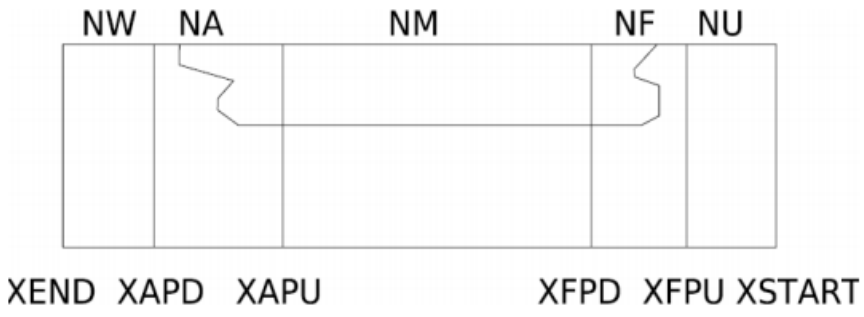

Figure 48. x - plane distribution

Table 42. The x - coordinates of the domain grid

XSTART	XFPU	XFPD	XAPU	XAPD	XEND
-0.5	-0.1	0.2	0.8	1.2	2.5

Finally, the domain of the computation is shown in Figure 49. The domain covers 0.5 ship length upstream of the bow, 3 ship lengths out from the side and bottom of the hull, and 1.5 ship length downstream of the stern. A no slip boundary condition was enforced at the hull surface, where the first grid point from the body surface was located at around y+=1 for turbulence modeling considerations.

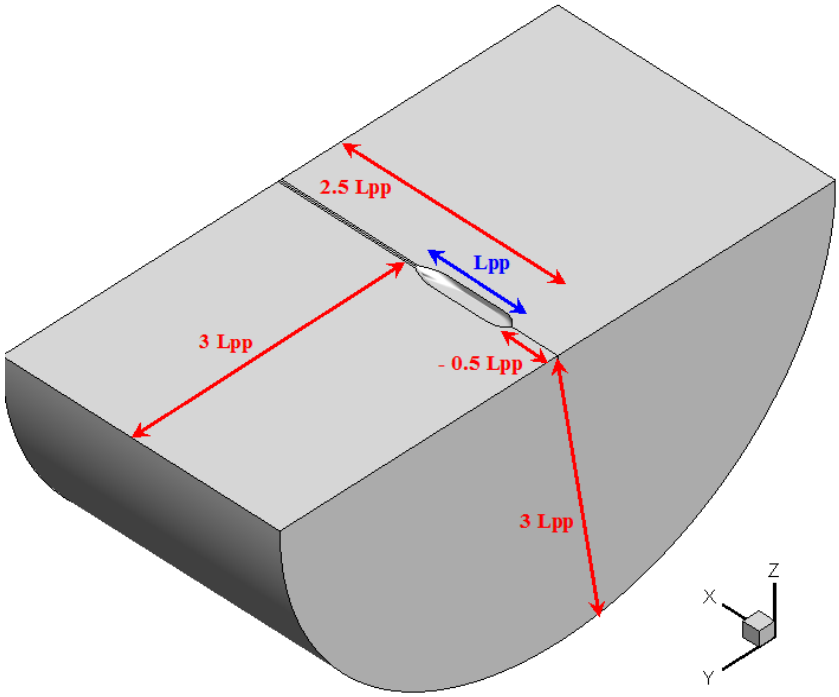

Figure 49.Computational domain

NU, NF, NM, NA and NW are the grid parameters which define the number of planes in the longitudinal direction, as follow: NU is number of 15 planes in the longitudinal direction between coordinates XSTART and XFPU; NF is number of30 planes in the longitudinal direction between coordinates XFPU and XFPD; NM is number of50 planes in the longitudinal direction between coordinates XFPD and XAPU; NA is number 60 of planes in the longitudinal direction between coordinates XAPU and XAPD; NW is number 30 of planes in the longitudinal direction between coordinates XAPD and XEND. The values of the grid parameters have been chosen in order to get a proper balance between accuracy of the result and CPU resources. The parameters used in computation are presented in Table 43. The resulted grid, shown in Figure 50, a cylindrical mono-block structured grid of about 1.9

million cells has been generated to cover the entire computational domain. Finer grids are generated in the areas of interest that may require better resolution.

Table 43. Number of planes in longitudinal direction

NU	NF	NM	NA	NW
15	**30**	**50**	**60**	**30**

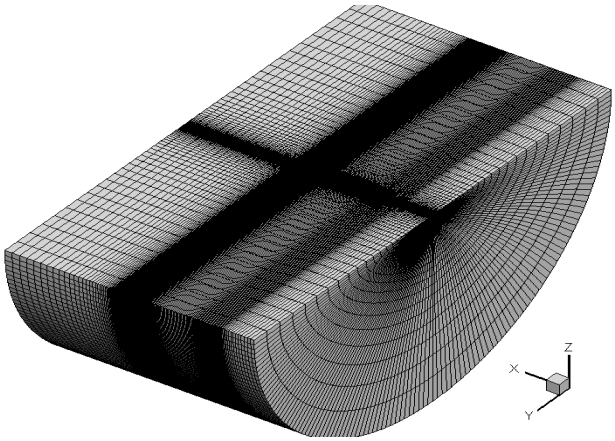

Figure 50. Grid of the domain of computation

3.3.3 Viscous Flow Computation

SHIPFLOW RANS solver, XCHAP has been employed to simulate viscous flow around the KVLCC2 bare hull model. The global characteristics of the flow as C_F, C_{PV} (viscous pressure resistance coefficient) and C_V (viscous resistance coefficient) has been computed. The results are tabulated in Table 44.

Table 44. Resistance coefficients in viscous flow

V (m/s)	Fn	C_F	C_{PV}	C_V
0.743	0.101	3.28E-03	1.12E-03	4.40E-03
0.8105	0.110	3.24E-03	1.11E-03	4.34E-03
0.8781	0.119	3.20E-03	1.09E-03	4.29E-03
0.9456	0.129	3.16E-03	1.09E-03	4.25E-03
0.9794	0.133	3.15E-03	1.08E-03	4.22E-03
1.0132	0.138	3.13E-03	1.07E-03	4.20E-03
1.0469	0.142	3.11E-03	1.07E-03	4.18E-03
1.0807	0.147	3.10E-03	1.07E-03	4.16E-03

a. Frictional resistance coefficient

The skin friction resistance coefficient computed by XCHAP is compared with the friction resistance coefficient determined by ITTC 1957, as one can see in Table 45 and Figure 51. They linearly decrease with increasing of Froude number.

Table 45. Comparison of C_F (Viscous flow) and C_F (ITTC 1957)

Fn	C_F(Viscous flow)	C_F(ITTC 1957)	Error (%)
0.101	3.28E-03	3.52E-03	-6.86%
0.110	3.24E-03	3.47E-03	-6.60%
0.119	3.20E-03	3.42E-03	-6.37%
0.129	3.16E-03	3.37E-03	-6.21%
0.133	3.15E-03	3.35E-03	-6.08%
0.138	3.13E-03	3.33E-03	-5.97%
0.142	3.11E-03	3.31E-03	-5.89%
0.147	3.10E-03	3.29E-03	-5.80%

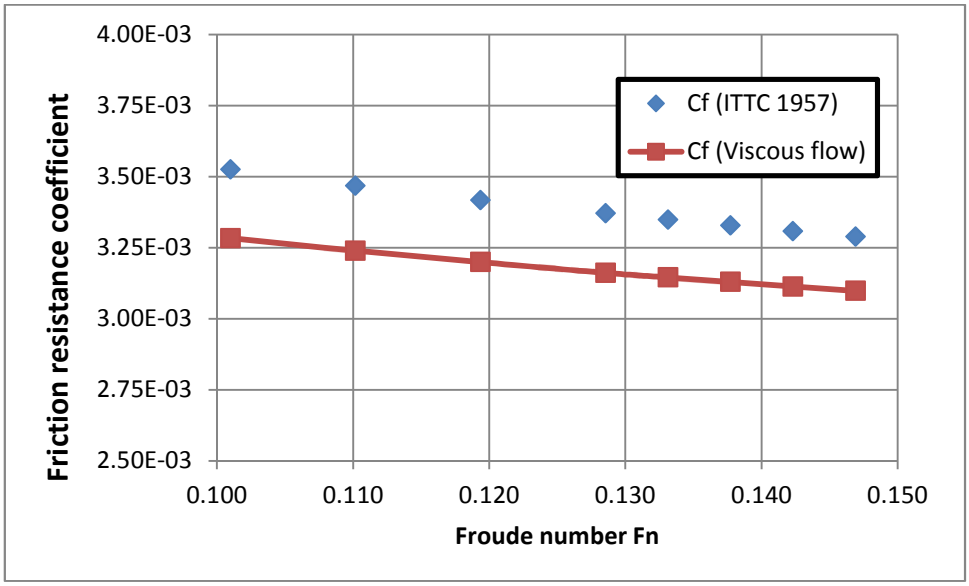

Figure 51. Comparison of C_F (Viscous flow) and C_F(ITTC 1957)

b. Viscous resistance coefficient

The viscous resistance coefficient computed by viscous flow method in SHIPFLOW is compared with the viscous resistance coefficient from experimental results, determined by the following relation:

$$C_{V,Exp} = (1 + k) * C_{F,ITTC\ 1957} \quad (54)$$

The results are presented in Table 46 and Figure 52. The numerical and experimental viscous resistance coefficients decrease with increasing of Froude number.

Table 46.Comparison between $\boldsymbol{C_V}$ (Viscous flow) and $\boldsymbol{C_V}$ Exp

Fn	C_V (Viscous flow)	C_V, Exp	Error (%)
0.101	4.40E-03	4.28E-03	2.89%
0.110	4.34E-03	4.21E-03	3.20%
0.119	4.29E-03	4.15E-03	3.52%
0.129	4.25E-03	4.09E-03	3.85%
0.133	4.22E-03	4.06E-03	3.95%
0.138	4.20E-03	4.04E-03	4.08%
0.142	4.18E-03	4.01E-03	4.21%
0.147	4.16E-03	3.99E-03	4.34%

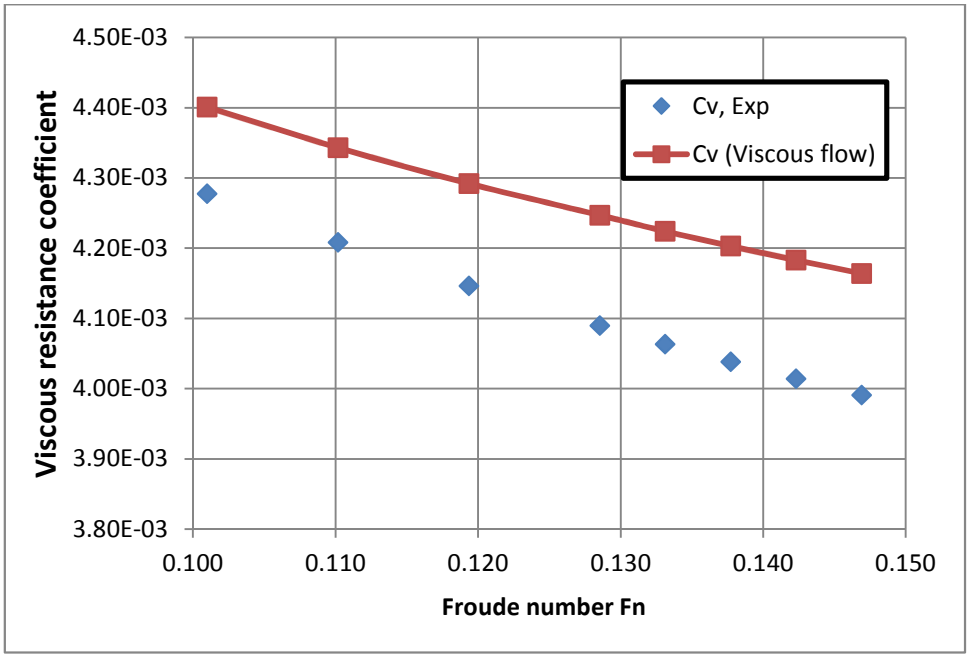

Figure 52. Comparison between $\boldsymbol{C_V}$(Viscous flow) and $\boldsymbol{C_V}$Exp

c. Total resistance coefficient

The total resistance coefficient in viscous flow method was calculated by the relation:

$$C_T(Viscous\ flow) = C_V(Viscous\ flow) + C_{WTWC}(Potential\ flow) \quad (55)$$

All the viscous flow computations have been performed in double model conditions, which there is no free surface elevation. In order to determine the total resistance, the wave cut resista0nce coefficient from the potential flow result has been taken in account. Resistance coefficient obtained as mentioned before is compared with the total resistance coefficient from experiments, as it can be seen in Table 47 and Figure 53. The difference is about 3%, where the computed values are bigger than the experimental.

Table 47.Comparison between C_T (viscous flow) and C_T (Exp)

Fn	CT (Viscous flow)	CT Exp	Error (%)
0.101	4.41E-03	4.29E-03	2.60%
0.110	4.35E-03	4.24E-03	2.54%
0.119	4.31E-03	4.20E-03	2.47%
0.129	4.27E-03	4.16E-03	2.68%
0.133	4.25E-03	4.14E-03	2.63%
0.138	4.24E-03	4.13E-03	2.74%
0.142	4.23E-03	4.11E-03	2.78%
0.147	4.22E-03	4.10E-03	2.89%

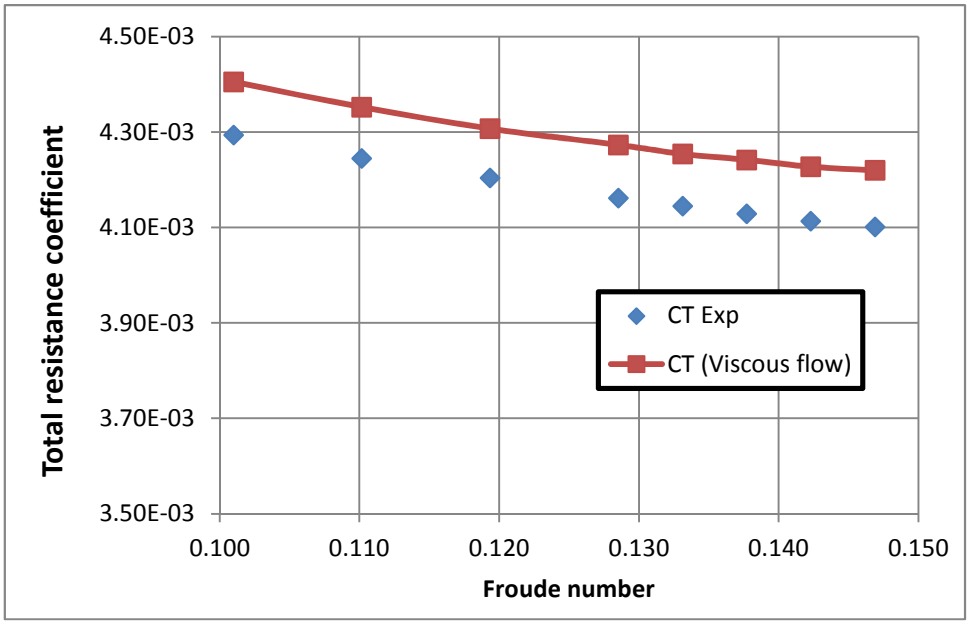

Figure 53. Comparison between C_T (viscous flow) and C_T (Exp)

4. CFD ANALYSIS OF THE FLOW AROUND THE KVLCC2 HULL WITH DRIFT ANGLE

4.1 Modeling conditions

In the present chapter, XCHAP solver based on RANS method has been used to simulate the flow around the KVLCC2 bare hull model. A set of seven computations have been carry out in order to determine hydrodynamic force acting on the hull. This is well known as static drift test. The computations have been performed for a range of drift angle from β=0° to β=12° with an increment of 2°.The hydrodynamic forces coefficients targeted by the static drift test are longitudinal force coefficient, X', lateral force coefficient Y' and yaw moment coefficient N'.

In SHIPFLOW the attack inflow angle is taken as positive value to the portside with is specified a command *osfl(flow=[α])*, which is corresponds to the drift angle β positive to the starboard, as indicated in Figure 54.

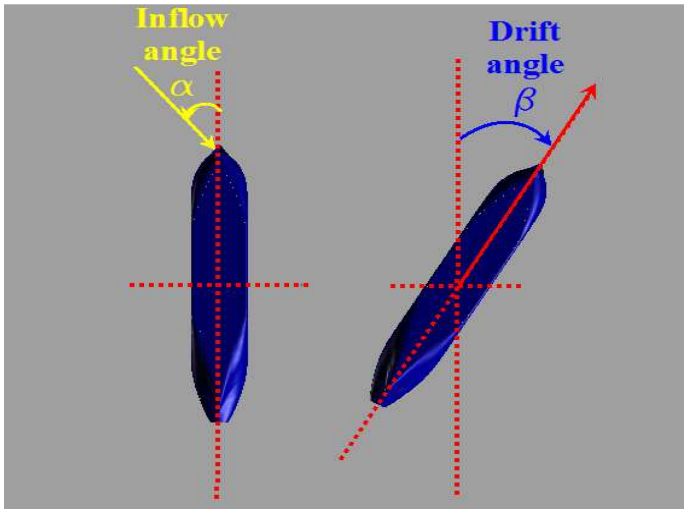

Figure 54. The drift angle β

The grid used for the flow computations is the same grid (1.9 million cells) which has been generated for the ship resistance simulations in CHAPTER 3.

To validate CFD results, the hydrodynamics forces coefficients X', Y' and moment N' are compared with the experimental results conducted by Instituto Nazionale Per Studi Ed Esperienze Di Architettura Navale (INSEAN) for the SIMMAN 2008 Worshop [14], Fabbri et al. [13]. The PMM tests of this model were conducted by INSEAN in deep water with scale factor of the model (1/45.714), at Froude number Fn=0.142 and Reynolds number

Re=3.7*10^6 .The measurement of the forces and moments in steady drift motion has been measured for drift angle β=0,3°, 0.5°, 0.9°, 1°, 1.8°, 2°, 4° and 6° and has been reported in [15]. The main dimensions of this model ship at INSEAN are shown in the Table 48.

Table 48. Characteristics of the model

	Full SCALE	INSEAN
Scale	1	45.714
Length between perpendicular Lpp (m)	320.0	7.000
Length waterline Lwl (m)	325.5	7.1204
Breadth Bwl (m)	58	1.2688
Draft T (m)	20.8	0.4550
Wetted surface area WSA (m^2)	27194	13.0129

4.2 Hydrodynamics Forces and moments with drift angle influence

The coefficients of the hydrodynamics forces X', Y' and yaw moment N' from the experimental PMM test (INSEAN) [15], (see Table49) are in function of the drift angle. The experimental results were taken in the absolute values, because of the difference of the sign convention and of the coordinate systems of the model hull, in order to easily compare the both results.

Table49. The coefficients of the Hydrodynamics forces and moment from INSEAN

Exp INSEAN			
Drift β (°)	**X'**	**Y'**	**N'**
0.3	0.017	0.001	0
0.5	0.016	0.0025	0.001
0.9	0.031	0.019	0.01
1	0.016	0.003	0.002
1.8	0.019	0.009	0.005
2	0.015	0.008	0.005
4	0.016	0.015	0.011
6	0.017	0.024	0.017

Shipflow prints the results in non-dimensional form using FMREF command. The force coefficients are: non-dimensional pressure forces (X'_p,Y'_p) and yaw moment (N'_p) and non-dimensional friction force (X'_f,Y'_f) and yaw moment(N'_f).

The non-dimensionalization of pressure and friction forces and moment is done according with following expressions:

$$X'_p = \frac{X_p}{0.5 * \rho * U^2 * Lpp * T}$$

$$Y'_p = \frac{Y_p}{0.5 * \rho * U^2 * Lpp * T}$$

$$N'_p = \frac{N_p}{0.5 * \rho * U^2 * Lpp^2 * T}$$

$$X'_f = \frac{X_f}{0.5 * \rho * U^2 * Lpp * T} \quad (56)$$

$$Y'_f = \frac{Y_f}{0.5 * \rho * U^2 * Lpp * T}$$

$$N'_f = \frac{N_f}{0.5 * \rho * U^2 * Lpp^2 * T}$$

where:

$\rho$is freshwater density [1000 kg/m³];

$U$is model speed [m/s];

$Lpp$is length between perpendicular of the model [m];

$T$is the draft of the model [m].

The coefficients of the total hydrodynamic forces X', Y' and moment N' has been calculated as sum of the pressure component and the frictional component as follow:

$$X' = X'p + X'f$$

$$Y' = Y'p + Y'f \quad (57)$$

$$N' = N'p + N'f$$

4.2.1 Longitudinal hydrodynamic force coefficient X'

The non-dimensional force X' represent the surge force acting on the model in the x-direction forward of the ship. SHIPFLOW gave the non-dimensional pressure force X_p' and

non – dimensional friction force Y_f' in negative value. The sum of these components determines the total non-dimensional force X' (see Table 50).

The comparison of the non-dimensional force X' computed by author and measured at INSEAN are compared in Figure 55.

Table 50. The non-dimensional force X' with drift angle influence

	SHIPFLOW		
Drift β (°)	**X'p**	**X'f**	**X'**
0	0.0047	0.0139	0.0186
2	0.0048	0.0139	0.0187
4	0.0050	0.0140	0.0190
6	0.0052	0.0142	0.0195
8	0.0055	0.0144	0.0200
10	0.0057	0.0145	0.0202
12	0.0060	0.0147	0.0206

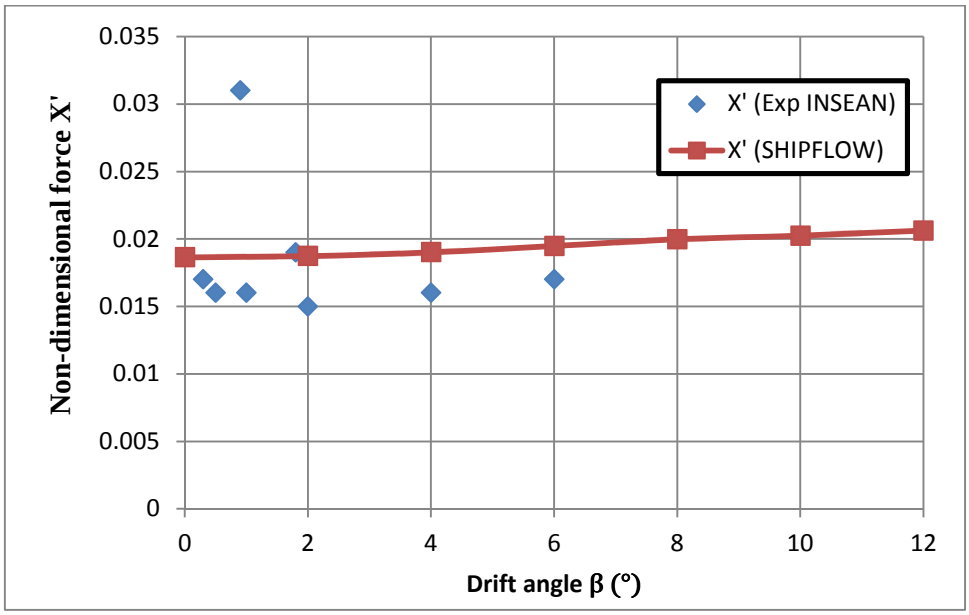

Figure 55.Comparison of non-dimensional force X' computed and measured

The numerical and experimental values of the non–dimensional force X' start to be closer for drift angle β> 2°. However, the experimental values have significant fluctuations in the range of the small drift angle (between β = 0.3° - 1.8°), probably caused by some experimental errors.

4.2.2 Lateral hydrodynamic force coefficient Y'

The non-dimensional force Y' represents the sway force in y-direction (in starboard). SHIPFLOW code computes the non-dimensional values of the pressure force Y'p, friction force Y'f and total force Y' (calculated as the sum of the pressure and friction components) as function of the drift angle β. The hydrodynamic coefficients have been computed for a range of drift angles β between 0° and 12°, as one can see in Table51. In Figure 56the comparison between of computed non-dimensional force Y' and experimental result (INSEAN) is depicted.

Table 51. The non-dimensional forces Y'with drift angle influence

	SHIPFLOW		
Drift β (°)	**Y'p**	**Y'f**	**Y'**
0	0	0	0
2	0.0076	0.0003	0.0079
4	0.0155	0.0005	0.0161
6	0.0263	0.0008	0.0270
8	0.0400	0.0010	0.0410
10	0.0561	0.0012	0.0573
12	0.0728	0.0015	0.0743

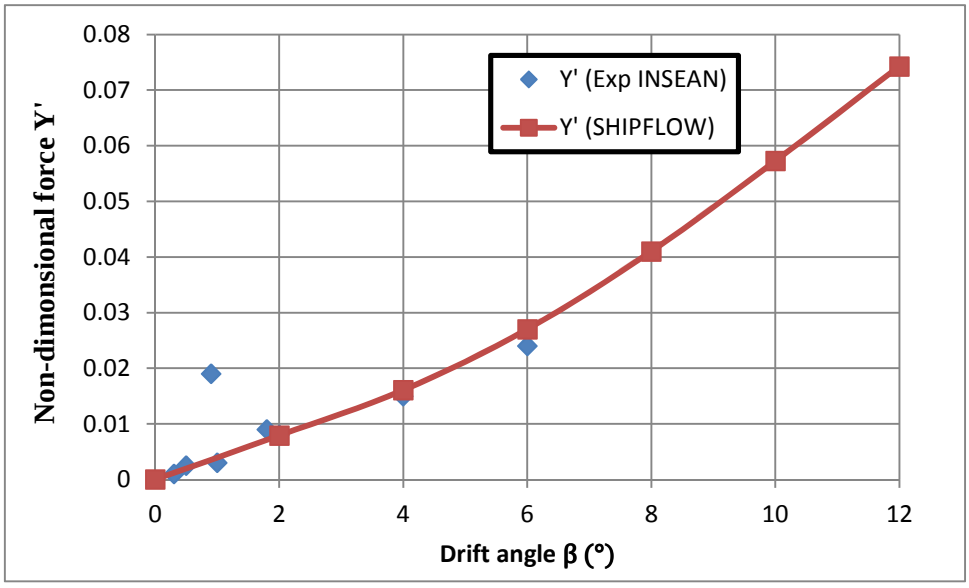

Figure 56. Comparison of non-dimensional force Y' computed and measured INSEAN

At drift angle β = 0 there is no lateral force, which means that the non-dimensional force Y'= 0.

The same fluctuation of the experimental values can be observed, at the small drift angles. For drift angle β>2° the experimental and SHIPFLOW values are superposed. The non-dimensional force Y' increases with the drift angle.

4.2.3 Yaw hydrodynamic moment coefficient N'

The non-dimensional hydrodynamic moment N' represents the yaw moment acting on the ship. The results obtained in SHIPFLOW are non-dimensional moment pressure N_p' and non-dimensional moment friction N_f'. Total non-dimensional moment N' is calculated as the sum of the two components (pressure and friction). These results are presented in Table 52as function of the drift angle β. Figure 57 shows the comparison of computed non-dimensional total yaw moment N' and the experiment measurement (INSEAN)as function of drift angle.

Table 52. The non-dimensional moment N' with drift angle influence

	SHIPFLOW		
Drift β (°)	**N'p**	**N'f**	**N'**
0	0.00	0.00	0.00
2	0.0051	2.54E-05	0.0051
4	0.0106	4.84E-05	0.0106
6	0.0154	6.83E-05	0.0155
8	0.0197	8.11E-05	0.0198
10	0.0236	9.10E-05	0.0237
12	0.0273	1.25E-04	0.0275

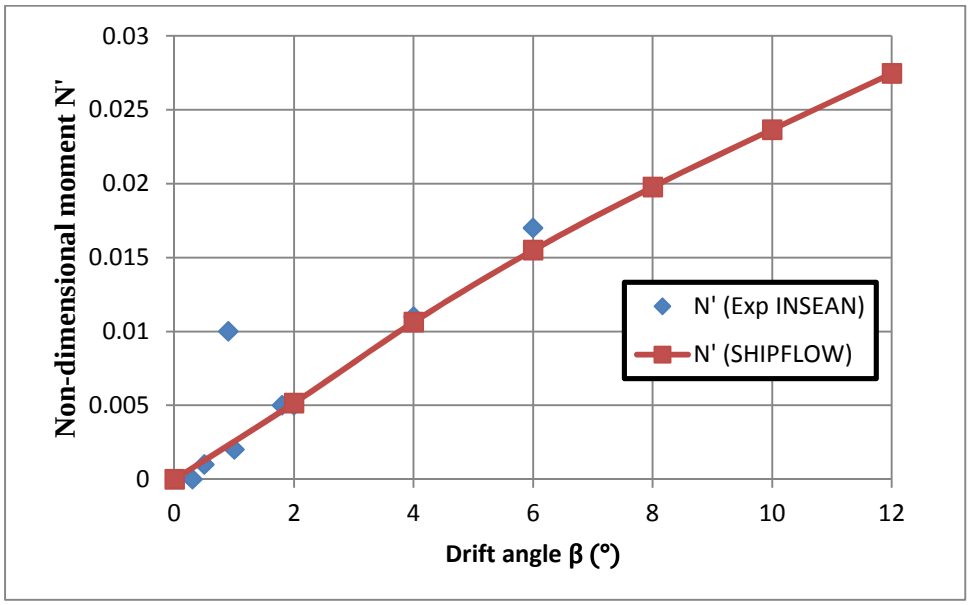

Figure 57. Comparison of non-dimensional yaw moment N' computed and measured

According to the Figure 57, a satisfactory agreement between the numerical and experimental values of the non-dimensional yaw moment N' may be observed, especially for drift angle β> 2°. Also, the total moment increases with drift angle. The same fluctuation of the experimental values can be observed, at the small drift angles.

4.3 Numerical study of the flow with drift angle influence

The present chapter depicts the numerical introspection of the incident flow developed around the hull without rudder in the presence of a given drift angle. An accurate image of the flow pattern developed in the stern area can be depicted by analyzing the flow behavior in the propeller plane, for all considered cases. The axial velocity has been investigated in order to study the influence of the drift angle on the flow propeller plane, which it is positioned at x/L=0.9825. The axial velocity contours has been plotted for all drift angles cases (β = 0°, 2°, 4°, 6°, 8°, 10° and 12°). The evolution of vortical structures in the propeller plane is revealed in Figures 58 - 64.

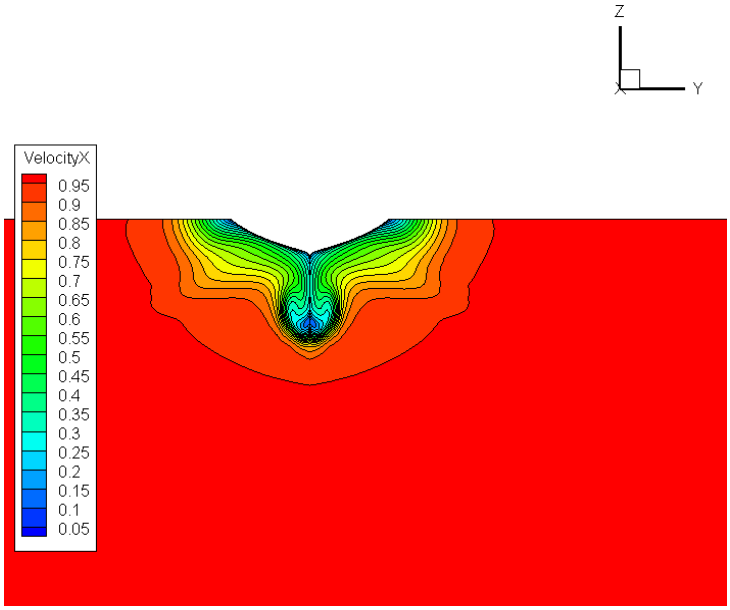

Figure 58. Axial velocity at x/L=0.9825 with drift angle β = 0°

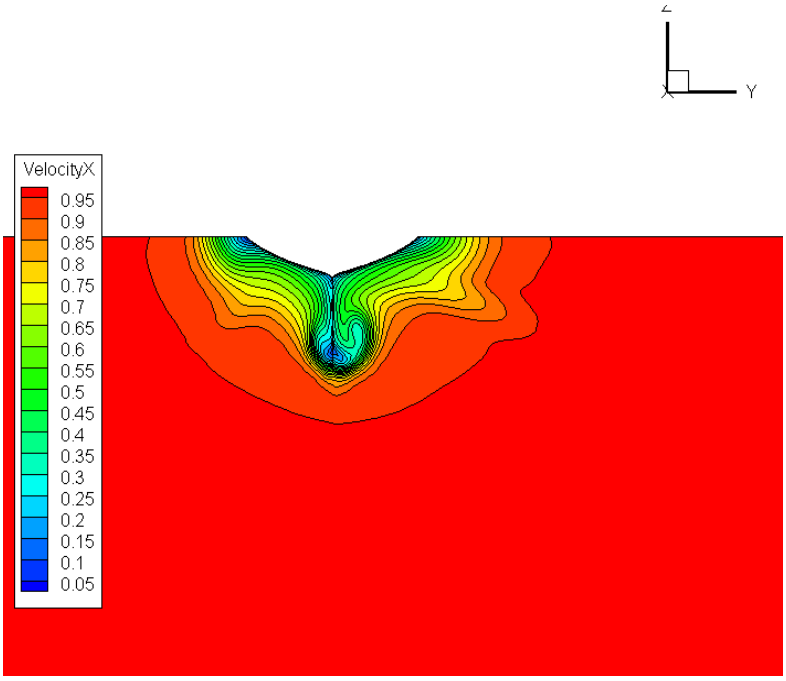

Figure 59. Axial velocity at x/L=0.9825 with drift angle β = 2°

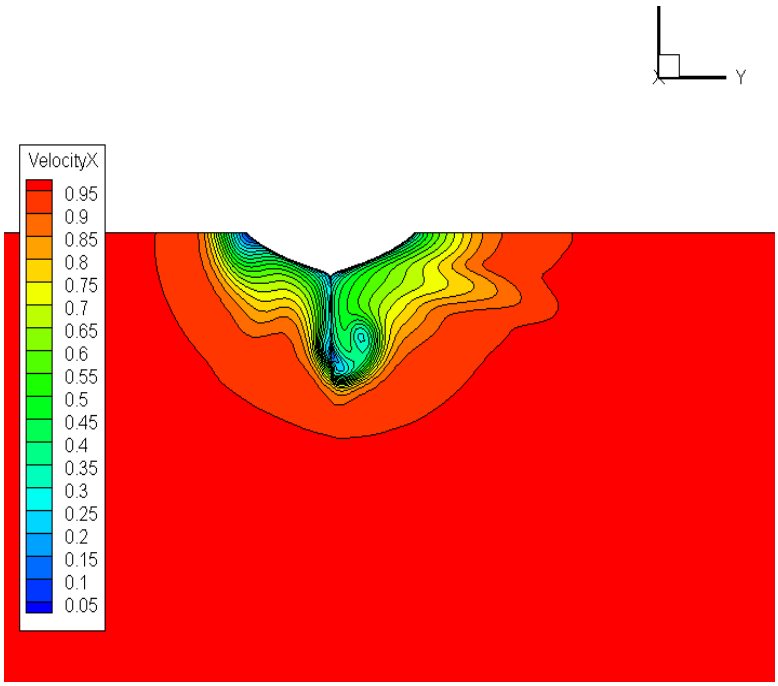

Figure 60. Axial velocity at x/L=0.9825 with drift angle β = 4°

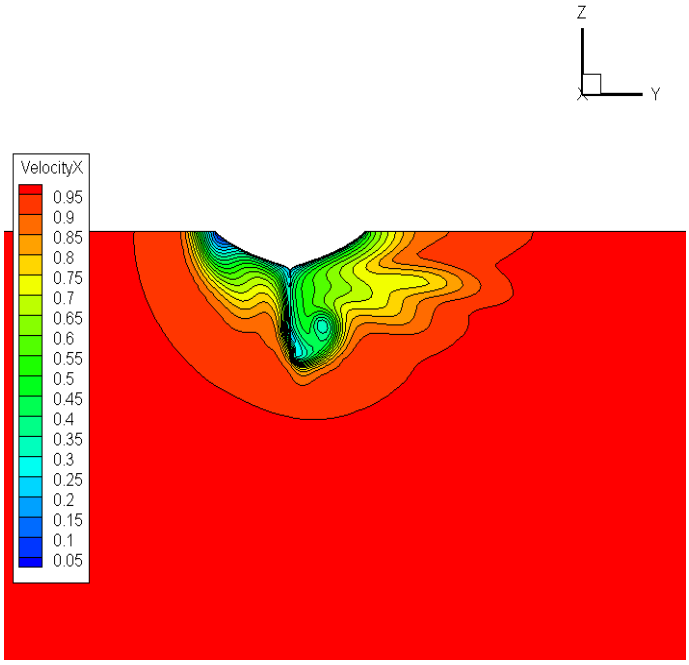

Figure 61. Axial velocity at x/L=0.9825 with drift angle β = 6°

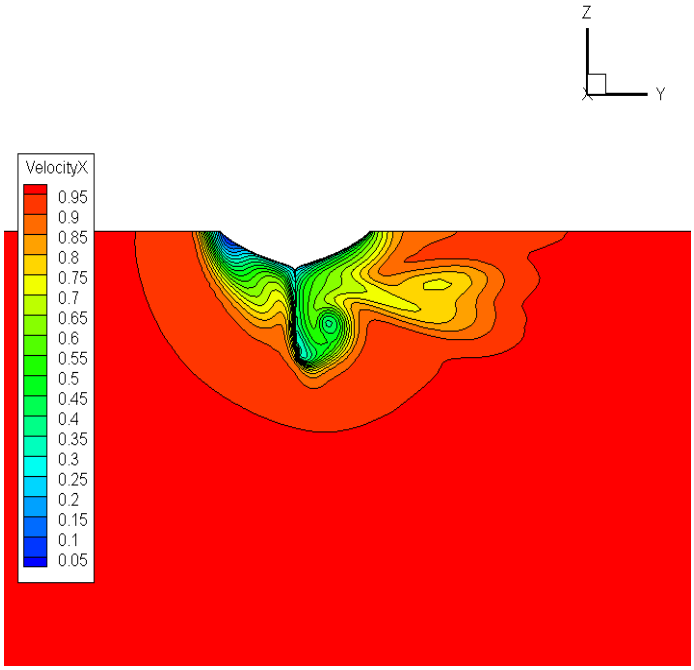

Figure 62. Axial velocity at x/L=0.9825 with drfit angle β = 8°

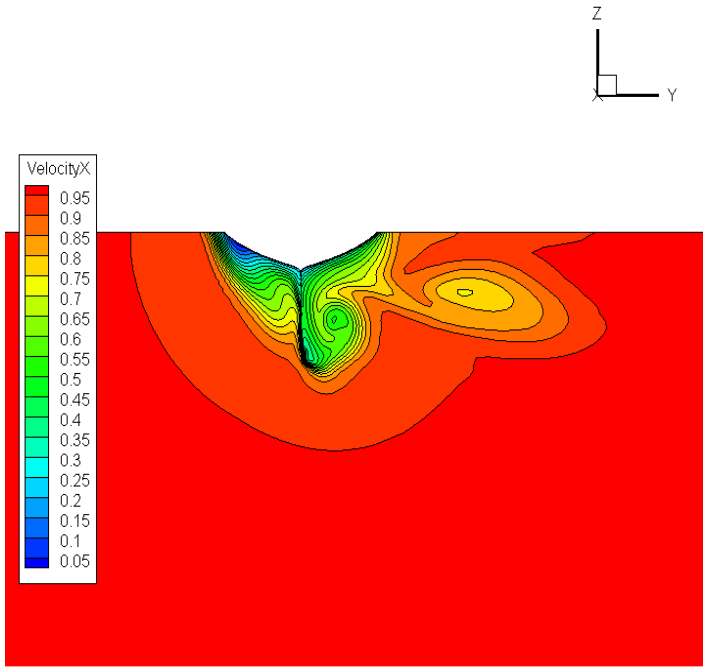

Figure 63. Axial velocity at x/L=0.9825 with drift angle β = 10°

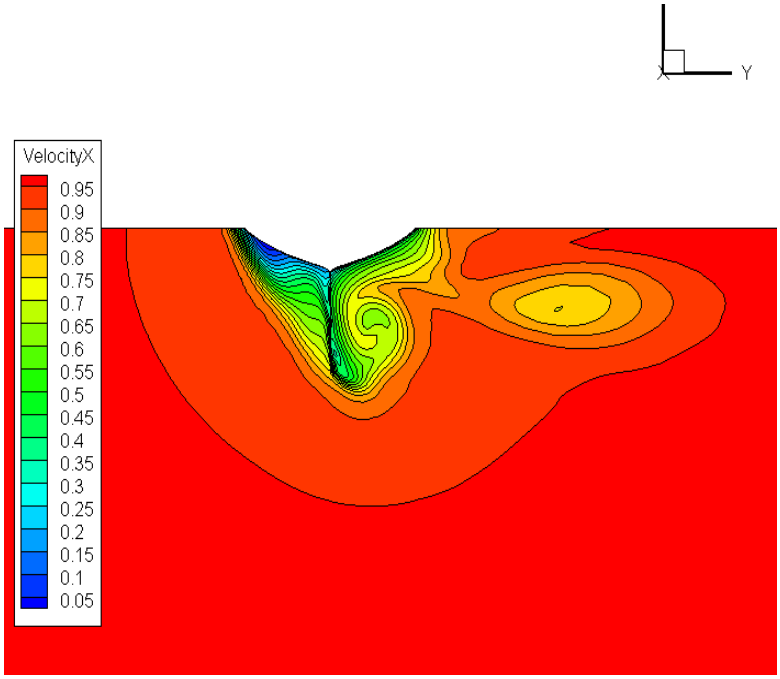

Figure 64. Axial velocity at x/L = 0.9825 with drift angle β = 12°

4.3.1 Comparison axial velocity with the experimental

The axial velocity contours computed in the propeller plane have been plotted for angle of β = 0° and β = 12° in order to be compared with experimental result from [13], [14], as follows:

a. <u>At the drift angle β = 0°</u>

The axial velocity contours measured from experimental at drift angle β = 0° are presented in Figure 65 and the CFD results in Figure 66.

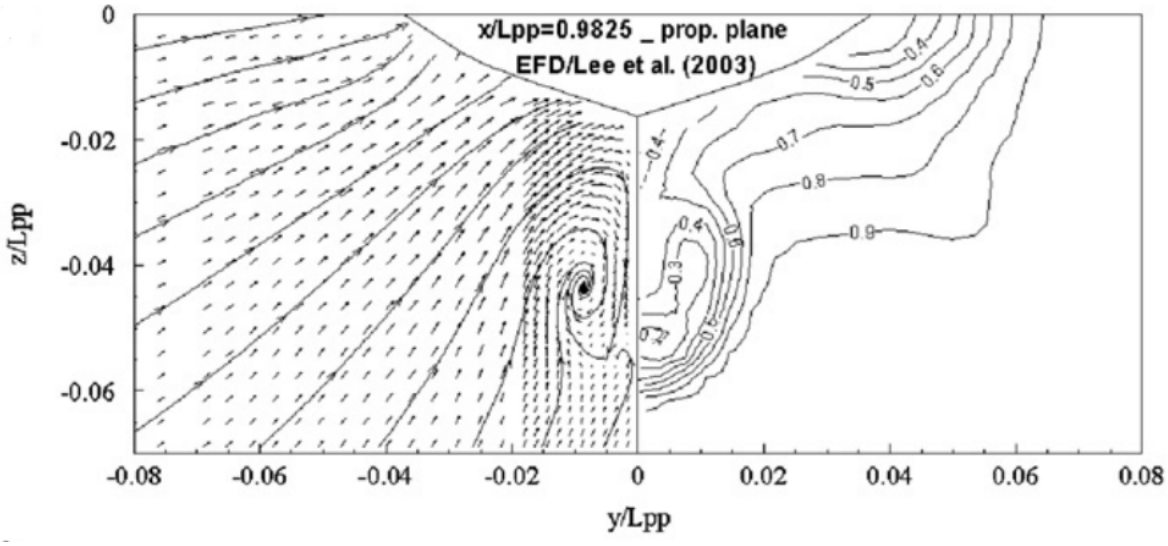

Figure 65. Axial velocity at x/Lpp=0.9825 from Experimental with β = 0° (right panel) [17].

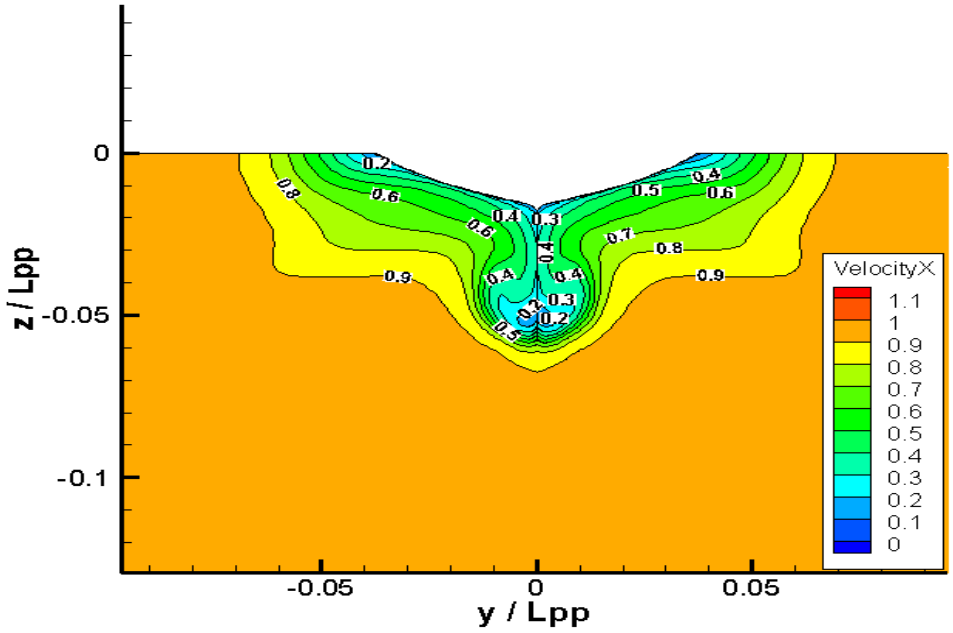

Figure 66. Axial velocity at x/Lpp=0.9825 from SHIPFLOW with β = 0°

Two stern bilge vortices can be observed on the both sides of the symmetry plane. The comparison based on the Figure 65 and Figure 66show a good agreement between measured and computed results. The case with β = 0° is represented as the axial advance velocity of the propeller, in order to determine the wake fraction factor.

b. At the drift angle β = 12°

The angle β=12° has been the maximum drift angle used in the CFD analysis of the flow around the KVLCC2 hull. The axial velocity contours measured at drift angle β = 12° are presented in Figure 67 and the CFD results are depicted in Figure 68.

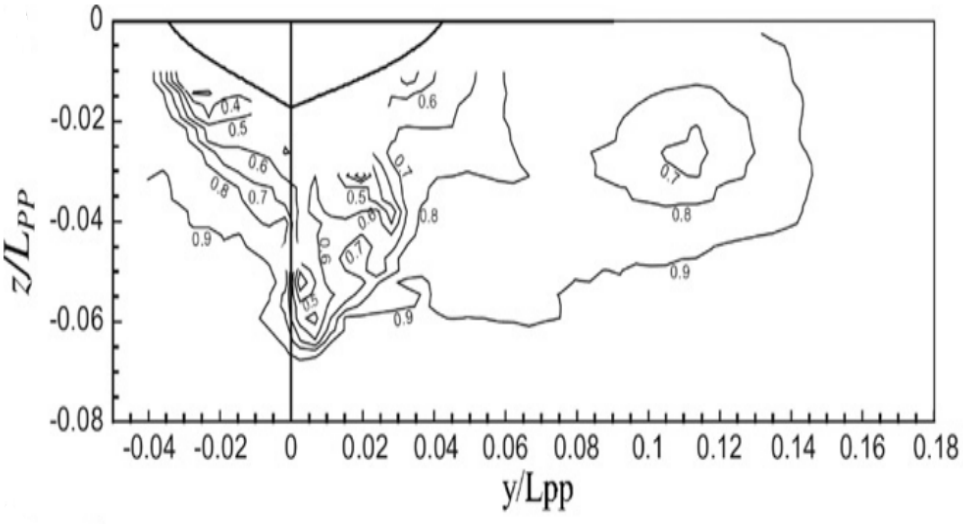

Figure 67. Axial velocity at x/Lpp=0.9825 from Experimental at β = 12° [17]

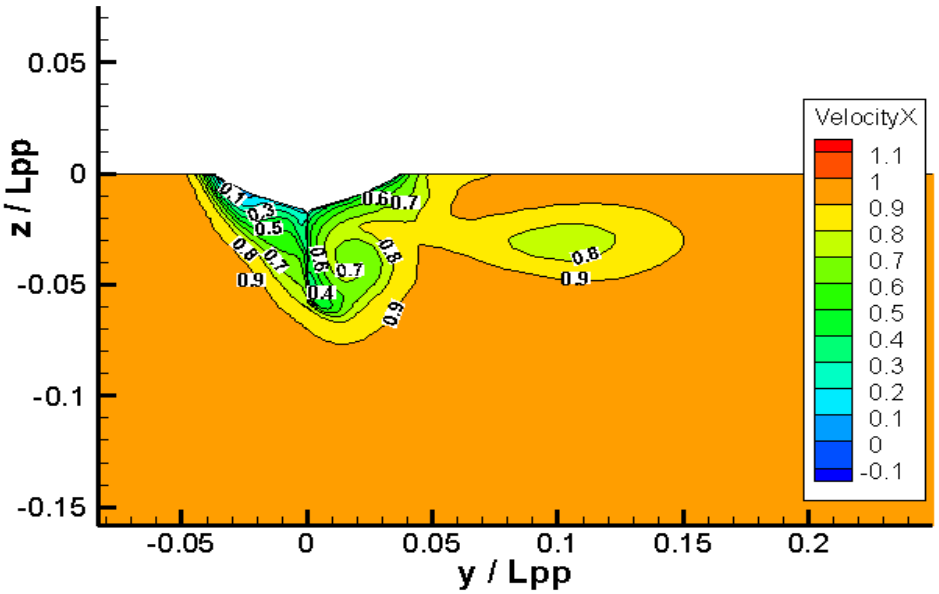

Figure 68. Axial velocity at x/Lpp=0.9825 from SHIPFLOW at β =12°

The comparison of the Figures67 and Figure68 revealed that flow behavior seems to be the same, in both numerical and experimental analysis.

5. CFD ANALYSIS OF THE FLOW AROUND THE KVLCC2 HULL WITH DRIFT ANGLE AND RUDDER ANGLE

5.1 Modeling conditions

In the present chapter XCHAP has been employed to simulate the static drift maneuvering test for hull with deflected rudder. For each drift angle case that was analyzed for bear hull, nine simulations have been performed for rudder angle δ from 40° to -40° with of incrementof10° (static rudder & drift tests).When the rudder is deflected in starboard, positive angles are considered. The KVLCC2model scale is 1/45.714. The computation has been performed in infinite water depth, at Froude number Fn=0.142 and Reynolds number $Re=3.7*10^6$.

The XCHAP solver can handle overlapping grids. A boundary fitted structured grid have been generated around the rudder. Thus, the resulting composite overleaping grid consists of almost 2.1 million cells. The rudder surface grid is depicted in Figure 69.

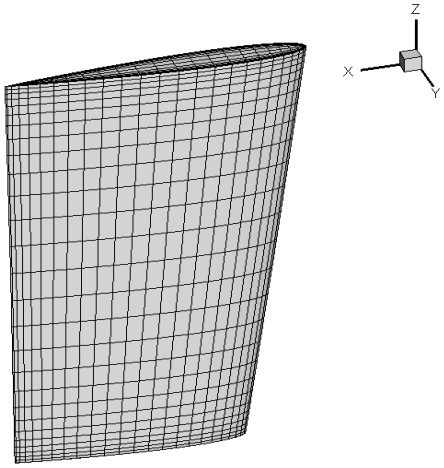

Figure 69. Grid of the rudder

5.2 Hydrodynamics forces and moments with drift angle and rudder angle influences

5.2.1*Longitudinal hydrodynamic force coefficient X'*

Non-dimensional longitudinal forces, *X'*, resulted from the computations for each drift angle (β = 0°, 2°, 4°, 6°, 8°, 10° and 12°) and each rudder angle (δ = -40°,-30°, -20°, -10°, 0°, 10°, 20°, 30°, 40°) have been tabulated in Table 53. The study of the influences of the rudder

angle and drift angle, on the longitudinal non-dimensional force *X'* may be performed using the Figure 70.

Table 53. Non-dimensional longitudinal force X' with drift and rudder influences

	Non – dimensional longitudinal force X'						
δ (°)	**β = 0°**	**β =2°**	**β = 4°**	**β = 6°**	**β = 8°**	**β = 10°**	**β = 12°**
-40	0.0226	0.0230	0.0250	0.0280	0.0298	0.0301	0.0300
-30	0.0214	0.0217	0.0233	0.0256	0.0270	0.0272	0.0274
-20	0.0201	0.0204	0.0213	0.0227	0.0238	0.0243	0.0243
-10	0.0191	0.0192	0.0197	0.0206	0.0214	0.0218	0.0219
0	0.0188	0.0189	0.0192	0.0196	0.0200	0.0201	0.0203
10	0.0191	0.0191	0.0195	0.0200	0.0203	0.0202	0.0203
20	0.0201	0.0201	0.0203	0.0211	0.0217	0.0215	0.0213
30	0.0214	0.0213	0.0216	0.0228	0.0239	0.0234	0.0230
40	0.0226	0.0226	0.0230	0.0244	0.0251	0.0251	0.0254

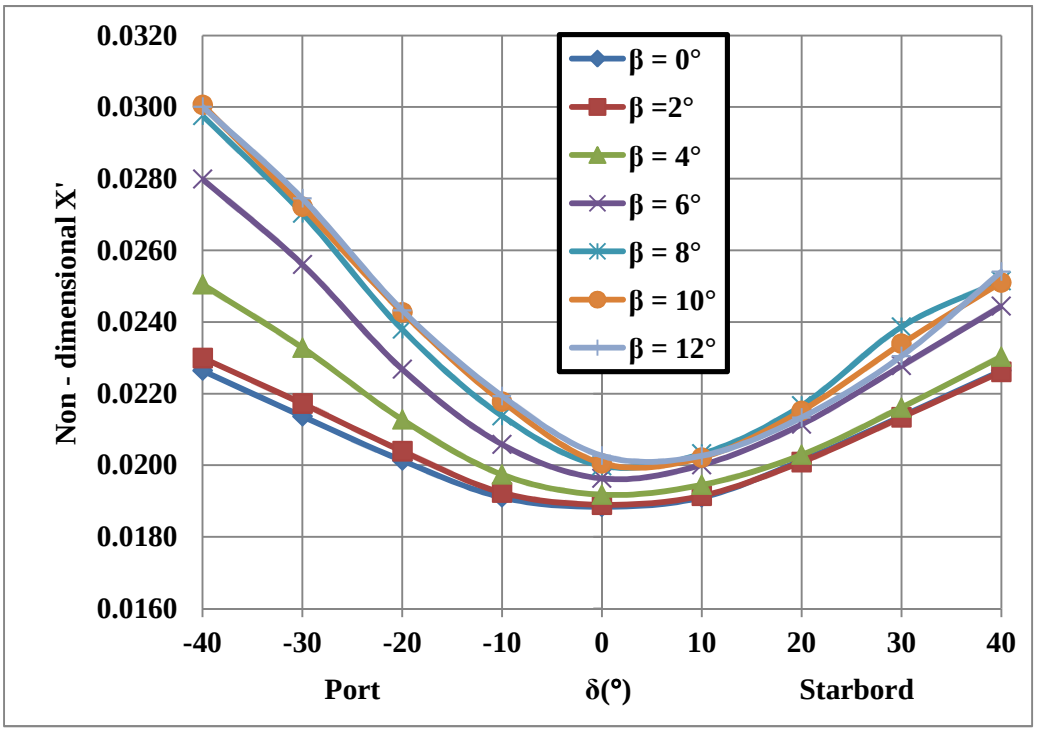

Figure 70. The non-dimensional longitudinal force X' with drift and rudder angles influences

The non–dimensional longitudinal force *X'* increases with the increasing of the drift angle β and rudder angle δ, in the analyzed domain. The values of drift angle β are positive at starboard. The non–dimensional longitudinal force *X'* is bigger when the rudder is deflected to portside than when the rudder is deflected to starboard, for significant drift angle ($\beta \geq 4°$). For example, at drift angle $\beta = 12°$ the non-dimensional longitudinal force is *X'*=0.03 where the rudder angle $\delta = -40°$ and *X'*=0.0254 where the rudder angle $\delta = 40°$. The influence of the rudder angle is significant when the drift angle is increased.

5.2.2 Lateral hydrodynamic force coefficient Y'

The results obtained for the non-dimensional lateral force Y' are presented in Table 54 and Figure 71, for the drift and rudder angles mentioned above.

Table 54. Non-dimensional lateral force *Y'* with drift and rudder angles influences

	Non – dimensional lateral force Y'						
δ (°)	**β = 0°**	**β =2°**	**β = 4°**	**β = 6°**	**β = 8°**	**β = 10°**	**β = 12°**
-40	0.0095	0.0186	0.0298	0.0455	0.0615	0.0779	0.0943
-30	0.0093	0.0183	0.0300	0.0460	0.0623	0.0781	0.0951
-20	0.0083	0.0168	0.0279	0.0426	0.0588	0.0756	0.0920
-10	0.0059	0.0144	0.0243	0.0378	0.0534	0.0702	0.0869
0	0.0000	0.0088	0.0177	0.0295	0.0443	0.0614	0.0790
10	-0.0059	0.0027	0.0111	0.0212	0.0348	0.0515	0.0696
20	-0.0083	-0.0010	0.0075	0.0156	0.0276	0.0436	0.0630
30	-0.0093	-0.0011	0.0065	0.0147	0.0258	0.0421	0.0606
40	-0.0095	-0.0006	0.0074	0.0154	0.0269	0.0420	0.0593

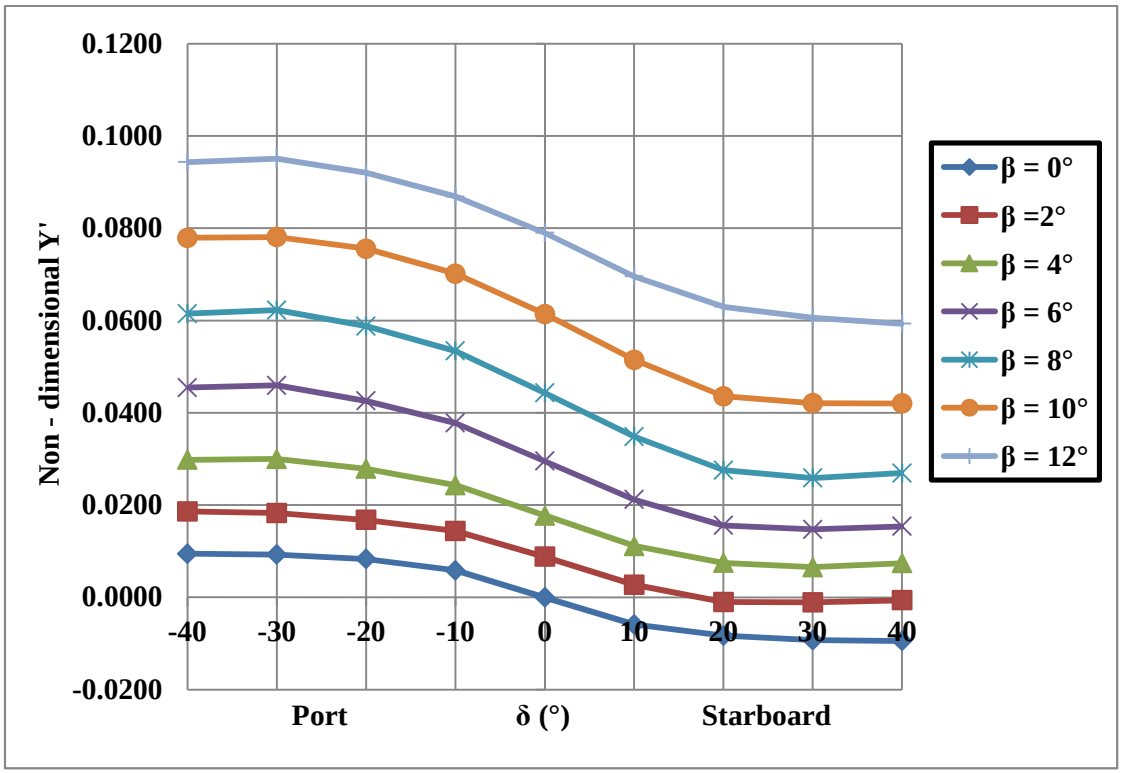

Figure 71. The non-dimensional lateral force Y' with drift and rudder influences

For different drift angle β, the non–dimensional lateral force Y’ increases when the rudder angle is deflected from the maximum starboard (δ = 40°) to the maximum portside (δ = - 40°). The drift angle β is positive to starboard. At the drift angle β = 0°, the non-dimensional lateral force Y’ has symmetric values, when the rudder is deflected to the starboard and to portside.

5.2.3 Yaw hydrodynamic moment coefficient N’

The influence of the rudder angle and the drift angle on the non–dimensional yaw moment *N’* are presented in Table 55 and Figure72.

Table55. Non-dimensional yaw moment N' with drift and rudder angles influences

Non – dimensional yaw moment N’							
δ (°)	β = 0°	β =2°	β = 4°	β = 6°	β = 8°	β = 10°	β = 12°
-40	-0.0043	0.0003	0.0043	0.0070	0.0103	0.0142	0.0183
-30	-0.0043	0.0004	0.0042	0.0068	0.0100	0.0141	0.0180
-20	-0.0038	0.0011	0.0052	0.0084	0.0116	0.0153	0.0193
-10	-0.0026	0.0022	0.0069	0.0106	0.0141	0.0178	0.0217
0	0.0000	0.0048	0.0099	0.0144	0.0183	0.0217	0.0252
10	0.0026	0.0075	0.0129	0.0181	0.0225	0.0261	0.0295
20	0.0038	0.0092	0.0146	0.0207	0.0258	0.0297	0.0325
30	0.0043	0.0093	0.0150	0.0211	0.0266	0.0304	0.0336
40	0.0043	0.0091	0.0147	0.0207	0.0260	0.0304	0.0342

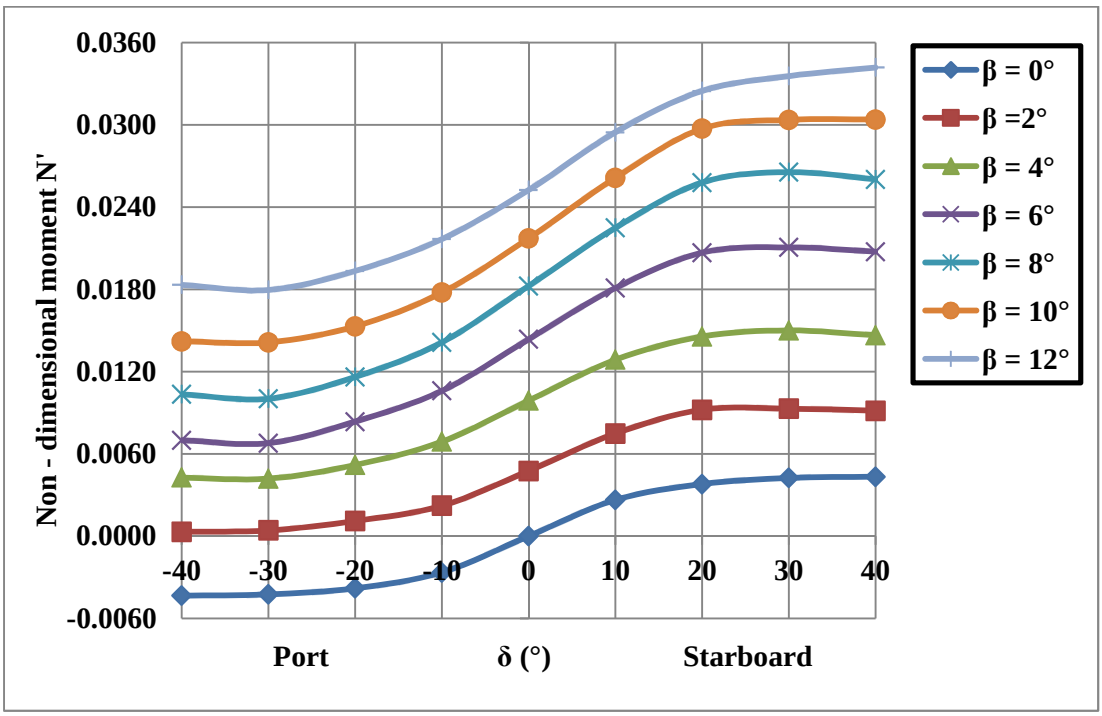

Figure 72. The non-dimensional yaw moment N' with drift and rudder angles influences

For a given rudder angle, the increase of the drift angle generates the increase of the non–dimensional yaw moment N'. For a given drift angle, the non–dimensional yaw moment N' is increased when the rudder is deflected from the maximum angle at portside (δ = -40°) to the maximum angle at starboard (β = 40°). It is the opposite of the non-dimensional lateral force Y'.At the drift angle β = 0°, the non-dimensional yaw moment N'has symmetric values, when the rudder is deflected to the starboard and to portside.

5.3 Numerical study of the flow with drift angle and rudder angle influences

Viscous free-surface flow calculations provide a detailed insight into the hydrodynamics phenomena, allowing the user to introspect the flow characteristics as pressure distribution, axial velocity contours, flow detachment and also help to understand the physical phenomena. In the following, two sets of pressure distribution on rudder have been plotted, in order to perform a systematically analyze of the physical phenomena.

For the first set of results, the 0° rudder angle and drift angle of β = 0°, 4°, 8° and 12° have been considered (the ship was deflected in starboard, the incident flow acts on portside). The cases analyzed have been presented in Figure 73. The pressure distributions for starboard side (SB) and port side (PS) of the rudder have been depicted for each combination of rudder and drift angles in Figure 74. Analyzing the plotted results one can clearly see that portside of the rudder is the pressure side and starboard is suction side, as it is expected.

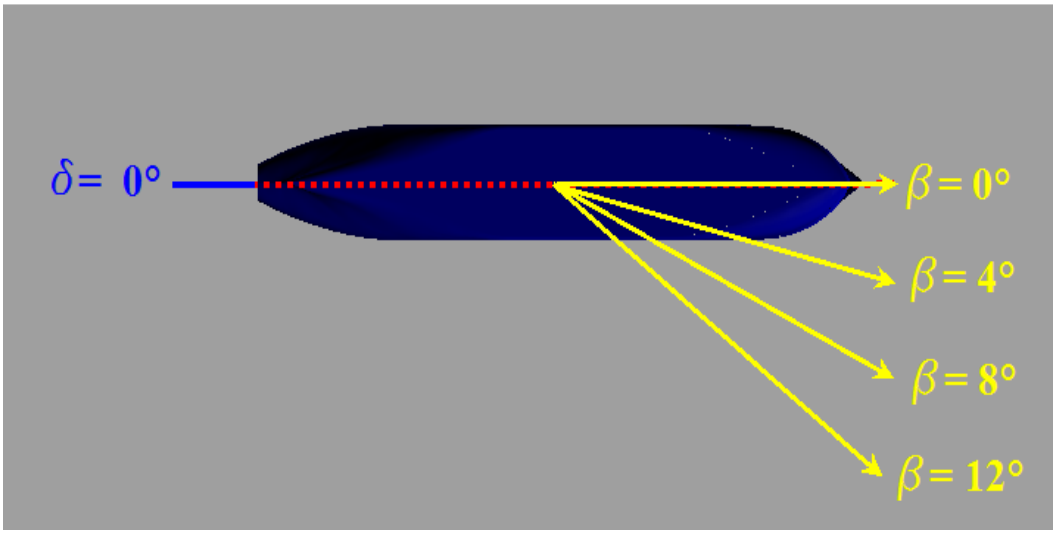

Figure 73. Cases analyzed (without rudder deflection)

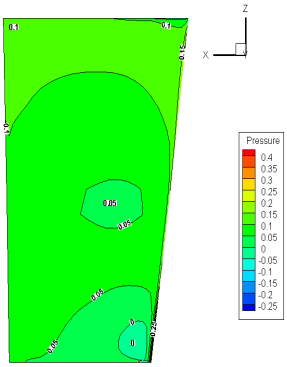

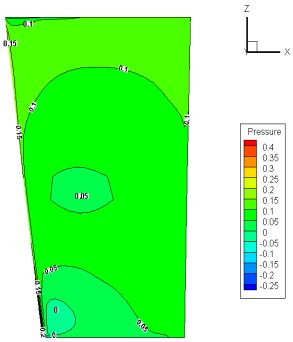

Suction side (SB) Pressure side (PS)

Drift angle 0° at rudder angle δ = 0°

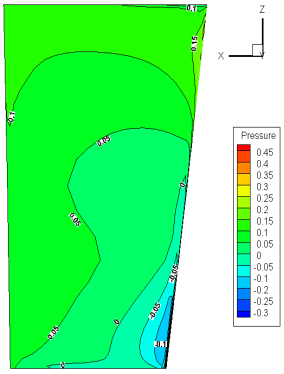

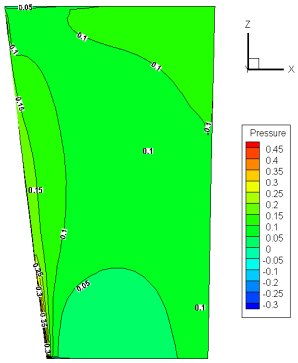

Suction side(SB) Pressure side (PS)

Drift angle 4° at rudder angle δ = 0°

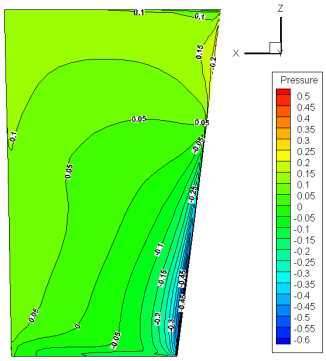

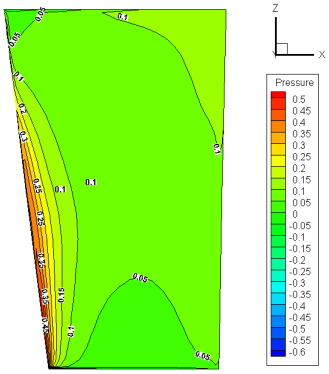

Suctionside (SB) Pressure side(PS)

Drift angle 8° at rudder angle δ = 0°

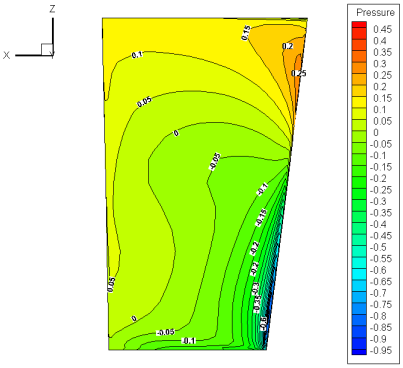

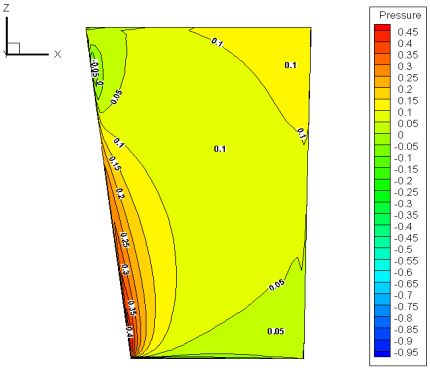

Suctionside (SB) Pressure side(PS)

Drift angle 12° at rudder angle δ = 0°

Figure 74. Pressure distribution on rudder

For the second study, two rudder angle, δ = -30° (in port side) and 30° (in starboard) and the same drift angles, as in the previous set of results, has been considered (see Figure 75). First, the pressure distributions for starboard and port side of the rudder have been depicted for each combination of drift angles and fixed rudder angle, of -30° in port side, as shown in Figure 76. On the other hand, when the pressure distribution has been plotted for the case of deflected rudder equal with 30° in starboard, the starboard side of the rudder becomes pressure side (see Figure 77).

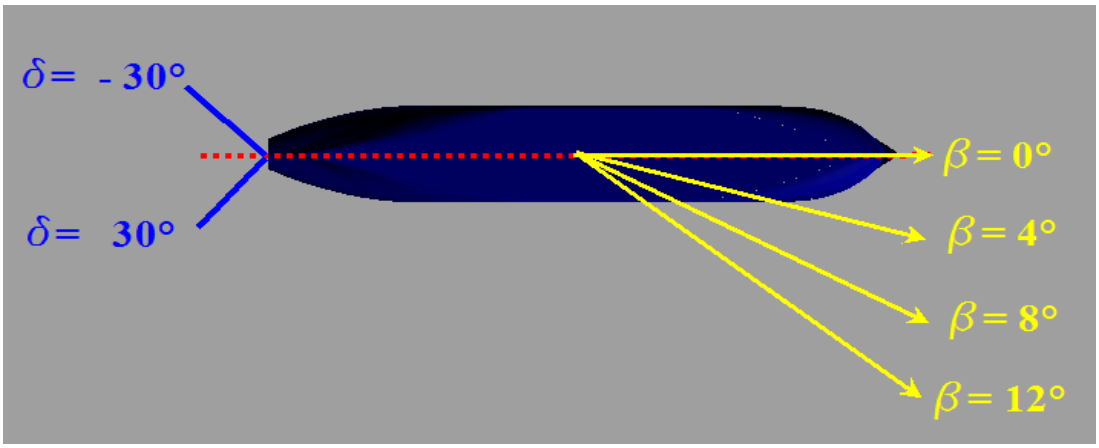

Figure 75. Cases analyzed (including rudder deflection)

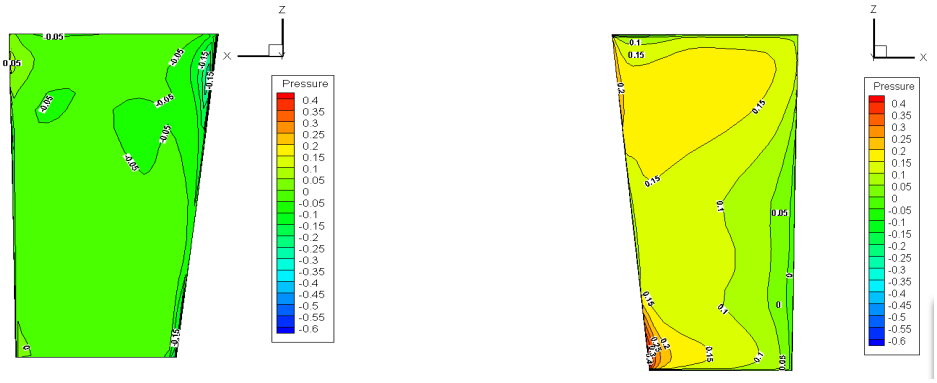

Suction side (SB) Pressure side (PS)

Drift angle 0° at rudder angle δ = -30°

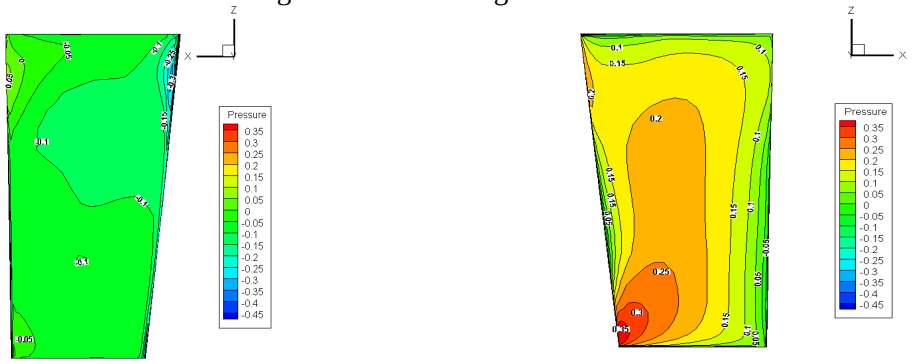

Suction side (SB) Pressure side(PS)

Drift angle 4° at rudder angle δ = -30°

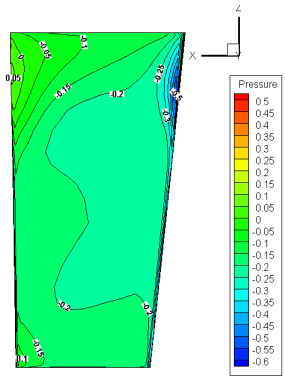

Suction side (SB)

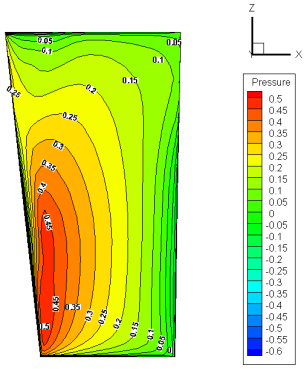

Pressure side(PS)

Drift angle 8° at rudder angle δ = -30°

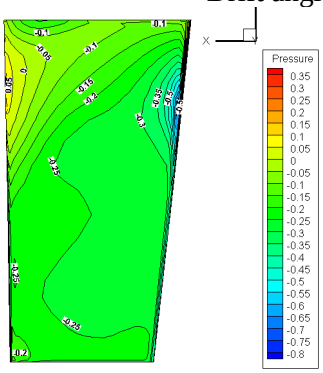

Suction side (SB)

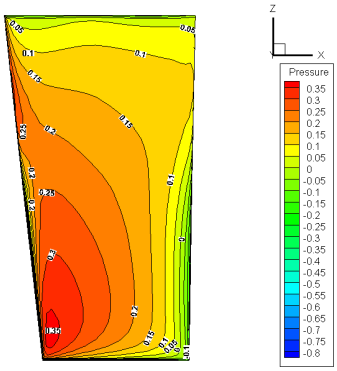

Pressure side(PS)

Drift angle 12° at rudder angle δ = -30°

Figure 76. Pressure distribution on deflected rudder in port side

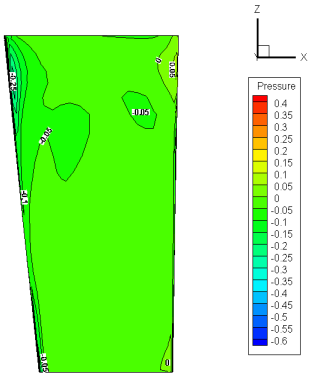

Suction side(PS)

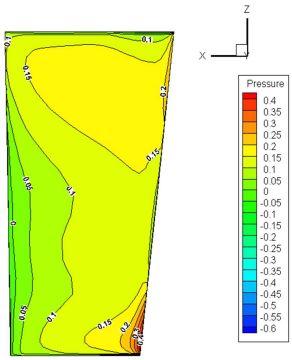

Pressure side(SB)

Drift angle 0° at rudder angle δ = 30°

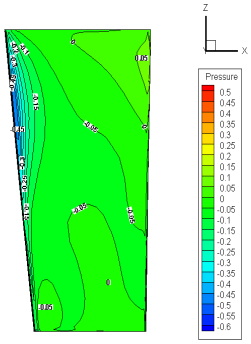

Suction side(PS)

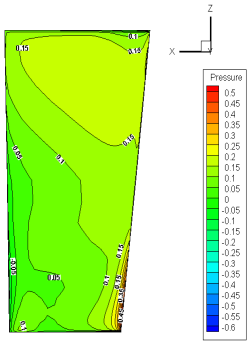

Pressure side(SB)

Drift angle 4° at rudder angle δ = 30°

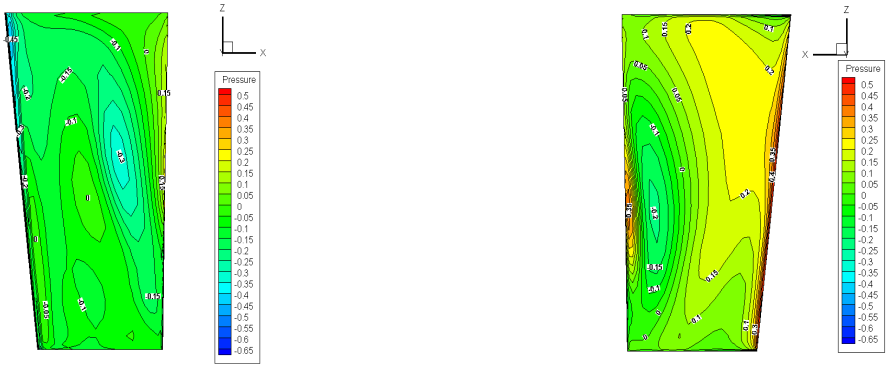

Suction side(PS) Pressure side(SB)

Drift angle 8° at rudder angle δ = 30°

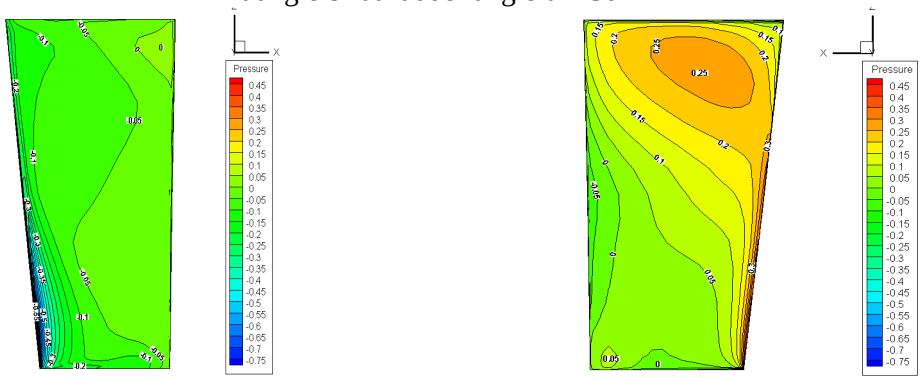

Suction side(PS) Pressure side(SB)

Drift angle 12° at rudder angle δ = 30°

Figure 77. Pressure distribution on deflected rudder in starboard

The Figure 78 presents the comparison between pressure distribution on the suction side corresponding to the -30° and 30°rudder angle. Finally, in the same manner, the pressure side is compared in Figure 79.

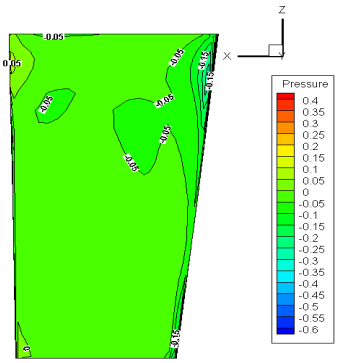

Suction side(SB)
Drift angle 0° at rudder angle δ = -30°

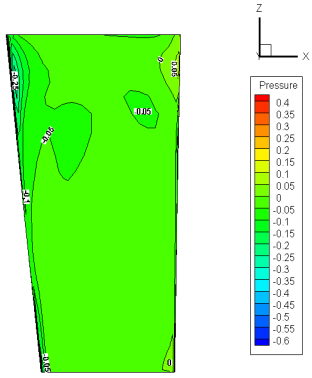

Suction side (PS)
Drift angle 0° at rudder angle δ = 30°

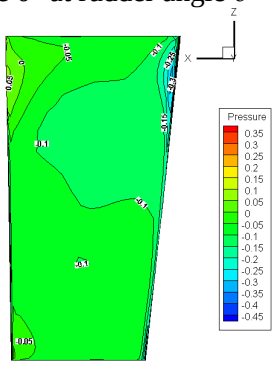

Suction side (SB)
Drift angle 4° at rudder angle δ = -30°

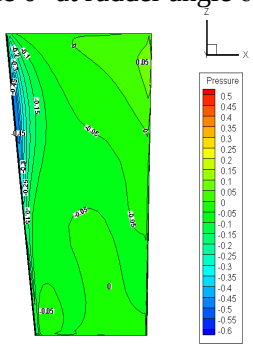

Suction side(PS)
Drift angle 4° at rudder angle δ = 30°

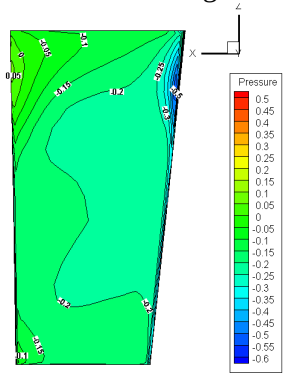

Suction side(SB)
Drift angle 8° at rudder angle δ = -30°

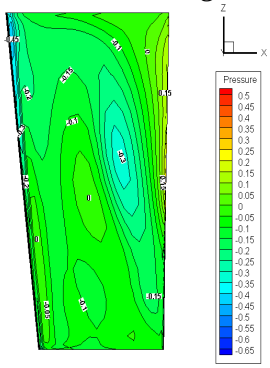

Suction side (PS)
Drift angle 8° at rudder angle δ = 30°

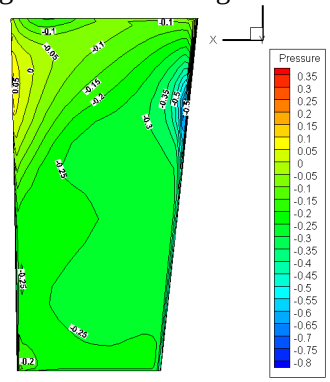

Suction side (SB)
Drift angle 12° at rudder angle δ = -30°

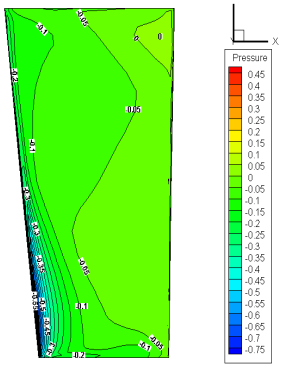

Suction side(PS)
Drift angle 12° at rudder angle δ = 30°

Figure 78. Pressure distribution on suction side of the rudder

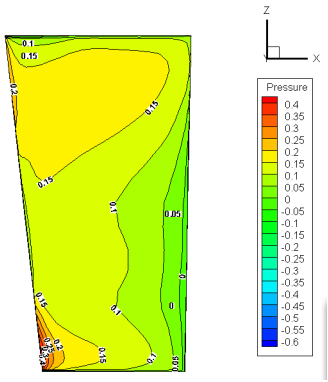

Pressure side(PS)
Drift angle 0° at rudder angle δ = -30°

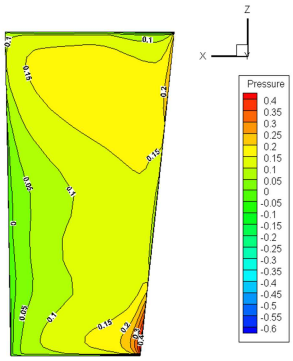

Pressure side(SB)
Drift angle 0° at rudder angle δ = 30°

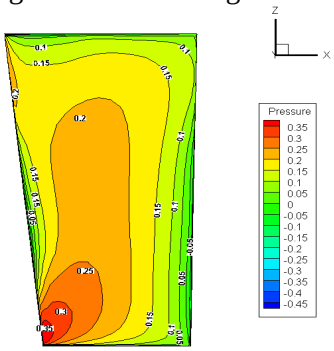

Pressure side(PS)
Drift angle 4° at rudder angle δ = -30°

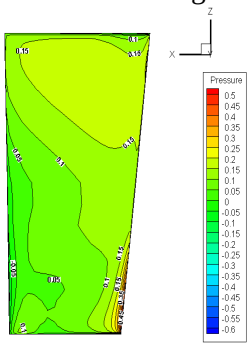

Pressure side (SB)
Drift angle 4° at rudder angle δ = 30°

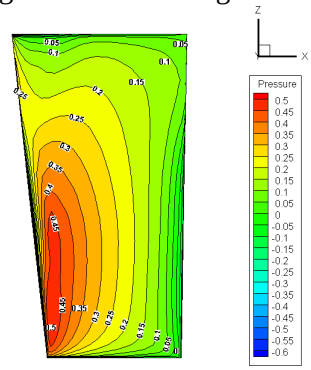

Pressure side(PS)
Drift angle 8° at rudder angle δ = -30°

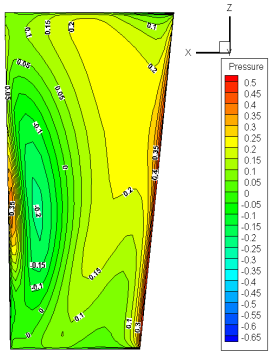

Pressure side(SB)
Drift angle 8° at rudder angle δ = 30°

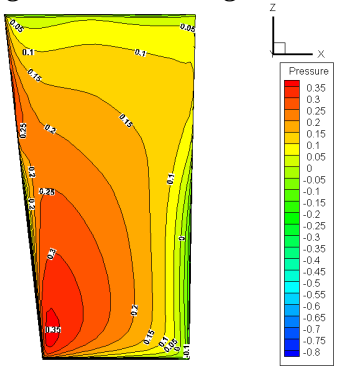

Pressure side (PS)
Drift angle 12° at rudder angle δ = -30°

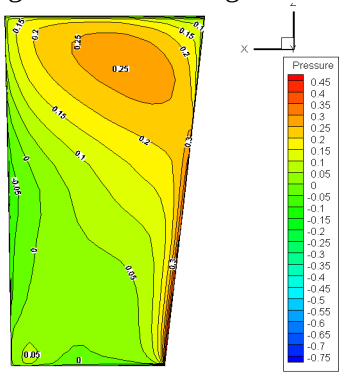

Pressure side (SB)
Drift angle 12° at rudder angle δ = 30°

Figure 79. Pressure distribution on pressure side of rudder

One may note that, in the case of fixed rudder angle (Figures 76 and 77),if the drift angle is increased, the pressure difference (on the rudder) between the pressure side and the suction side is increased. As a consequence, the lateral hydrodynamic forces will increase.

In the case of each fixed drift angle in starboard, the pressure distribution on the suction side (Figure 78) and pressure side (Figure 79) of the deflected rudder with -30° (in portside) will be greater than the case of the deflected rudder with 30° (in starboard).

Also, the same pressure distribution may be observed for the following cases, which means that the CFD results are according with physical phenomena:

- Rudder angle δ =0° and drift angle β = 0°, on the rudder sides (Figure 74);
- Drift angle β = 0°, rudder angle δ =30° and drift angle β = 0°, rudder angle δ =-30° on the suction side of the rudder (Figure 78);
- Drift angle β = 0°, rudder angle δ =30° and drift angle β = 0°, rudder angle δ =-30° on the pressure side of the rudder (Figure 79).

6. CONCLUSION

The objective of this master thesis (described in **Chapter 1**) was to predict and to validate the hydrodynamics performance (resistance, powering and manoeuvring) of the KVLCC2 ship in the initial design stage. It was carried out with two different tools:

- CAD-CAE (**AVEVA-Tribon ID** code and **PHP** code, performed in Chapter 2);
- CFD (**SHIPFLOW** code, used in the Chapters 3-5).

The main conclusions detached from the chapters dedicated to the hydrodynamics analysis are presented in the following.

Chapter 2

- AVEVA-Tribon ID code calculations was performed to evaluate the total resistance of the ship KVLCC2 at design speed, using Holtrop and Mennen method. The parameters of KVLCC2 ship are in the range of limitations of this method. Thus, the brake power was determined in order to select the size and propulsion power of the engine, suitable for the KVLCC2 ship. Also, the optimum hydrodynamic characteristics of the propeller were calculated in open water condition, using Wageningen B-Series.
- By means of PHP (Preliminary Hydrodynamics Performances) code, the hydrodynamics of the rudder (including the maximum torque related to the rudder axis) were performed, in order to select the steering gear used to provide the rudder deflection from one side to the other side, at maximum ship speed. Also, the preliminary checking of the cavitations risk was performed, using Brix' method.
- The analysis of the standard manoeuvring tests (turning circle manoeuvre, Zig-Zag manoeuvre and spiral manoeuvre) of KVLCC2 ship reveals a good course keeping stability on route and satisfactory manoeuvring performances ,the IMO criteria being fulfilled.

Chapter 3

- The numerical results of potential flow resistance computations were carried out by Shipflow and validated by the experimental data from MOERI. The error of the

comparison is less than 1%. Also, a satisfactory agreement was obtained by comparing the numerical wave pattern with experiment results.

- Also, the analysis of the flow around the hull was performed based on viscous flow theory. The numerical results were validated with the MOERI experimental results. The error of the comparison was less than 3% and the results could be more accurate with more refining the computational grid.

Chapter 4

- The non-dimensional hydrodynamics forces X', Y' and non-dimensional yaw moment N' of the bare hull model were predicted, using SHIPFLOW code, by simulating the oblique flow (typical for manoeuvres of the ship), with different static drift angle, between 0-12 degrees and the increment equal with 2 degrees. The numerical results obtained are in a good agreement with the experimental results providing from INSEAN.
- Also, the comparison of the numerical axial velocity in the propeller plane with experimental results from INSEAN reveals a good correlation.

Chapter 5

- The hydrodynamics forces and moment acting on the ship model in horizontal plane were computed for different rudder and drift angles. The numerical results were checked with the diagrams and tables obtained on the basis of the experimental tests with MARINER model, described in references [18] (M. S. CHISLETT & J. STROM-TEJSEN). Even if KVLCC2 and MARINER are different types of ships, the evolution of the non-dimensional forces and moment acting in horizontal plane in function of drift and rudder angles is similar, the forms of the diagrams being correlated.

On the basis of the numerical analysis performed with mentioned CAD-CAE and CFD codes, one may conclude that these codes may be used in naval architecture applications, in order to predict the resistance and propulsion performances and to optimize the shape of the hull. Also, the hydrodynamics forces and moment acting on the ship model in horizontal plane may be evaluated, for different rudder angle and drift angle, with CFD instruments. As a consequence, the static hydrodynamics derivatives used in the nonlinear mathematical models of the ship manoeuvring may be calculated, on the basis of the CFD results.

The **future work recommendation** is to continue this analysis and to determine the hydrodynamics derivatives from the non-dimensional forces and yaw moment acting on the ship model in horizontal plane, obtained in the master thesis. These hydrodynamics derivatives can be implemented in the differential equations of the ship motion in horizontal plane, in order to simulate the standard manoeuvres of the ship and to evaluate the manoeuvrability performances in still water.

7. REFERENCES

Journal article	[2]. Holtrop, J., Mennen, G.G.J., 1982, An approximate power prediction method, International Shipbuilding Progress.
	[9]. Dawson, C., 1977, A Practical Computer Method for Solving Ship Wave Problems, *2nd International Conference on Numerical Hydrodynamics,* Berkley.
	[13]. L. Fabbri, L Benedetti, B. Bouscasse, F.L.Gala and C.Lungni, October 2006, An experimental study of the maneuverability of a blunt ship: the effect of the water depth, *In 9thNutts Numerical Towing Tank Symposium*, La Croisie, France.
	[14]. F. Stern and K. Agdrup, April 2008, *SIMMAN Workshop on Verification and Validation of Ship Manoeuvring Simulation* Methods, Copenhagen, Danemark.
	[16]. Lee, S,-J, Kim, H,-R, Kim, W,-J, Van, S,-H, 2003, *Wind tunnel tests on flow characteristic of the KRISO 3,600 TEU containership and 300K VLCC double deck ship models*.J. Ship Res, 47 (1), 24-38
	[17]. Tao Xing, Shanti Bhushan, Frederick Stern, 2012.Vortical and turbulent structures for KVLCC2 at drift angle. *Ocean Engineering*, 55 (2012), 23–43
	[18]. Chislett, M. S. and Strom-Tejsen, J, April 1965,*Planar Motion Mechanism Test and Full-Scale Steering and Manoeuvring Predictions for a MARINER Class Vessel*, Hydro-and Aerodynamic Laboratory, Report No. Hy-6
Book	[4]. Abkowitz, M.A., 1964. *Lectures on Ship Hydrodynamics-Steering and Manoeuvrability*, Report No.Hy-5, Hydro- and Aerodynamics laboratory, Lyngby, Denmark.
	[6]. Bertram, V., *Practical Ship Hydrodynamics,* Butter Heinemann, Oxford, 2000
	[7]. Brix, J., *Manoeuvring Technical Manual,* Seehafen Verlag, Hamburg, 1993
	[8]. Voitkounski, Y.I., *Spravocinik po teoria Korablea,* Ed. Sudostroenie, Sankt Petersburg, 1985 (in Russian)
Chapter	[3]. Michael G. Parsons. Parametric Design, Chapter11, pages 1 – 50
	[12]. W. J. Kim, S. H. Van, D. H. Kim, 2001, *Measurement of flows around modern commercial ship model,* Springer-Verlag 2001, Experiments in Fluids 31: 567-578

Internet document	[1].http://www.simman2008.dk/KVLCC/KVLCC2/kvlcc2_geometry.html
	[10].http://nas.tinyla.idv.tw/~F96525033/Instruction/Flowtech%20Shipflow/).
Newspaper article	[5]. IMO, 2002. Explanatory notes to the standard for ship manoeuvrability
Thesis	[15]. Toxopeus, S, 2001. *Practical application of viscous-flow calculations for the simulation of manoeuvring ship*. Thesis (Ph.D). Universiteit Delft.
	[8]. Janson, C-E., 1997. *Potential Flow Panel Methods for the Calculation of Free Surface Flows with Lift*, Thesis (Ph.D), Chalmers University of Technology.
	[11]. Koen van Mierlo, 2006. *Trend validation of SHIPFLOW based on the bare hull upright resistance of Delft Series*, Thesis (Master), Delft Univeristy of Technology.

APPENDIX

APPENDIX A1 Hydrostatic calculation of KVLCC2

Draft (m)	Displt (t)	LCB (m)	VCB (m)	WPA (m^2)	LCF (m)	KML (m)	KMT (m)	WSA (m^2)	TPC (t/cm)	MTC (t-m/cm)
0.50	5496.97	177.507	0.258	11479.03	177.103	9018.795	434.790	11532.02	117.66	1549.21
1.00	11593.40	177.166	0.518	12246.98	176.680	4947.730	230.653	12388.92	125.53	1792.34
1.50	17997.12	176.951	0.779	12714.38	176.497	3468.076	158.694	12987.50	130.32	1950.04
2.00	24607.63	176.829	1.040	13066.22	176.484	2690.305	122.135	13494.61	133.93	2068.01
2.50	31372.49	176.745	1.301	13324.99	176.377	2211.312	99.178	13944.98	136.58	2166.67
3.00	38260.30	176.667	1.562	13550.56	176.238	1887.859	83.924	14370.29	138.89	2255.32
3.50	45255.30	176.592	1.823	13740.22	176.142	1650.870	72.970	14775.46	140.84	2332.13
4.00	52339.27	176.527	2.084	13901.17	176.089	1468.109	64.747	15164.42	142.49	2397.83
4.50	59501.20	176.471	2.345	14045.42	176.027	1323.864	58.385	15544.33	143.97	2457.25
5.00	66733.79	176.418	2.605	14177.57	175.940	1207.217	53.337	15918.13	145.32	2512.13
5.50	74031.45	176.366	2.866	14299.54	175.832	1110.596	49.253	16286.76	146.57	2562.71
6.00	81389.27	176.313	3.127	14412.53	175.742	1028.865	45.904	16651.24	147.73	2608.88
6.50	88804.55	176.260	3.388	14526.57	175.598	960.598	43.135	17014.52	148.90	2656.40
7.00	96279.10	176.201	3.649	14640.98	175.402	902.615	40.818	17378.12	150.07	2704.74
7.50	103809.23	176.136	3.910	14741.90	175.201	851.108	38.794	17739.72	151.10	2748.34
8.00	111387.08	176.066	4.171	14828.47	175.003	804.784	37.002	18098.87	151.99	2786.81
8.50	119006.75	175.992	4.432	14905.50	174.827	763.197	35.423	18456.61	152.78	2821.81
9.00	126665.48	175.915	4.694	14983.19	174.591	726.884	34.046	18815.08	153.58	2858.64
9.50	134364.89	175.831	4.955	15063.32	174.294	695.079	32.848	19174.30	154.40	2897.77
10.00	142105.36	175.738	5.216	15142.55	173.947	666.497	31.802	19534.31	155.21	2936.61
10.50	149884.36	175.633	5.477	15214.46	173.493	639.864	30.875	19894.12	155.95	2971.40
11.00	157700.69	175.515	5.738	15288.98	173.010	616.062	30.066	20255.69	156.71	3007.76
11.50	165555.85	175.385	6.000	15365.19	172.495	594.824	29.350	20620.32	157.49	3046.35
12.00	173449.63	175.241	6.262	15439.42	171.949	575.499	28.704	20987.48	158.25	3085.44
12.50	181380.89	175.084	6.524	15511.44	171.373	557.729	28.123	21356.28	158.99	3124.32
13.00	189348.42	174.915	6.786	15580.95	170.761	541.245	27.602	21726.54	159.70	3162.47
13.50	197350.96	174.734	7.048	15648.34	170.113	525.946	27.135	22098.38	160.40	3200.16
14.00	205388.38	174.540	7.310	15717.77	169.426	512.010	26.724	22472.99	161.11	3239.36
14.50	213462.24	174.333	7.572	15790.59	168.699	499.395	26.367	22850.87	161.85	3280.80
15.00	221574.38	174.113	7.835	15866.63	167.944	487.989	26.057	23231.79	162.63	3324.68
15.50	229725.44	173.880	8.098	15942.49	167.173	477.549	25.776	23615.28	163.41	3370.15
16.00	237915.31	173.635	8.362	16017.80	166.368	467.869	25.526	24001.24	164.18	3416.37
16.50	246143.24	173.379	8.625	16090.50	165.524	458.653	25.304	24389.83	164.93	3461.60
17.00	254407.39	173.109	8.889	16159.18	164.650	449.737	25.108	24780.64	165.63	3504.84
17.50	262705.79	172.828	9.153	16224.44	163.763	441.140	24.935	25172.96	166.30	3546.41

Draft (m)	Displt (t)	LCB (m)	VCB (m)	WPA (m^2)	LCF (m)	KML (m)	KMT (m)	WSA (m^2)	TPC (t/cm)	MTC (t-m/cm)
18.00	271037.36	172.536	9.418	16289.15	162.881	433.032	24.787	25566.13	166.96	3587.98
18.50	279402.66	172.234	9.682	16357.61	162.042	425.704	24.666	25958.53	167.67	3632.42
19.00	287805.65	171.926	9.947	16434.21	161.343	419.550	24.565	26345.91	168.45	3683.94
19.50	296246.37	171.616	10.212	16503.82	160.758	413.183	24.478	26727.92	169.16	3730.58
20.00	304720.83	171.307	10.477	16566.42	160.287	406.639	24.404	27104.68	169.81	3772.46
20.50	313226.30	171.003	10.743	16625.16	159.931	400.155	24.344	27477.35	170.41	3811.69
20.80	318343.79	170.823	10.902	16659.21	159.767	396.334	24.315	27699.27	170.76	3834.37
21.00	321761.18	170.705	11.008	16680.92	159.675	393.776	24.299	27846.45	170.98	3848.74

APPENDIX A2 Sectional area calculation of KVLCC2

WL ST	0.00	1.00	2.00	3.00	4.00	5.00	6.00	7.00	8.00	9.00	10.00
-0.125	0.000	0.000	0.000	0.000	0.000	0.000	0.000	0.000	0.000	0.000	0.000
0.000	0.000	0.000	0.000	0.000	0.000	0.000	0.000	0.000	0.000	0.000	0.000
0.250	0.000	0.000	0.000	0.000	0.000	0.000	0.000	0.000	0.000	0.180	2.099
0.500	0.000	1.318	5.034	9.663	14.944	20.335	25.433	30.207	34.504	38.305	42.049
0.750	0.000	1.925	8.908	16.839	25.960	35.801	45.729	55.718	66.318	76.591	86.970
1.000	0.000	6.982	17.598	29.600	42.790	56.593	70.951	86.018	101.926	118.791	137.159
1.500	0.000	13.560	31.697	52.148	74.495	98.346	123.794	151.134	180.494	212.370	246.862
2.000	0.000	20.881	47.471	77.590	110.871	147.051	185.679	226.663	269.833	315.092	362.146
2.500	0.000	29.458	65.820	106.456	150.452	197.031	245.853	296.499	348.581	402.059	456.438
3.000	0.000	40.145	86.498	136.136	187.688	241.063	295.562	351.039	407.467	464.396	521.664
3.500	0.000	49.121	102.870	158.206	214.435	271.206	328.472	386.235	444.293	502.353	560.412
4.000	0.000	55.364	112.714	170.538	228.437	286.367	344.329	402.321	460.321	518.321	576.321
5.000	0.000	55.699	113.242	171.202	229.202	287.202	345.202	403.202	461.202	519.202	577.202
6.000	0.000	55.699	113.242	171.202	229.202	287.202	345.202	403.202	461.202	519.202	577.202
6.500	0.000	55.709	113.261	171.221	229.225	287.233	345.247	403.265	461.281	519.292	577.298
7.000	0.000	55.699	113.242	171.202	229.202	287.202	345.202	403.202	461.202	519.202	577.202
7.500	0.000	52.974	109.148	166.285	223.771	281.425	339.243	397.225	455.279	513.323	571.357
8.000	0.000	46.173	97.288	150.251	204.883	260.673	316.929	373.647	430.801	488.117	545.520
8.500	0.000	38.055	82.061	129.472	178.797	229.724	281.991	334.914	388.458	442.595	497.089
9.000	0.000	26.768	60.449	98.222	138.606	181.270	225.447	271.037	317.717	365.086	413.141
9.250	0.000	15.156	39.567	68.655	100.843	135.514	172.177	210.732	250.526	291.086	332.341
9.500	0.000	11.717	30.480	53.222	78.934	106.938	136.950	168.439	201.283	234.958	269.382
9.750	0.000	1.510	8.826	20.223	34.550	51.127	69.918	89.703	111.285	134.373	158.347
10.000	0.000	0.000	1.373	5.769	12.337	20.741	30.781	42.079	54.488	67.536	81.111
10.125	0.000	0.000	0.000	0.000	0.000	0.000	0.441	3.314	8.038	14.125	20.996
10.250	0.000	0.000	0.000	0.000	0.000	0.000	0.000	0.000	0.000	0.000	0.019

WL ST	11.00	12.00	13.00	14.00	15.00	16.00	17.00	18.00	19.00	20.00
-0.125	0.000	0.000	0.000	0.000	0.000	0.000	0.000	0.000	2.141	10.001
0.000	0.000	0.000	0.000	0.000	0.000	0.000	0.000	2.206	11.015	24.740
0.250	4.740	7.252	9.341	11.252	13.722	18.931	29.236	44.553	64.042	86.817
0.500	46.087	50.610	56.601	64.578	76.459	93.312	114.913	140.402	168.877	199.768
0.750	98.368	112.432	128.735	148.488	172.091	199.492	230.013	263.229	298.518	335.650
1.000	157.210	179.756	205.365	234.648	267.101	302.372	340.185	379.991	421.574	464.361
1.500	284.052	323.763	365.828	409.904	455.787	503.216	551.901	601.786	652.534	704.092
2.000	410.947	461.165	512.687	565.399	618.951	673.319	728.394	783.948	839.973	896.407
2.500	511.563	567.425	623.766	680.468	737.533	794.865	852.354	909.999	967.781	1025.630
3.000	579.273	637.121	695.013	752.945	810.915	868.899	926.889	984.885	1042.878	1100.850
3.500	618.472	676.509	734.514	792.487	850.433	908.389	966.361	1024.350	1082.346	1140.332
4.000	634.321	692.321	750.321	808.321	866.321	924.321	982.321	1040.321	1098.321	1156.321
5.000	635.202	693.202	751.202	809.202	867.202	925.202	983.202	1041.202	1099.202	1157.202
6.000	635.202	693.202	751.202	809.202	867.202	925.202	983.202	1041.202	1099.202	1157.202
6.500	635.299	693.298	751.298	809.298	867.299	925.299	983.298	1041.299	1099.299	1157.298
7.000	635.202	693.202	751.202	809.202	867.202	925.202	983.202	1041.202	1099.202	1157.202
7.500	629.380	687.392	745.394	803.385	861.368	919.352	977.342	1035.338	1093.338	1151.344
8.000	603.009	660.569	718.148	775.744	833.356	890.976	948.596	1006.216	1063.838	1121.476
8.500	551.883	606.978	662.310	717.803	773.457	829.267	885.199	941.244	997.405	1053.674
9.000	461.715	510.574	559.716	609.109	658.669	708.392	758.284	808.383	858.696	909.225
9.250	374.115	416.190	458.550	501.072	543.664	586.410	629.214	672.046	715.079	758.256
9.500	304.345	339.613	375.176	410.850	446.569	482.320	518.049	553.748	589.463	625.272
9.750	182.606	206.983	231.618	256.296	280.540	304.541	327.981	349.123	367.913	386.007
10.000	94.826	108.505	121.893	134.652	146.485	156.643	164.311	168.978	171.254	172.343
10.125	28.201	35.304	41.815	46.812	49.036	49.527	49.994	51.826	54.186	54.186
10.250	0.625	0.803	0.803	0.803	0.803	0.803	0.803	0.803	0.803	0.803

WL ST	20.80	21.00
-0.125	19.641	22.410
0.000	38.356	42.057
0.250	106.894	112.094
0.500	225.769	232.446
0.750	366.352	374.141
1.000	499.409	508.271
1.500	745.853	756.336
2.000	941.736	953.093
2.500	1071.952	1083.539
3.000	1147.211	1158.799
3.500	1186.713	1198.308
4.000	1202.721	1214.321
5.000	1203.602	1215.202
6.000	1203.602	1215.202
6.500	1203.699	1215.298
7.000	1203.602	1215.202
7.500	1197.753	1209.355
8.000	1167.603	1179.136
8.500	1098.764	1110.047
9.000	949.833	960.011
9.250	792.930	801.649
9.500	653.988	661.180
9.750	401.126	405.065
10.000	172.589	172.629
10.125	54.186	54.186
10.250	0.803	0.803